Universidade do Minho
Escola de Ciências

Marco Ivan Novais Ribeiro Silva Brito

Ultralight Bosonic Fields and Black Holes

julho de 2021

Ultralight Bosonic Fields and Black Holes
Marco Brito
UMinho | 2021

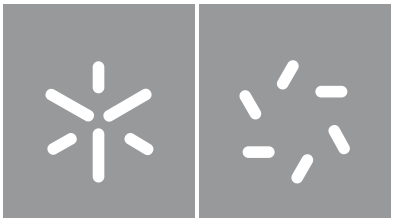

Universidade do Minho
Escola de Ciências

Marco Ivan Novais Ribeiro Silva Brito

Ultralight Bosonic Fields and Black Holes

Dissertação de Mestrado
Mestrado em Física

Trabalho efetuado sob a orientação do
Professor Doutor Carlos Alberto Ruivo Herdeiro
Professor Doutor António Joaquim Onofre Abreu Ribeiro Gonçalves

julho de 2021

Acknowledgments

I would like to thank my thesis advisors, namely Professor Carlos Herdeiro and Professor António Onofre. I thank Professor Herdeiro, who guided my work in these last 10 months by proposing a subject for this master thesis and being available to answer my doubts, giving me suggestions and guidance. I thank Professor Onofre, who advised me on doing a thesis related to astrophysics and made efforts so that would be possible. I would also like to thank Nuno Santos from the University of Aveiro, for spending his own time answering my doubts as well as reviewing my work, pointing out some errors and giving suggestions.

STATEMENT OF INTEGRITY

I hereby declare having conducted this academic work with integrity. I confirm that I have not used plagiarism or any form of undue use of information or falsification of results along the process leading to its elaboration.

I further declare that I have fully acknowledged the Code of Ethical Conduct of the University of Minho.

Campos Bosónicos Ultra-leves e Buracos Negros

Resumo

Nesta dissertação de mestrado, vão ser estudadas as perturbações escalares e tensoriais em buracos negros. Depois de uma introdução, com o intuito de fazer uma revisão sobre buracos negros e ondas gravitacionais, são obtidas numericamente as frequências dos estados quasi-ligados de campos massivos escalares nas geometrias de Schwarzschild e Kerr, assim como as frequências dos modos quasi-normais para campos escalares sem massa, a que se segue uma discussão dos resultados. Também se obtêm os modos quasi-normais para perturbações tensoriais sem massa (perturbações gravíticas) tanto no caso de Schwarzschild (onde, apenas neste caso, vai ser deduzida uma equação de onda para as mesmas perturbações) assim como para o caso de Kerr. Para a determinação numérica das frequências vai ser utilizado o método da fração infinita continuada (método de Leaver). Estuda-se também o fenómeno da superradiância em buracos negros de Kerr com o objetivo de obter uma condição para a instabilidade superradiante causada por um campo escalar massivo. Conclui-se que só para campos ultraleves é que a instabilidade é relevante. No capítulo 6 vai-se aplicar os valores obtidos para as frequências dos modos quasi-normais de perturbações gravíticas em Kerr a um sinal de ondas gravitacionais obtido pelo LIGO, nomeadamente o evento GW190521. Tenta-se ajustar uma função de onda com as frequências dos modos dominantes e encontra-se um bom acordo entre experiência e teoria.

Palavras chave: Buracos negros, Relatividade Geral, estados quasi-ligados, modos quasi-normais, perturbações, Schwarzschild, Kerr, campos bosónicos ultra-leves, ondas gravitacionais, método de Leaver, equação de Klein-Gordon, equação de Teukolsky, superradiância.

Ultralight Bosonic Fields and Black Holes

Abstract

In this master's thesis, we will study scalar and tensor perturbations on black holes. After an introduction, with the objective of doing a review about black holes and gravitational waves, the frequencies of quasi-bound states of massive scalar fields are obtained numerically on the Schwarzschild and Kerr geometries, as well as the frequencies of quasi-normal modes for massless scalar fields, followed by a discussion of results. We too obtain the quasi-normal modes for massless tensor perturbations (gravitational perturbations) for the Schwarzschild case (where, in this case only, we will derive a wave equation for those perturbations) and for the Kerr case. For the numerical determination of the frequencies the infinite continued fraction method (Leaver's method) will be used. We also study the phenomena of super-radiance on Kerr black holes with the purpose of obtaining a condition for the super-radiant instability caused by a massive scalar field. We conclude that only for ultralight fields the instability is relevant. In chapter 6, we will apply the obtained values for the quasi-normal frequencies of gravitational perturbations on Kerr to a gravitational wave signal obtained by LIGO, namely the event GW190521. We try to adjust a wave function with the frequencies of the dominant modes and we find a good agreement between experiment and theory.

Keywords: Black holes, General Relativity, quasi-bound states, quasi-normal modes, perturbations, Schwarzschild, Kerr, ultralight bosonic fields, gravitational waves, Leaver's method, Klein-Gordon equation, Teukolsky equation, super-radiance.

Contents

Constants and Conventions

Our conventions and notations below are essentially the same as in Misner *et al.* (2017), unless defined otherwise. We will also make use of the Einstein summation convention. Further we use Greek letters for spacetime indices and lower case Latin letters for 3-space indices. In this thesis we shall use geometrized units.

Fundamental Constants

$c = 1$	Speed of light in a vacuum inertial frame
$G = 1$	Gravitational constant
$\hbar = 2.612 \times 10^{-70}\,\mathrm{m}^2$	Reduced Planck's constant

Sign Conventions

$g_{\mu\nu} \to (-,+,+,+)$	Metric signature (Landau-Lifshitz Spacelike Convention)
$+R^{\alpha}{}_{\beta\mu\nu} = 2\Gamma^{\alpha}{}_{\beta[\nu,\mu]} + \Gamma^{\alpha}{}_{\sigma\mu}\Gamma^{\sigma}{}_{\beta\nu} - \Gamma^{\alpha}{}_{\sigma\nu}\Gamma^{\sigma}{}_{\beta\mu}$	Riemann sign
$G^{\mu\nu} + \Lambda g^{\mu\nu} = +8\pi T^{\mu\nu}$	Einstein sign

Mathematical Symbols

$\vec{V}$	Four vector
$\mathbf{A}$	Tensor

$\boldsymbol{r}$ or $\boldsymbol{R}$	Three vector
$\tilde{p}$	n-form
$\vec{e}_\mu$	Basis vector
$\tilde{\omega}^\mu$	Basis one-form
$V^{\mu'} = \Lambda^{\mu'}{}_{\nu} V^\nu$	$V^{\mu'}$ denotes the μth vector component in the newly transformed basis
$\tilde{\mathrm{d}}\tilde{p} = \dfrac{\partial \omega_i}{\partial x^j}\, \tilde{\mathrm{d}}x^j \wedge \tilde{\mathrm{d}}x^{i_1} \wedge \ldots \wedge \tilde{\mathrm{d}}x^{i_n}$	Exterior derivative of a n-form
$\partial f / \partial x^\mu \equiv \partial_\mu f \equiv f_{,\mu}$	Partial derivative
$(\nabla \mathbf{T})^{\alpha_1 \cdots}{}_{\beta_1 \ldots \mu} \equiv T^{\alpha_1 \cdots}{}_{\beta_1 \ldots ; \mu} \equiv \nabla_\mu T^{\alpha_1 \cdots}{}_{\beta_1 \ldots , \mu}$	Covariant derivative
$\ldots\ldots \overset{*}{=} \ldots\ldots$	Equality only valid in a local Lorentzian frame

Physical Quantities

$\omega = \omega_R + \mathrm{i}\omega_I$	Frequency eigenvalue
M	Mass of a black hole
a	Angular momentum per unit of mass of a black hole
$r_\pm = M \pm \sqrt{M^2 - a^2}$	Location of the outer(inner) event horizons of a Kerr black hole
$\mu = \mathcal{M}/\hbar$	Mass of a scalar field divided by $\hbar$ (it will be referred as the mass of the field nonetheless)
$\Omega_H = a/(r_+^2 + a^2)$	Black hole horizon angular velocity

List of Figures

List of Tables

1 Introduction

In the last decade, due to the first detections of gravitational waves, there has been a new impetus in the research field of gravitational physics. For the first time in history we can probe astrophysical phenomena, such as black hole collisions and gravitational waves generated a few instants after the Big Bang, without depending on electromagnetic signals, which are absorbed by whatever matter they find along the way. Gravitational waves, since they barely interact with matter due to the very weak coupling of gravity to matter, are excellent probes to study astronomical and cosmological physics.

Given our ability to detect such signals, we are able to test General Relativity in the strong gravity regime, test it against other theories, and even detect the presence of other fields of matter beyond the standard model which may give us clues to the problem of dark matter.

In this thesis, we shall study scalar and tensorial perturbations of Kerr black holes (and in the special case of Kerr, the Schwarzschild metric) using numerical methods. We begin with a general overview of the main results of the Schwarzschild and Kerr solutions to the Einstein equations and a brief overview on light bosonic fields and gravitational waves. We later study bound and unbound modes of scalar fields on black holes followed by gravitational perturbations on a black hole geometry which gives rise to gravitational waves. In the last chapter we try to fit our results of gravitational perturbations to a specific gravitational wave event, GW190521, and see if our results describe the wave-form of the detected waves.

1.1 Black Holes and General Relativity

General Relativity predicts that the gravitational collapse of matter, if not stopped by pressure, will eventually collapse into a region of infinite density, hidden from the outside universe by an event horizon, a region from which nothing can emerge. Several solutions for Einstein equations giving rise to black holes were found in the past, although only two of them are generically thought to describe the spacetime geometry of real black holes. Such solutions are the Schwarzschild solution, Schwarzschild (1916), for a non-rotating black hole and the Kerr solution, Kerr (1963) (Schwarzschild is a particular case of this solution), for rotating black holes, which we shall explore in more detail in the following.

1.1.1 Schwarzschild black hole

1.1.1.1 The Schwarzschild solution

Outside a spherically symmetric distribution of matter (like a star) we expect to find a spherical symmetrically spacetime of the form

$$\mathrm{d}s^2 = -\mathrm{e}^{2\Phi(t,r)}\mathrm{d}t^2 + \mathrm{e}^{2\Pi(t,r)}\mathrm{d}r^2 + r^2\left(\mathrm{d}\theta^2 + \sin^2\theta\,\mathrm{d}\phi^2\right) \tag{1.1.1}$$

where Φ and Π are functions of t and r only so that the line element remains spherically symmetric. As for possible cross terms $\mathrm{d}r\mathrm{d}t$, they vanish under an appropriate coordinate transformation[1]. In order to get a solution to Einstein equations in vacuum our metric must satisfy

$$R_{\mu\nu} = 0 \tag{1.1.2}$$

[1] See Misner *et al.* (2017), page 594.

considering a zero cosmological constant. The tr component of equation (1.1.2) gives $R_{tr} = 2\Pi_{,t}/r = 0$, which implies that $\Pi(t,r) = \Pi(r)$. The remaining components of equation (1.1.2)

$$\begin{cases} R_{tt} = \frac{\mathrm{e}^{2\Phi-2\Pi}\left[(2-r\Pi')\Phi'+r\Phi'^2+r\Phi''\right]}{r} \\ R_{rr} = \frac{\Pi'(r\Phi'+2)-r\left(\Phi'^2+\Phi''\right)}{r} \\ R_{\theta\theta} = \mathrm{e}^{-2\Pi(r)}\left(-r\Phi'+r\Pi'+\mathrm{e}^{2\Pi(r)}-1\right) \\ R_{\phi\phi} = \sin^2\theta\, R_{\theta\theta} \end{cases}$$

where $' \equiv \partial_r$. To solve the Einstein equations $R_{\mu\nu} = 0$, we could differentiate the $R_{\theta\theta} = 0$ component with respect to t. Then $-r\partial_t\Phi' = 0$ and $\partial_t\partial_r\Phi = 0$ which can only be true generally if

$$\Phi = f(t) + g(r). \tag{1.1.3}$$

Our line element becomes

$$\mathrm{d}s^2 = -\mathrm{e}^{2f(t)+2g(r)}\mathrm{d}t^2 + \mathrm{e}^{2\Pi(r)}\mathrm{d}r^2 + r^2\left(\mathrm{d}\theta^2 + \sin^2\theta\,\mathrm{d}\phi^2\right). \tag{1.1.4}$$

In order to remove the time dependence of g_{tt} we make the following coordinate transformation $t' = \int \mathrm{e}^{f(t)}\mathrm{d}t$ and we get

$$\mathrm{d}s^2 = -\mathrm{e}^{2g(r)}\mathrm{d}t^2 + \mathrm{e}^{2\Pi(r)}\mathrm{d}r^2 + r^2\left(\mathrm{d}\theta^2 + \sin^2\theta\,\mathrm{d}\phi^2\right)$$

where we dropped the prime. Applying Einstein equations again we get

$$\begin{cases} R_{tt} = \frac{\mathrm{e}^{2g(r)-2\Pi(r)}}{r}\left(rg''(r) + g'(r)\left(2 - r\Pi'(r)\right) + rg'^2(r)\right) = 0 \\ R_{rr} = g''(r) - g'(r)\Pi'(r) - g'^2(r) + \frac{2\Pi'(r)}{r} = 0 \\ R_{\theta\theta} = \mathrm{e}^{-2\Pi(r)}\left(rg'(r) + r\Pi'(r) + \mathrm{e}^{2\Pi(r)} - 1\right) = 0 \\ R_{\phi\phi} = R_{\phi\phi} = \sin^2\theta\, R_{\theta\theta} = 0. \end{cases} \tag{1.1.5}$$

Summing the first two equations we get

$$g(r) = -\Pi(r) + C,$$

where the constant C is determined by applying our boundary conditions. We impose that the metric must be asymptotically flat at infinity so both $g(r)$ and $\Pi(r) \underset{r\to\infty}{\to} 0$, which implies that $C = 0$. Now with the $R_{\theta\theta} = 0$ equation we obtain

$$\partial_r(r\mathrm{e}^{2g(r)}) = -1 \qquad\qquad \Rightarrow \mathrm{e}^{2g(r)} = 1 - \frac{\text{const.}}{r}$$

which results in a line element

$$\mathrm{d}s^2 = -\left(1 - \frac{\text{const.}}{r}\right)\mathrm{d}t^2 + \left(1 - \frac{\text{const.}}{r}\right)^{-1}\mathrm{d}r^2 + r^2(\mathrm{d}\theta^2 + \sin^2\theta\,\mathrm{d}\phi^2).$$

This constant is twice the mass of the central object deforming this spacetime, as one can see by going to the Newtonian limit of the metric. The Schwarzschild solution is given then by

$$\mathrm{d}s^2 = -\left(1 - \frac{2M}{r}\right)\mathrm{d}t^2 + \left(1 - \frac{2M}{r}\right)^{-1}\mathrm{d}r^2 + r^2(\mathrm{d}\theta^2 + \sin^2\theta\,\mathrm{d}\phi^2). \tag{1.1.6}$$

As a secondary result of this derivation, we have also shown that, by assuming spherical symmetry only, every metric that obeys the vacuum Einstein equations must be the Schwarzschild metric. This is known as the Birkhoff theorem, Birkhoff (1923). In particular it establishes the remarkable conclusion that in vacuum, spherical symmetry implies time independence; that is there can be no spherical pure gravitational dynamics in GR (no spherical gravitational waves).

1.1.1.2 General orbits in Schwarzschild spacetime

Since the Schwarzschild solution is both static and spherically symmetric, two of its killing vectors are $\vec{k} = \partial/\partial t$ and $\vec{m} = \partial/\partial\phi$. This means there will be two conserved quantities along geodesics, namely $p_0 \equiv E$, the energy at infinity and $p_\phi = L$, the angular momentum[2] of a particle.

Let us suppose that a particle with mass m and four-momentum $\vec{p}$ is orbiting a Schwarzschild black hole in the equatorial plane[3] (and it remains there during the whole motion since the angular momentum

[2] Both of these identifications come from the fact that in the Newtonian limit, these quantities correspond to the total energy (kinetic and potential) and to the angular momentum. Moreover, the energy at infinity has the additional meaning of being the energy measured by an observer at rest at infinity.

[3] It is irrelevant to the problem because, due to spherical symmetry, we just need to rotate the coordinates to put the motion of the particle lying on a plane.

is conserved) with $\theta = \pi/2$ and $p_\theta = 0$. From the normalization of four-momentum

$$g_{\alpha\beta}p^\alpha p^\beta = g^{\alpha\beta}p_\alpha p_\beta = -m^2 \tag{1.1.7}$$

from which we obtain

$$-\frac{(p_0)^2}{1-2M/r} + \frac{m^2}{1-2M/r}\left(\frac{\mathrm{d}r}{\mathrm{d}\tau}\right)^2 + \frac{L^2}{r^2} = -m^2,$$

where τ is the proper time of the particle. Solving in order to $(\mathrm{d}r/\mathrm{d}\tau)^2$ we end up with

$$\left(\frac{\mathrm{d}r}{\mathrm{d}\tau}\right)^2 = \tilde{E}^2 - (1-2M/r)(1+\tilde{L}^2/r^2). \tag{1.1.8}$$

where $\tilde{E} \equiv E/m$ and $\tilde{L} = L/m$. For massless particles we have $\vec{p}\cdot\vec{p} = 0$ so

$$\left(\frac{\mathrm{d}r}{\mathrm{d}\lambda}\right)^2 = E^2 - (1-2M/r)\frac{L^2}{r^2}, \tag{1.1.9}$$

where λ is an affine parameter for massless particles, since we cannot define proper time τ for such particles. We can too define effective potentials for massive and massless particles from equations (1.1.8) and (1.1.9)

$$\tilde{V}_{\text{eff}}^2 = (1-2M/r)(1+\tilde{L}^2/r^2) \tag{1.1.10}$$

$$V_{\text{eff}}^2 = (1-2M/r)\frac{L^2}{r^2}. \tag{1.1.11}$$

Photon sphere For massless particles there are no bound orbits, as one can see in Figure 1.1, except at the maximum of the potential located at $r = 3M$, where a massless particle could have a circular orbit around the black hole. However, the orbits there are unstable since a slight change in the radial coordinate makes the particle go to infinity or into the black hole.

From equation (1.1.9), in order to get circular orbits $\mathrm{d}r/\mathrm{d}\lambda = 0$, we must have the conditions

$$E^2 - (1-2M/r)\frac{L^2}{r^2} = 0 \tag{1.1.12}$$

and

$$\frac{\mathrm{d}V}{\mathrm{d}r} = 0,$$

where the solution for r is the maximum of the potential where $r = 3M$. This is an unstable orbit and any small disturbance will send the particle to $r = 0$ or to $r = \infty$.

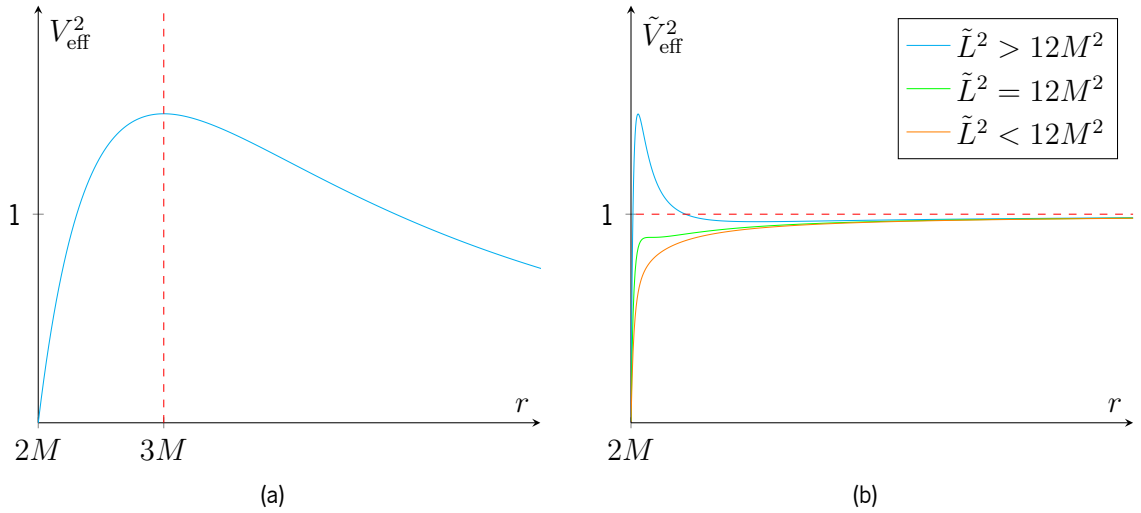

Figure 1.1: Effective potential for massive and massless particles. In order to get a potential well in $\tilde{V}^2_{\text{eff}}$ (Figure 1.1b), $\tilde{L}^2 > 12M^2$.

1.1.1.3 Singularities and event horizon

At first sight it appears that there are two issues with the Schwarzschild solution. At $r = 2M$ and $r = 0$ the metric element becomes infinite. However, only the singularity at $r = 0$ is a true singularity. The singularity at $r = 2M$ is only a coordinate singularity, removable by a suitable change of coordinates.

At the surface $r = 2M$ the components g_{tt} and g_{rr} of the metric go to zero and infinity respectively. But let's change coordinates to ingoing Eddington-Finkelstein coordinates, where

$$v = t + r + 2M \ln |r/2M - 1|. \tag{1.1.13}$$

Then the line element written in these coordinates is

$$\mathrm{d}s^2 = -\left(1 - \frac{2M}{r}\right) \mathrm{d}v^2 + 2\mathrm{d}v\mathrm{d}r + r^2(\mathrm{d}\theta^2 + \sin^2\theta\, \mathrm{d}\phi^2). \tag{1.1.14}$$

At $r = 2M$ only $g_{vv} = 0$ and the determinant of the metric is $g \neq 0$. Therefore metric is perfectly defined at this surface.

Other tests could have been used to show that we are dealing with a coordinate problem here. For example, an infalling particle takes infinite coordinate time t in order to cross $r = 2M$, yet it takes finite

proper time to reach and cross that surface. This shows that there is no problem with the geometry, but with coordinate time itself. This gives rise to the well known situation where an observer at infinity can never see something falling at the black hole in finite time (since his proper time is the coordinate time at infinity). One can also check the square of the Riemann tensor (Kretschmann scalar)

$$R^{\alpha\beta\mu\nu}R_{\alpha\beta\mu\nu} = 48M^2/r^6 \tag{1.1.15}$$

which is finite at $r = 2M$. These tests can be seen in standard General Relativity textbooks like Schutz (2009) or Misner *et al.* (2017).

The boundary $r = 2M$ is called the event horizon. Inside the event horizon, equation (1.1.6) tells us that the t and r coordinate reverse roles, meaning that now the basis vectors $\vec{e}_t = \partial/\partial t$ and $\vec{e}_r = \partial/\partial r$ become spacelike and timelike, respectively. This means that our new time is given by coordinate r. If an astronaut falls inside the event horizon it becomes impossible for the astronaut to go back, since the particle can only travel in timelike paths (time always moves forwards and now that translates to a decrease of the r coordinate) meaning that the astronaut will reach $r = 0$ in a finite time. Even on a non-geodesic trajectory, like a spaceship using its thrusters, any massive body must travel on a timelike path. The instant a particle crosses $r = 2M$, it will, no matter what, reach $r = 0$ in finite proper time which can be computed using the equations of motion for the Schwarzschild geometry obtained above (assuming a radial trajectory).

However at $r = 0$ we are faced with a true spacetime singularity. The square of Riemann blows up showing there is a curvature singularity at the center of the black hole.

1.1.2 The Kerr black hole

1.1.2.1 Kerr metric

Unlike the Schwarzschild solution, the Kerr metric describes a rotating stationary black hole. The problem of finding the metric of a rotating black hole is very complicated and such solution was only found in the 1960s (compare to the Schwarzschild solution which was obtained one month after Einstein published

the theory of General Relativity). Since the derivation of this result is very long, we shall just quote the line element which is

$$\mathrm{d}s^2 = -\frac{\Delta}{\rho^2}(\mathrm{d}t - a\sin^2\theta)^2 + \frac{\rho^2}{\Delta}\mathrm{d}r^2 + \frac{\sin^2\theta}{\rho^2}\left[a\mathrm{d}t - (r^2+a^2)\mathrm{d}\phi\right]^2 \tag{1.1.16}$$

where $\Delta \equiv r^2 - 2Mr + a^2$, $\rho^2 \equiv r^2 + a^2\cos^2\theta$, M is the mass of the black hole, J its angular momentum and $a \equiv J/M$, the angular momentum per unit mass, assuming the black hole rotates in the ϕ direction. It is easy to see that it reduces to the Schwarzschild solution when $M \to 0$, showing that Schwarzschild is nothing else than a particular case of the Kerr geometry. Although the metric is no longer static nor spherically symmetric, $\vec{k} = \partial/\partial t$ and $\vec{m} = \partial/\partial\phi$ are still Killing vectors of this geometry, therefore conserved quantities like the energy or angular momentum of a particle are still conserved here.

1.1.2.2 Dragging of inertial frames and ergoregion

The existence of a cross term $\mathrm{d}t\mathrm{d}\phi$ in the line element gives rise to an interesting property: even particles with zero angular momentum rotate in the direction of rotation of the black hole itself. Defining angular velocity measured by an observer at infinity as

$$\Omega \equiv \frac{\mathrm{d}\phi}{\mathrm{d}t} = \frac{p^\phi}{p^t}$$

it is easy to obtain, for a particle with $p_\phi = 0$, that its angular velocity will be

$$\Omega = \frac{g^{\phi\phi}p_\phi + g^{\phi t}p_t}{g^{tt}p_t + g^{t\phi}p_\phi} = \frac{g^{\phi t}}{g^{tt}} \neq 0. \tag{1.1.17}$$

But even observers that try to remain static ($\Omega = 0$) might not be able to do it even if they fire their thrusters to keep them in place. From the line element, considering $\mathrm{d}\theta = \mathrm{d}r = 0$, we see that

$$\mathrm{d}s^2 = g_{tt}\mathrm{d}t^2 + 2g_{t\phi}\mathrm{d}\phi\mathrm{d}t + g_{\phi\phi}\mathrm{d}\phi^2 < 0$$

dividing by $\mathrm{d}t^2$

$$\Rightarrow g_{tt} + 2g_{t\phi}\Omega + g_{\phi\phi}\Omega^2 < 0,$$

we find that

$$\Omega_{\min} < \Omega < \Omega_{\max} \tag{1.1.18}$$

where

$$\Omega_{min} = -\frac{g_{t\phi}}{g_{\phi\phi}} + \sqrt{\frac{(g_{t\phi})^2}{(g_{\phi\phi})^2} - \frac{g_{tt}}{g_{\phi\phi}}}$$

and

$$\Omega_{max} = -\frac{g_{t\phi}}{g_{\phi\phi}} - \sqrt{\frac{(g_{t\phi})^2}{(g_{\phi\phi})^2} - \frac{g_{tt}}{g_{\phi\phi}}}.$$

This means that there's a lower and an upper limit on the angular velocity. However, when $g_{tt} = 0$ (the line element remains finite here) $\Omega_{\min} = 0$ which happens when

$$r_0 = M + \sqrt{M^2 - a^2 \cos^2\theta}. \tag{1.1.19}$$

On and below this surface $\Omega_{\min} \geq 0$ and all particles (even light traveling on the opposite direction of rotation of the black hole) are forced to rotate in the direction of the rotation of the black hole. This region is called the ergoregion and allows for interesting phenomena like the Penrose process (Penrose (1969)) or super-radiance as we shall see later on.

1.1.2.3 Event horizon

The horizons appear when $g_{rr} = \infty$, at surfaces of radius

$$r_\pm = M \pm \sqrt{M^2 - a^2} \tag{1.1.20}$$

where we call r_+ the outer horizon and r_- the inner horizon. Only the outer horizon is the true event horizon, from which no particle can come out from after crossing it.

The event horizon coincides with the ergoregion at the poles ($\theta = 0, \pi$) where it is tangent to it. The minimum and maximum angular velocity become equal, meaning that there can never be stationary observers at the horizon.

This imposes certain restrictions for the mass and angular momentum of the black hole. Astrophysical black holes must have $M^2 > a^2$ or $M^2 = a^2$ at the very least (although very unlikely). Black holes

satisfying the latter are known as the *extreme* Kerr black holes. If $M^2 < a^2$, there will be no horizons and the black hole will be in fact a *naked singularity*, uncovered by an horizon, meaning that the singularity can be seen by observers at infinity. It is believed that gravitational collapse can not give existence to such objects. Such conjecture is known as the Cosmic Censorship Hypothesis and was formulated by Penrose (1969).

1.1.2.4 Singularity

In order to find the curvature singularity of the Kerr metric we can use the squared Riemann scalar. It is given by

$$R_{\alpha\beta\mu\nu}R^{\alpha\beta\mu\nu} = \frac{48M^2\left(r^2 - a^2\cos^2\theta\right)\left(\rho^4 - 16a^2r^2\cos^2\theta\right)}{\rho^{12}} \tag{1.1.21}$$

therefore the singular "point" is given by $\rho^2 = r^2 + a^2\cos^2\theta = 0$. The condition is only satisfied if $r = 0,\ \theta = \pi/2$, but the resulting singularity is not a point in space. In Kerr-Schild coordinates[4] (the equivalent Cartesian coordinates for this metric) we have $x^2 + y^2 = (r^2 + a^2)\sin^2\theta$ and $z = r\cos\theta$ and therefore $r = 0$ is in fact a ring singularity in the equatorial plane defined by

$$x^2 + y^2 = a^2. \tag{1.1.22}$$

1.2 Ultralight bosons around black holes

Many theories in particle physics postulate the existence of ultralight bosons, scalar or vector, with masses between $10^{-33}$and $10^{-8}\,\mathrm{eV}$: from the QCD axion, dark photons (another vector field like the photon), string theory axions[5], cold dark matter hypothesis, to hypothesis where the photon has a non-zero mass[6]. The existence of these particles could be deduced by their gravitational wave signatures, when they are around black holes.

[4]The Kerr spacetime metric in Kerr-Schild coordinates is given by $g_{\mu\nu} = \eta_{\mu\nu} + f k_\mu k_\nu$ where $f = 2Mr^3/\left(r^4 + a^2z^2\right)$, $(k_0, k_x, k_y, k_z) = \left(1, \frac{rx+ay}{r^2+a^2}, \frac{ry-ax}{r^2+a^2}, \frac{z}{r}\right)$ and r is a function of the coordinates defined implicitly by $\frac{x^2+y^2}{r^2+a^2} + \frac{z^2}{r^2} = 1$, which reduces to the usual $r = \sqrt{x^2+y^2+z^2}$ when $a \to 0$.

[5]See Arvanitaki *et al.* (2010)

[6]See Zyla *et al.* (2020) for estimated upper bounds on the mass of the photon.

Scalar particles, as it is well known, are described by the Klein-Gordon equation, which is separable in the Kerr background. We begin our study by scalar fields since they are much simpler to work with than vector (Proca) and tensor (gravitational) particles. Scalar massless fields can be used as a toy model in order to understand how to obtain the frequencies of oscillation and decay rates of these fields around black holes, which will be qualitatively similar to the other perturbations types, namely gravitational perturbations.

If we consider massive fields, we get an analogue of the bound states of the electron in an hydrogen atom, but in our case, the energy of the field will decay in time due to the presence of an event horizon. The main importance of astrophysical massive bosonic fields is, however, that these fields around rotating black holes, under the condition $\omega < m\Omega_H$, where m is the azimuthal angular momentum quantum number, can grow exponentially. After a certain period of time they are large enough to back-react on the black hole geometry, slowing its rotation and emitting gravitational waves in the process, which in principle can be detected on the Earth. The detection of such waves could signal the existence of an ultralight particle in nature.

1.3 Gravitational waves

General Relativity predicts the existence of gravitational waves, that is, perturbations that propagate in space and time at the speed of light which can be felt by changes in the curvature of spacetime. These waves are generated when there is a change in the curvature of spacetime, just like electrodynamics where an accelerated charge emits electromagnetic radiation. They can be generated by binaries of stars, planets orbiting stars, the merger of black holes and the non-spherical collapse of stars.

A major difficulty in detecting gravitational waves is that their amplitude is very weak leading to very small stretching of spacetime. However, the new generation of detectors (e.g. LIGO and VIRGO) in the 21st century is able to detect waves emitted by highly energetic events in the universe, such as the collision of two neutron stars or black holes. In 2015 the LIGO collaboration, Abbott *et al.* (2016), announced that they had detected the waves from the merger of two black holes, confirming, at last, a well known prediction

of General Relativity. Many more signals have been detected so far. This has caused an increase in the gravitational wave research since now we can compare the obtained signals with the predictions of General Relativity and other theories, as well as the physics of black holes and other astrophysical phenomena. This is possible because gravitational waves travel almost undisturbed by matter, unlike electromagnetic radiation which is easily absorbed by matter.

One of our objectives is to understand how to obtain the frequencies of such gravitational waves for Schwarzschild and Kerr black holes and compare them to the signals of waves that have been detected.

1.3.1 Existence of gravitational waves in Minkowski spacetime

We can write small perturbations in Minkowski spacetime as

$$g_{\mu\nu} = \eta_{\mu\nu} + h_{\mu\nu}, \tag{1.3.1}$$

where, $\eta_{\mu\nu}$ is the Minkowski metric and $|h_{\mu\nu}| \ll 1$[7]. Under a Lorentz transformation we get

$$\begin{aligned} g_{\alpha'\beta'} &= \Lambda^{\mu}{}_{\alpha'}\eta_{\mu\nu}\Lambda^{\nu}{}_{\beta'} + \Lambda^{\mu}{}_{\alpha'}h_{\mu\nu}\Lambda^{\nu}{}_{\beta'} \\ &= \eta_{\alpha'\beta'} + h_{\alpha'\beta'}, \end{aligned}$$

where $h_{\alpha'\beta'} \equiv \Lambda^{\mu}{}_{\alpha'}h_{\mu\nu}\Lambda^{\nu}{}_{\beta'}$. In a certain way a weak gravitational field behaves as a Lorentzian tensor, since $h_{\mu\nu}$ transforms as a tensor considering only Lorentz transformations.

We can now define gauge transformations just like in electromagnetism. A gauge transformation of the potential in classical electromagnetism, $\boldsymbol{A} \to \boldsymbol{A}' = \boldsymbol{A} + \nabla\chi(t, \boldsymbol{r})$ and $\phi \to \phi' = \phi - \partial_t\chi(t, \boldsymbol{r})$, has no influence on the electric and magnetic fields $\boldsymbol{E} = -\nabla\phi - \frac{\partial \boldsymbol{A}}{\partial t}$, $\boldsymbol{B} = \nabla \times \boldsymbol{A}$ respectively, which are the fields with physical significance. We can then make analogous transformations in the weak field theory of gravitation, as long as we require that the physical field that we can measure, the Riemann tensor remains unchanged. We begin by defining a coordinate transformation like

$$x^{\mu'} = x^{\mu} + \xi^{\mu}(x^{\nu}),\ |\partial_{\rho}\xi^{\mu}| \ll 1. \tag{1.3.2}$$

[7] In fact the perturbation should be written as $\varepsilon h_{\mu\nu}$, since from perturbation theory a perturbation series is given by $g_{\mu\nu} = \eta_{\mu\nu} + \varepsilon h^{(1)}_{\mu\nu} + \varepsilon^2 h^{(2)}_{\mu\nu} + \ldots$ where ε is a very small constant. This automatically makes $|\varepsilon h_{\mu\nu}| \ll 1$ and $|\partial_{\alpha}(\varepsilon h_{\mu\nu})| \ll 1$. But we shall always write $\varepsilon h_{\mu\nu} \equiv h_{\mu\nu}$ because this is the most common notation in most textbooks. As a counterexample, d'Inverno (1992) uses the $\varepsilon h_{\mu\nu}$ notation.

The transformation matrix is $\Lambda^{\alpha}{}_{\mu'} = \delta^{\alpha}{}_{\mu} - \xi^{\alpha}{}_{,\mu}$ so the new transformed metric becomes

$$g_{\mu'\nu'} = \eta_{\mu\nu} + h_{\mu\nu} - \xi_{\mu,\nu} - \xi_{\nu,\mu} + \mathcal{O}\left((\xi^{\alpha}{}_{,\beta})^2\right), \tag{1.3.3}$$

where we use $\eta_{\mu\nu}$ to raise and lower indices. It corresponds to raising indices with the full metric up to first order.

We can now define that under a gauge transformation the perturbation transforms as $h^{\text{new}}_{\mu\nu} \equiv h^{\text{old}}_{\mu\nu} - \xi_{\mu,\nu} - \xi_{\nu,\mu}$ and it is easy to see that the Riemann tensor

$$R_{\alpha\beta\mu\nu} = \frac{1}{2}(h_{\alpha\nu,\beta\mu} + h_{\beta\mu,\alpha\nu} - h_{\alpha\mu,\beta\nu} - h_{\beta\nu,\alpha\mu}) \tag{1.3.4}$$

is completely unaffected by gauge transformations.

Defining the trace reverse of $h_{\mu\nu}$ as

$$\overline{h}^{\mu\nu} \equiv h^{\mu\nu} - \frac{1}{2}(\eta^{\mu\nu}h^{\alpha}{}_{\alpha})$$

the Einstein tensor becomes

$$G_{\alpha\beta} \approx -\frac{1}{2}\left(\overline{h}_{\alpha\beta,\mu}{}^{,\mu} + \eta_{\alpha\beta}\overline{h}_{\mu\nu}{}^{,\mu\nu} - \overline{h}_{\alpha\mu,\beta}{}^{,\mu} - \overline{h}_{\beta\mu,\alpha}{}^{,\mu}\right).$$

We can choose a certain ξ^{α} so that we can make $\overline{h}^{\mu\nu}{}_{,\mu} = 0$ in order to simplify the Einstein tensor ending up with

$$G_{\alpha\beta} = -\frac{1}{2}\Box\overline{h}^{\alpha\beta}.$$

Therefore the linearized Einstein equations are

$$\Box\overline{h}^{\mu\nu} = -16\pi T^{\mu\nu}.$$

In vacuum $\mathbf{T} = 0$, so we end up with

$$\Box\overline{h}^{\mu\nu} = \left(-\frac{\partial^2}{\partial t^2} + \nabla^2\right)\overline{h}^{\mu\nu} = 0, \tag{1.3.5}$$

where ∇^2 is the Cartesian Laplacian. Equation (1.3.5) is the well known wave equation, meaning that metric perturbations propagate in space and time like waves at the speed of light. Such waves are the so called gravitational waves.

In principle every spacetime can be perturbed just like the Minkowski metric, although the complexity increases and even in the Schwarzschild case the problem is very complex. We will do it for Schwarzschild spacetime in chapter 3 when studying the gravitational quasi-normal modes for that geometry.

1.4 Perturbations around black holes

1.4.1 Quasi-bound states

An electron around an hydrogen atom must obey the Schrödinger equation

$$\left(-\frac{\hbar^2}{2\mu}\nabla^2 - \frac{e^2}{4\pi\varepsilon_0 r}\right)\psi(r,\theta,\phi) = E\psi(r,\theta,\phi), \tag{1.4.1}$$

where μ is the reduced mass of the electron-proton system, e the elementary electric charge and ε_0 the vacuum dielectric constant. The wave equation of the electron is given by

$$\Psi_n = \mathrm{e}^{-\mathrm{i}Et/\hbar}\psi_n \propto \mathrm{e}^{-\mathrm{i}Et/\hbar - r/na_0} \tag{1.4.2}$$

where a_0 is the Bohr radius. This means, that at infinity the wave function of the electron goes to zero. The electron is then bound to the hydrogen atom. This is due to the boundary conditions, where we make the wave function vanish at the origin and at infinity, which also quantizes the energy levels.

Black holes might be surrounded by massive scalar or vector fields which might too become bound to the black hole, since they both obey a similar Schrodinger type equation. Far away from the black hole their wave function obeys

$$\Phi(x^\mu) \propto \mathrm{e}^{-\mathrm{i}\omega t}\mathrm{e}^{-r\sqrt{\mu^2-\omega^2}},$$

where $\mu^2 > \omega^2$ in order to decay at infinity. This is one of the reasons why there is no bound gravitational perturbations because $\mu = 0$ for gravitons. Furthermore the potential of the black hole for massless particles forbids the existence of bound states.

However, due to the existence of a causal boundary at the event horizon, there cannot be any outgoing waves. This must be taken into account when formulating the boundary conditions to the problem. Similarly to the hydrogen atom problem, the new boundary conditions will quantize the frequencies (energy) of

the field, but instead of a purely real energy value we get a complex value. That will make our field decay (or grow) in time. Then such bound states are not stationary and are called quasi-bound states due to the shared similarities with bound states in a potential.

1.4.2 Quasi-normal modes

A string on a guitar, when perturbed, will vibrate in discrete modes with a distinct frequency. Since a string must obey the wave equation

$$\frac{1}{v^2}\frac{\partial^2 y(t,x)}{\partial t^2} = \frac{\partial^2 y(t,x)}{\partial x^2} \tag{1.4.3}$$

with solution

$$y(t,x) \propto \cos(\omega t - \omega v x), \tag{1.4.4}$$

the boundary conditions $y(t,0) = y(t,L) = 0$, where L is the length of the string, imply that the frequency spectrum is discrete $\omega_n = \frac{\pi n}{L} v$.

In black holes we can perturb surrounding scalar or vector fields and even the geometry of the black hole itself. In order to get normal modes the field at infinity should obey

$$\Phi(x^\mu) \propto \mathrm{e}^{-\mathrm{i}\omega t}\mathrm{e}^{\mathrm{i}r\sqrt{\omega^2-\mu^2}},$$

where $\mu^2 < \omega^2$. Here we can have gravitational quasi-normal modes since the energy of a perturbation is always greater than the mass of the graviton, which is zero.

Imposing the appropriate boundary condition at the horizon and imposing a wave-like behavior at infinity, the frequency of the perturbation is again quantized, but it will be complex due to the boundary at the event horizon. That will make the field's waves decay in time and this is why they are called quasi-normal modes[8], since the system is dissipative.

[8] In a way, a vibrating string has in fact quasi-normal modes, since in a non-ideal situation the string loses energy to the surrounding environment.

1.4.3 The infinite continued fraction method for quasi-bound(normal) frequencies

The differential equations that give rise to quasi-bound(normal) modes in black hole geometry cannot be solved analytically with the help of elementary functions. Over the years several methods to solve the differential equations have been developed, ranging from analytical approximations to numerical solving of the equations. One of the most well known methods is the infinite continued fraction method, proposed by Leaver (1985). It consists in solving the time-independent differential equation of the system by proposing an ansatz of the solution of the form

$$R(r) = f(r) \sum_{n=0}^{\infty} g^n(r) a_n,$$

where the function must obey the specified boundary conditions. Replacement of the solution ansatz in the differential equation results in a three term recursion

$$\alpha_n a_{n+1} + \beta_n a_n + \gamma_n a_{n-1} = 0$$

which can be re-expressed as an infinite continued fraction

$$F(M\omega) \equiv \frac{\beta_0}{\alpha_0} - \cfrac{\gamma_1}{\beta_1 - \cfrac{\alpha_1\gamma_2}{\beta_2 - \cfrac{\alpha_2\gamma_3}{\beta_3 - \ddots}}} = 0.$$

It can be solved for ω using standard numerical root finding methods, avoiding completely numerical integration. It's a very accurate method even for higher order overtones, since it agrees with other methods in all domains of validity. It becomes unstable for frequencies with large imaginary parts, but that problem can be solved by modifying the method, as done by Nollert (1993). It can be applied to both Schwarzschild and Kerr black holes, as well as their charged counterparts, whether for quasi-bound or quasi-normal modes. This is the method we will use in this thesis to obtain our values for the quasi-bound(normal) frequencies.

Compared to methods which integrate directly the differential equation, it is more accurate since it only depends on solving an algebraic equation, as opposed to solving a differential equation. Others methods, like WKB approximation or the method of matched asymptotic expansions, have the advantage to obtain analytical approximations to the values of the frequencies, although only in a certain range of validity. Although the infinite continued fraction method is more accurate, we can't obtain an explicit expression for ω, whose value must be obtained numerically.

An overview of other methods to obtain quasi-normal frequencies can be found in Baumann *et al.* (2019) and Kokkotas and Schmidt (1999).

2 Test Scalar Fields on Schwarzschild Black Holes

2.1 The Klein-Gordon equation in Schwarzschild spacetime

A scalar field is described by the Klein-Gordon equation. By the Einstein Equivalence Principle[1] the laws of physics in local inertial frames must be the same as in Special Relativity. So at a point $\mathcal{P}$ in a local inertial frame the Klein-Gordon equation is given by

$$\partial^\nu \partial_\nu \Phi \overset{*}{=} \mu^2 \Phi, \tag{2.1.1}$$

where Φ is the field's wave function, $\mu \equiv m^2/\hbar^2$ where m is the field's mass (though we shall usually call μ the field's mass for convenience), and $\overset{*}{=}$ means the equality is only valid in a local frame at a point $\mathcal{P}$. Since the Christoffel symbols at $\mathcal{P}$ in a local frame vanish then

$$\Box \Phi \overset{*}{=} \mu^2 \Phi. \tag{2.1.2}$$

This is now a tensor equation (both sides of the equation transform equally under a transformation of basis) so this must be true in every frame and, since our point $\mathcal{P}$ is arbitrary, then at any point in a curved spacetime the Klein-Gordon equation becomes

$$\Box \Phi = \mu^2 \Phi. \tag{2.1.3}$$

[1] See for example Schutz (2009).

where

$$\Box = \frac{1}{\sqrt{-g}} \frac{\partial}{\partial x^\mu} \left(\sqrt{-g} g^{\mu\nu} \frac{\partial}{\partial x^\nu} \right). \tag{2.1.4}$$

The geometry of spacetime for a Schwarzschild black hole is given by the following line element in Schwarzschild coordinates (t, r, θ, ϕ)

$$\mathrm{d}s^2 = -\left(1 - \frac{2M}{r}\right) \mathrm{d}t^2 + \left(1 - \frac{2M}{r}\right)^{-1} \mathrm{d}r^2 + r^2 \left(\mathrm{d}\theta^2 + \sin^2\theta \, \mathrm{d}\phi^2\right). \tag{2.1.5}$$

In Schwarzschild coordinates, the Klein-Gordon equation in Schwarzschild spacetime is given by

$$\left[-\left(1 - \frac{2M}{r}\right)^{-1} \frac{\partial^2}{\partial t^2} + \frac{1}{r^2} \hat{\boldsymbol{L}}^2 + \frac{1}{r^2} \frac{\partial}{\partial r} \left(r^2 \left(1 - \frac{2M}{r}\right) \frac{\partial}{\partial r} \right) \right] \Phi = \mu^2 \Phi, \tag{2.1.6}$$

where

$$\left(\frac{1}{\sin^2\theta} \frac{\partial^2}{\partial \phi^2} + \cot\theta \frac{\partial}{\partial \theta} + \frac{\partial^2}{\partial \theta^2} \right) = \hat{\boldsymbol{L}}^2 \tag{2.1.7}$$

is the square of the angular momentum operator.

The equation is separable in all coordinates as $\psi(r, \theta, \phi) = \eta(t)\rho(r)Y^{\ell,m}(\theta, \phi)$, where $Y^{\ell,m}$ is the standard spherical harmonic, the eigenfunction of $\hat{\boldsymbol{L}}^2$. The complete calculation can be found in appendix A. We will just quote the main results here.

Separation of the time coordinate leads to

$$\eta(t) = A\mathrm{e}^{-\mathrm{i}\omega t} + B\mathrm{e}^{\mathrm{i}\omega t} \tag{2.1.8}$$

where we have chosen the negative exponent solution. As for the angular coordinates we have

$$\hat{\boldsymbol{L}}^2 Y^{\ell,m}(\theta, \phi) = \lambda Y^{\ell,m}(\theta, \phi) \tag{2.1.9}$$

and the eigenvalues are

$$\lambda = -\ell(\ell + 1) \tag{2.1.10}$$

where $\ell = 0, 1, 2 \ldots$ is the quantum number of angular momentum and $m = -\ell, \ldots, \ell$ is the azimuthal angular momentum number. Separating the equation for the radial coordinate and making $R(r) \equiv \rho(r)/r$, results in

$$-\frac{\mathrm{d}^2 R(r)}{\mathrm{d}r^{*2}} + \left(1 - \frac{2M}{r}\right) \left(\frac{\ell(\ell+1)}{r^2} + \frac{2M}{r^3} + \mu^2 \right) R(r) = \omega^2 R(r), \tag{2.1.11}$$

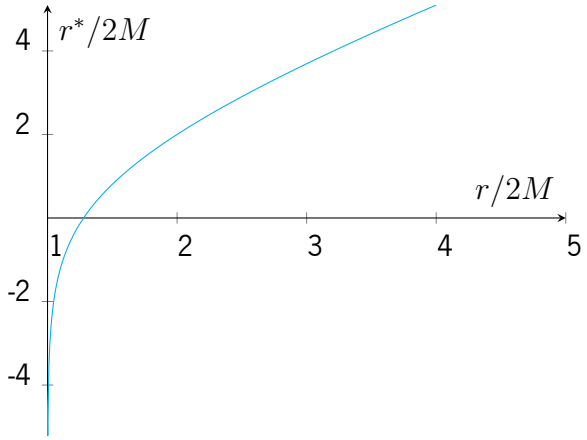

Figure 2.1: Regge-Wheeler coordinate r^* as a function of radial coordinate r.

or making

$$V_{\text{eff}}^2(r) = \left(1 - \frac{2M}{r}\right)\left(\frac{\ell(\ell+1)}{r^2} + \frac{2M}{r^3} + \mu^2\right) \tag{2.1.12}$$

we get

$$-\frac{\mathrm{d}^2R(r)}{\mathrm{d}r^{*2}} + V_{\text{eff}}^2(r)R(r) = \omega^2 R(r), \tag{2.1.13}$$

where and r^* is the Regge-Wheeler coordinate, introduced by Regge and Wheeler (1957). It is defined as

$$\mathrm{d}r^* = \frac{\mathrm{d}r}{\left(1 - \frac{2M}{r}\right)} \tag{2.1.14}$$

or

$$r^* = \int \frac{\mathrm{d}r}{1 - 2M/r} = r + 2M \ln\left|\frac{r}{2M} - 1\right|. \tag{2.1.15}$$

It is plotted against r in figure 2.1.

The effective potential can also be written as a function of r^*

$$V_{\text{eff}}^2(r^*) = \left[1 - \frac{M}{M\mathrm{W}\left(\mathrm{e}^{r^*/2M-1}\right) + M}\right]\left[\mu^2 + \frac{\ell(\ell+1)}{4\left[M\mathrm{W}\left(\mathrm{e}^{r^*/2M-1}\right) + M\right]^2} + \frac{M}{4\left[M\mathrm{W}\left(e^{r^*/2M-1}\right) + M\right]^3}\right] \tag{2.1.16}$$

where $\mathrm{W}(x)$ is the Lambert W function. Plots for the behavior of V_{eff}^2 when increasing the mass and the angular momentum are given by Figures 2.2 and 2.3 respectively. As the mass of the field and the angular

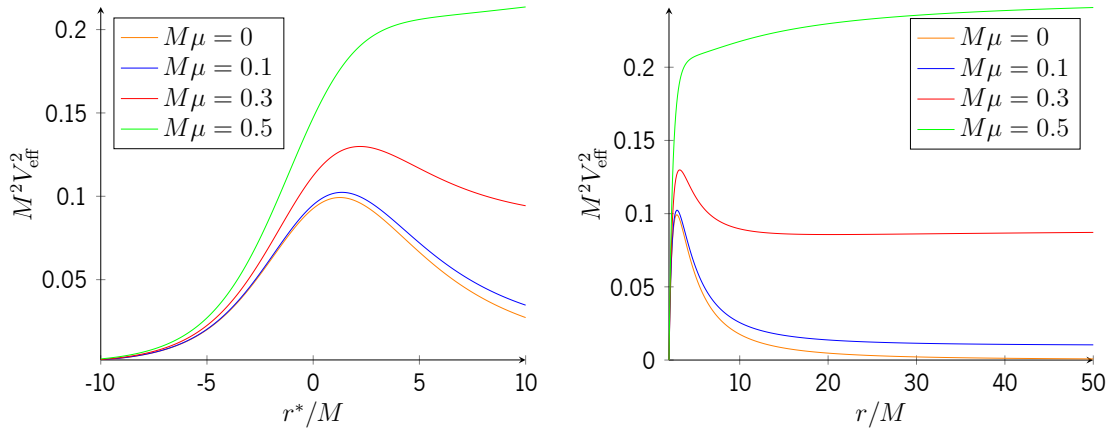

(a) (b)

Figure 2.2: Effective potential $M^2V_{\text{eff}}^2$ for $\ell = 1$ varying the field's mass μ. $M\mu = 0$ has no bound states since there is no potential well.

momentum increases so does the maximum of the potential. At infinity both functions go to the value of μ^2. As $r^* \to -\infty$, that is when $r \to 2M$, the effective potential goes to zero as expected.

For $\ell > 0$, V_{eff}^2 has extrema located at (for $\mu > 0$)

$$r_1 = \frac{1}{12\mu^2 M}\left[-\mathrm{i}2^{2/3}\left(\sqrt{3}-\mathrm{i}\right)\sqrt[3]{2\beta} + \frac{2\mathrm{i}\left(\sqrt{3}+\mathrm{i}\right)\gamma}{\beta^{1/3}} + 4\ell(\ell+1)\right] \tag{2.1.17}$$

$$r_2 = \frac{1}{12\mu^2 M}\left[\mathrm{i}2^{2/3}\left(\sqrt{3}+\mathrm{i}\right)\sqrt[3]{2\beta} - \frac{2\mathrm{i}\left(\sqrt{3}-\mathrm{i}\right)\gamma}{\beta^{1/3}} + 4\ell(\ell+1)\right] \tag{2.1.18}$$

where

$$\begin{aligned}
\alpha = &\Big[324\left(\ell^2+\ell-1\right)\left(\ell^2+\ell+1\right)^2\mu^6M^6 - 3\ell^2(\ell+1)^2 \\
&\left(\ell(\ell+1)(9\ell(\ell+1)+14)+9\right)\mu^4M^4 + 5184\mu^8M^8\Big]^{1/2} \\
\beta = &\ell^3(\ell+1)^3 - \frac{27}{2}\ell(\ell+1)\left(\ell^2+\ell-1\right)\mu^2M^2 + \frac{3}{2}\alpha - 108\mu^4M^4 \\
\gamma = &\ell^2(\ell+1)^2 - 9\left(\ell^2+\ell-1\right)\mu^2M^2.
\end{aligned}$$

In fact the effective potential has three extrema but on is located at a negative value of r, therefore it can be ignored. The necessary condition to have three **real values** for $r_{\max(\min)}$ is found in Barranco *et al.*

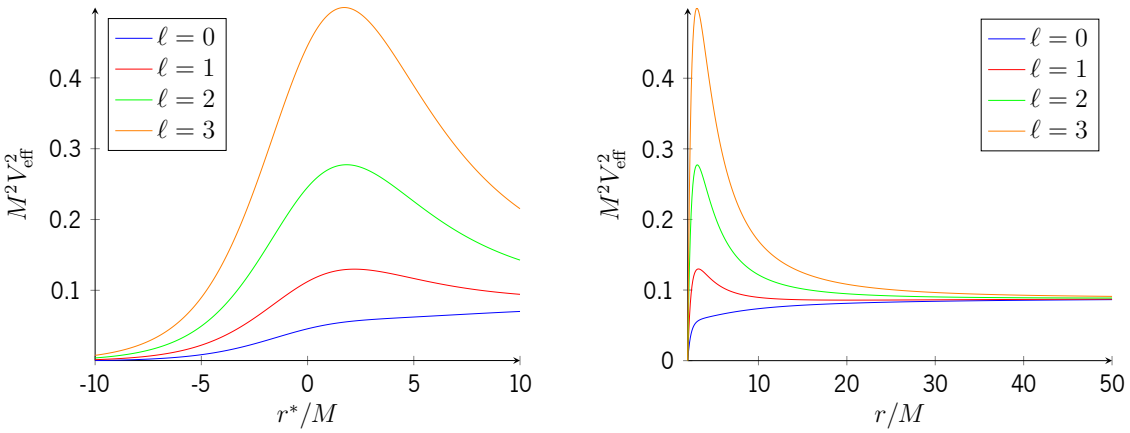

Figure 2.3: Effective potential $M^2V_{\text{eff}}^2$ for $M\mu = 0.3$ varying the field's angular momentum eigenvalue ℓ.

(2011). The mass of the field μ must satisfy the condition

$$M^2\mu^2 < -\frac{1}{32}(\ell^2+\ell-1)(\ell^2+\ell+1)^2 + \frac{1}{288}\sqrt{3(3\ell^4+6\ell^3+5\ell^2+2\ell+3)^3}. \tag{2.1.19}$$

Then for $\ell = 1$ in order to get maxima and minima for V_{eff}^2, $M\mu \lesssim 0.466$ and for $\ell > 1$ the maximum value for $M\mu$ is always larger than 0.466. For $\mu = 0$ we only have one extremum located at

$$r = \frac{3(\ell^2+\ell-1)M + \sqrt{(\ell(\ell+1)(9\ell(\ell+1)+14)+9)M^2}}{2\ell(\ell+1)}. \tag{2.1.20}$$

The condition (2.1.19) also predicts the existence of potential wells where bound states exist. They aren't, however, a necessary condition for the existence of bound states since for $\ell = 0$ or for $\ell = 1, \mu = 0.5$ we have no potential well, but bound states do exist because there is no potential barrier. It is analogous to the $\ell = 0$ Coulomb potential in the Schrödinger equation for the hydrogen atom, which has no classical equivalent.

We can now consider these locations as functions of ℓ and μ. As seen in Figure 2.4 when $\mu = 0$ and ℓ goes to infinite the maximum of the potential will go to $r = 3M$ which is precisely the location of the light ring of the Schwarzschild black hole. Actually even when $\mu \neq 0$ the location of the maximum is still $r = 3M$ when $\ell \to \infty$. This is not surprising since, even for classical particles in the Schwarzschild

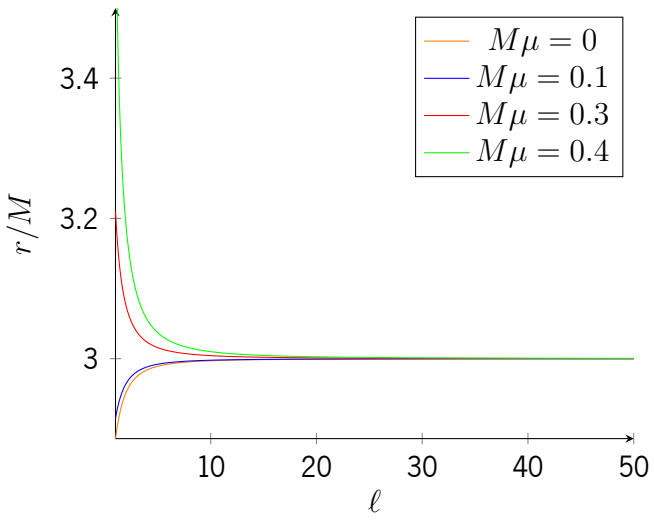

Figure 2.4: Location of the maximum of V^2_{eff} as ℓ and μ increase.

background, they will behave almost as massless particles when their angular momentum goes to infinity, see equation (1.1.10). The difference between the massless and massive case is that, for lower values of ℓ, the maximum of the potential is larger then for the massless case.

2.2 Asymptotic solutions

2.2.1 Near the horizon

Near the horizon of the black hole we have $r \approx 2M$, thus $V^2_{\text{eff}} \simeq 0$ since $\left(1 - \frac{2M}{r}\right) \to 0$ as $r \to 2M$, the Schwarzschild radius. Therefore

$$-\frac{\mathrm{d}^2 R(r)}{\mathrm{d}r^{*2}} \simeq \omega^2 R(r) \tag{2.2.1}$$

and the solution is

$$R(r) = A\mathrm{e}^{\mathrm{i}\omega r^*} + B\mathrm{e}^{-\mathrm{i}\omega r^*}. \tag{2.2.2}$$

The minus solution will be chosen since it corresponds to a wave falling into the black hole. Since there cannot be waves coming from the black hole we must reject the plus solution.

Replacing r^* in equation (2.2.2) by equation (2.1.15) we have

$$R(r) = \exp\left[-\mathrm{i}\omega\left(r + 2M\ln\left|\frac{r}{2M} - 1\right|\right)\right] \simeq (r/2M - 1)^{-\mathrm{i}\omega 2M} \tag{2.2.3}$$

since the logarithmic term dominates as $r \to 2M$.

2.2.2 Far from source

Very far from the black hole $r \to \infty$ and then expanding V_{eff}^2 in r^{-1} around $r^{-1} = 0$ we have to zeroth order

$$V_{\text{eff}}^2\left(r^{-1}\right) = V_{\text{eff}}^2(0) + \frac{\mathrm{d}V_{\text{eff}}^2\left(r^{-1}\right)}{\mathrm{d}r^{-1}} r^{-1} + \cdots \tag{2.2.4}$$

$$\simeq \mu^2 + \mathcal{O}\left(r^{-1}\right) \tag{2.2.5}$$

so equation (2.1.13) becomes

$$\left(-\frac{\mathrm{d}}{\mathrm{d}r^{*2}} + \mu^2\right) R(r) = \omega^2 R(r).$$

Using the chain rule

$$-\left[\frac{\mathrm{d}^2R(r)}{\mathrm{d}r^2}\left(\frac{\mathrm{d}r}{\mathrm{d}r^{*2}}\right)^2 + \frac{\mathrm{d}R(r)}{\mathrm{d}r}\frac{\mathrm{d}^2r}{\mathrm{d}r^{*2}}\right] + \mu^2 R(r) = \omega^2 R(r) \tag{2.2.6}$$

$$-\left[\frac{\mathrm{d}^2R(r)}{\mathrm{d}r^2}\left(1 - \frac{2M}{r}\right)^2 + \frac{\mathrm{d}R(r)}{\mathrm{d}r}\frac{4M}{r^2}\left(1 - \frac{2M}{r}\right)\right] + \mu^2 R(r) = \omega^2 R(r). \tag{2.2.7}$$

When $r \to \infty$ then

$$\frac{\mathrm{d}^2R(r)}{\mathrm{d}r^2} = \left(\mu^2 - \omega^2\right) R(r) \tag{2.2.8}$$

and the solution is

$$R(r) = A\mathrm{e}^{-\sqrt{\mu^2-\omega^2}r} + B\mathrm{e}^{\sqrt{\mu^2-\omega^2}r}. \tag{2.2.9}$$

If we want bound states then $\omega^2 < \mu^2$

$$R(r) = \mathrm{e}^{-r\sqrt{\mu^2-\omega^2}} \tag{2.2.10}$$

where the minus solution was picked since we want a decaying wave function for bound states. In order to get normal modes we require $\omega > \mu$ and that means we want an outgoing wave at infinity so

$$R(r) = \mathrm{e}^{\mathrm{i}r\sqrt{\omega^2-\mu^2}} \tag{2.2.11}$$

which when $\mu = 0$ becomes

$$R(r) = \mathrm{e}^{\mathrm{i}\omega r}. \tag{2.2.12}$$

Now to first order in r^{-1} the effective potential is

$$V_{\text{eff}}^2 = \mu^2 \left(1 - \frac{2M}{r}\right) \tag{2.2.13}$$

so the equation becomes

$$-\frac{\mathrm{d}^2R(r)}{\mathrm{d}r^{*2}} + \mu^2\left(1 - 2M/r\right)R(r) = \omega^2 R(r) \tag{2.2.14}$$

and performing the chain rule we get at first order in r^{-1}

$$-\frac{\mathrm{d}^2R(r)}{\mathrm{d}r^2}\left(1 - 4M/r\right) + \mu^2\left(1 - 2M/r\right)R(r) = \omega^2 R(r). \tag{2.2.15}$$

The solution can be given by

$$A\mathrm{e}^{\sqrt{\mu^2-\omega^2}(4M-r)}U\left(\chi, 0, 2(r-4M)\sqrt{\mu^2-\omega^2}\right) + B\mathrm{e}^{\sqrt{\mu^2-\omega^2}(4M-r)}L_{-\chi}^{-1}\left(2(r-4M)\sqrt{\mu^2-\omega^2}\right) \tag{2.2.16}$$

where $A,\ B$ are constants and $U(\dots,\dots,\dots)$ is the confluent hyper-geometric function, L_b^a is the generalized Laguerre polynomial and $\chi \equiv \frac{M\mu^2-2M\omega^2}{\sqrt{\mu^2-\omega^2}}$. For the bound state condition we choose $B = 0$ since that solution diverges at $r \to \infty$. Then our solution up to first order is given by

$$R(r) \approx r^{-\chi}\mathrm{e}^{-r\sqrt{\mu^2-\omega^2}}. \tag{2.2.17}$$

As for the normal modes we must have $\omega > \mu$. When we choose $\mu = 0$ we have

$$-\frac{\mathrm{d}^2R(r)}{\mathrm{d}r^2}\left(1 - 4M/r\right) = \omega^2 R(r) \tag{2.2.18}$$

and the solution is

$$R(r) \approx r^{2\mathrm{i}M\omega}\mathrm{e}^{\mathrm{i}\omega r}. \tag{2.2.19}$$

2.3 Quasi-bound states

2.3.1 Recursion coefficients

Bound states happen when we require that $\omega < \mu$, meaning the wave function decays at $r \to \infty$. In this section we will show that in the Schwarzschild black hole we will have quasi-bound states (decaying states) because the frequency ω will have an imaginary part responsible for the decay in time since there cannot be any outgoing wave coming from the event horizon. That means that at infinity $R(r) \to r^{-\frac{\mu^2-2\omega^2}{\sqrt{\mu^2-\omega^2}}M} \exp\left(-r\sqrt{\mu^2-\omega^2}\right)$. Now such a solution could be given by a function like

$$R(r) = (r-2M)^{-2M\omega \mathrm{i}}\, r^{2M\omega \mathrm{i}+\chi} \mathrm{e}^{-r\sqrt{\mu^2-\omega^2}} \sum_{n=0}^{\infty} a_n \left(\frac{r-2M}{r}\right)^n \tag{2.3.1}$$

where $\chi = -\frac{\mu^2-2\omega^2}{\sqrt{\mu^2-\omega^2}}M$ (see Leaver (1985) where a similar ansatz is proposed for the quasi-normal modes situation), which at infinity satisfies our requirements for the quasi-bound states. The radial equation (2.1.13) expressed in the r coordinate is

$$-\frac{\mathrm{d}^2R(r)}{\mathrm{d}r^2}\left(1-\frac{2M}{r}\right)^2 - \left(1-\frac{2M}{r}\right)\frac{\mathrm{d}R(r)}{\mathrm{d}r}\frac{2M}{r^2} + \left(1-\frac{2M}{r}\right)\left(\frac{\ell(\ell+1)}{r^2}+\frac{2M}{r^3}+\mu^2\right)R(r) = \omega^2 R(r). \tag{2.3.2}$$

Replacing $R(r)$ by our ansatz in the previous equation gives rise to the following conditions (see section §B.1)

$$\alpha_0 a_1 + \beta_0 a_0 = 0 \tag{2.3.3}$$

$$\alpha_n a_{n+1} + \beta_n a_n + \gamma_n a_{n-1} = 0,\ n > 0 \tag{2.3.4}$$

where $\alpha_n, \beta_n, \gamma_n$ are given by

$$\begin{cases} \alpha_n = (n+1)\left(\mu^2-\omega^2\right)^{3/2}(n-4\mathrm{i}M\omega+1) \\ \beta_n = -\left(\ell^2+\ell+2n(n+1)+1\right)\left(\mu^2-\omega^2\right)^{3/2} + 4M^2\left(\mu^2-\omega^2\right)\left[4\omega^2\left(\sqrt{\mu^2-\omega^2}-\mathrm{i}\omega\right)+\right. \\ \qquad \left.-\mu^2\left(\sqrt{\mu^2-\omega^2}-3\mathrm{i}\omega\right)\right] - M(2n+1)\left(\mu^2-\omega^2\right)\left(-4\mathrm{i}\omega\sqrt{\mu^2-\omega^2}+3\mu^2-4\omega^2\right) \\ \gamma_n = M^2\left[\mu^4\left(\sqrt{\mu^2-\omega^2}-4\mathrm{i}\omega\right)+4\mu^2\omega^2\left(-2\sqrt{\mu^2-\omega^2}+3\mathrm{i}\omega\right)+8\omega^4\left(\sqrt{\mu^2-\omega^2}-\mathrm{i}\omega\right)\right] \\ \qquad +2Mn\left(\mu^2-\omega^2\right)\left(-2\mathrm{i}\omega\sqrt{\mu^2-\omega^2}+\mu^2-2\omega^2\right)+n^2\left(\mu^2-\omega^2\right)^{3/2}. \end{cases} \tag{2.3.5}$$

2.3.2 Quasi-bound frequencies

From equation (B.1.6) we have

$$\frac{\beta_0}{\alpha_0} = -\frac{a_1}{a_0} \tag{2.3.6}$$

and from equation (B.1.8)

$$a_0 = -\frac{\beta_1 a_1 + \alpha_1 a_2}{\gamma_1}$$

meaning that

$$\begin{aligned} \frac{\beta_0}{\alpha_0} &= \frac{a_1\gamma_1}{\beta_1 a_1 + \alpha_1 a_2} \\ &= \cfrac{\gamma_1}{\beta_1 + \alpha_1 \cfrac{a_2}{a_1}}. \end{aligned}$$

If we keep doing the analogous calculation for all the a_n *ad infinitum* we get an infinite continuous fraction

$$\frac{\beta_0}{\alpha_0} = \cfrac{\gamma_1}{\beta_1 - \cfrac{\alpha_1\gamma_2}{\beta_2 - \cfrac{\alpha_2\gamma_3}{\beta_3 - \ddots}}} \tag{2.3.7}$$

and to get the frequencies we just need to solve numerically the following equation

$$F(M\omega) \equiv \frac{\beta_0}{\alpha_0} - \cfrac{\gamma_1}{\beta_1 - \cfrac{\alpha_1\gamma_2}{\beta_2 - \cfrac{\alpha_2\gamma_3}{\beta_3 - \ddots}}} = 0. \tag{2.3.8}$$

It can be divided into two equations, one for the real part and another for the imaginary part

$$\Re\left[F(M\omega)\right] = 0; \;\; \Im\left[F(M\omega)\right] = 0. \tag{2.3.9}$$

Each function describes a surface on the complex plane $M\omega = M\omega_R + \mathrm{i}M\omega_I$, where ω_R and ω_I are the real and imaginary part of the frequency ω respectively. Setting the above equations to zero this is equivalent to two level curves. The intersections of the curve give the frequencies for which equations (2.3.9) are both satisfied.

The infinite fraction equation (2.3.8) was calculated up to 200 terms and the fundamental frequencies (the eigenvalues of the functions with no nodes) of the quasi-bound states are in Table 2.1. A plot for $M\mu = 0.3$ and $\ell = 1$ can be seen in Figure 2.5. It can be seen that the real part of the frequency increases with $M\mu$, while the imaginary part becomes more negative. Also there is a slight increase in the real part of the frequency with the angular momentum ℓ while the imaginary part approaches zero.

In Table 2.2 we can see that only for small values of $M\mu$ we see an appreciable change in the imaginary part of ω whereas for higher $M\mu$ the imaginary part practically doesn't change with the number of iterations, meaning that a higher level of precision is only required for smaller values of $M\mu$. As for the real part, it is very stable against the number of iterations, and up to 5 decimal places no difference can be found. We will keep using 200 iterations since it seems the perfect balance between accuracy and computation time, which is very important when one calculates the frequencies for a large number of ℓ.

Looking at equation (2.1.6) we can see that μ^{-1} is the Compton wavelength[2] of the field, so $M\mu$ is just the ratio between the black hole's radius[3] and the field's Compton wavelength. We expect these field

[2]The (reduced) Compton wavelength is given by $\mu^{-1} = \lambda_C = \hbar/m$.
[3]Ignoring a factor 2 since the Schwarzschild radius is $r_S = 2M$.

$M\mu$	$\ell = 0$		$\ell = 1$		$\ell = 2$		$\ell = 3$	
	$M\omega_R$	$-M\omega_I$	$M\omega_R$	$-M\omega_I$	$M\omega_R$	$-M\omega_I$	$M\omega_R$	$-M\omega_I$
0.1	0.09945	$1.5341 \cdot 10^{-05}$	0.09987	$1.3405 \cdot 10^{-11}$	0.09994	$5.7004 \cdot 10^{-15}$	0.09994	$-6.3693 \cdot 10^{-16}$
0.2	0.19508	$1.4872 \cdot 10^{-03}$	0.19895	$4.0604 \cdot 10^{-08}$	0.19955	$3.4580 \cdot 10^{-14}$	0.19955	$-5.8443 \cdot 10^{-17}$
0.3	0.28691	$9.6081 \cdot 10^{-03}$	0.29619	$9.4557 \cdot 10^{-06}$	0.29844	$4.9025 \cdot 10^{-11}$	0.29844	$5.1314 \cdot 10^{-15}$
0.4	0.37891	$2.5247 \cdot 10^{-02}$	0.38956	$5.6274 \cdot 10^{-04}$	0.39619	$1.1704 \cdot 10^{-08}$	0.39619	$3.1021 \cdot 10^{-14}$
0.5	0.47272	$4.6989 \cdot 10^{-02}$	0.47759	$5.5442 \cdot 10^{-03}$	0.49220	$1.2271 \cdot 10^{-06}$	0.49220	$1.2446 \cdot 10^{-11}$
0.6	0.56883	$7.3708 \cdot 10^{-02}$	0.56381	$1.7704 \cdot 10^{-02}$	0.58542	$6.9974 \cdot 10^{-05}$	0.58542	$1.5500 \cdot 10^{-09}$
0.7	0.66735	$1.0463 \cdot 10^{-01}$	0.65075	$3.6065 \cdot 10^{-02}$	0.67386	$1.4988 \cdot 10^{-03}$	0.67386	$1.1900 \cdot 10^{-07}$
0.8	0.13920	$1.3920 \cdot 10^{-01}$	0.73930	$5.9472 \cdot 10^{-02}$	0.75789	$8.1511 \cdot 10^{-03}$	0.75789	$6.1870 \cdot 10^{-06}$

Table 2.1: Quasi-bound fundamental frequencies (200 iterations). Red cells indicate a wrong value, due to numerical inaccuracies.

$M\mu$	50		100		200		400	
	$M\omega_R$	$-M\omega_I$	$M\omega_R$	$-M\omega_I$	$M\omega_R$	$-M\omega_I$	$M\omega_R$	$-M\omega_I$
0.1	0.09987	$1.6392 \cdot 10^{-11}$	0.09987	$1.3603 \cdot 10^{-11}$	0.09987	$1.3405 \cdot 10^{-11}$	0.09987	$1.3396 \cdot 10^{-11}$
0.2	0.19895	$4.0688 \cdot 10^{-08}$	0.19895	$4.0606 \cdot 10^{-08}$	0.19895	$4.0604 \cdot 10^{-08}$	0.19895	$4.0604 \cdot 10^{-08}$
0.3	0.29619	$9.4558 \cdot 10^{-06}$	0.29619	$9.4556 \cdot 10^{-06}$	0.29619	$9.4556 \cdot 10^{-06}$	0.29619	$9.4556 \cdot 10^{-06}$
0.4	0.38956	$5.6274 \cdot 10^{-04}$	0.38956	$5.6274 \cdot 10^{-04}$	0.38956	$5.6274 \cdot 10^{-04}$	0.38956	$5.6274 \cdot 10^{-04}$
0.5	0.47759	$5.5442 \cdot 10^{-03}$	0.47759	$5.5442 \cdot 10^{-03}$	0.47759	$5.5442 \cdot 10^{-03}$	0.47759	$5.5442 \cdot 10^{-03}$
0.6	0.56381	$1.7704 \cdot 10^{-02}$	0.56381	$1.7704 \cdot 10^{-02}$	0.56381	$1.7704 \cdot 10^{-02}$	0.56381	$1.7704 \cdot 10^{-02}$
0.7	0.65075	$3.6065 \cdot 10^{-02}$	0.65075	$3.6065 \cdot 10^{-02}$	0.65075	$3.6065 \cdot 10^{-02}$	0.65075	$3.6065 \cdot 10^{-02}$
0.8	0.73930	$5.9472 \cdot 10^{-02}$	0.73930	$5.9472 \cdot 10^{-02}$	0.73930	$5.9472 \cdot 10^{-02}$	0.73930	$5.9472 \cdot 10^{-02}$

Table 2.2: Frequency values for different iterations of the infinite fraction for $\ell = 1$ with five decimal places.

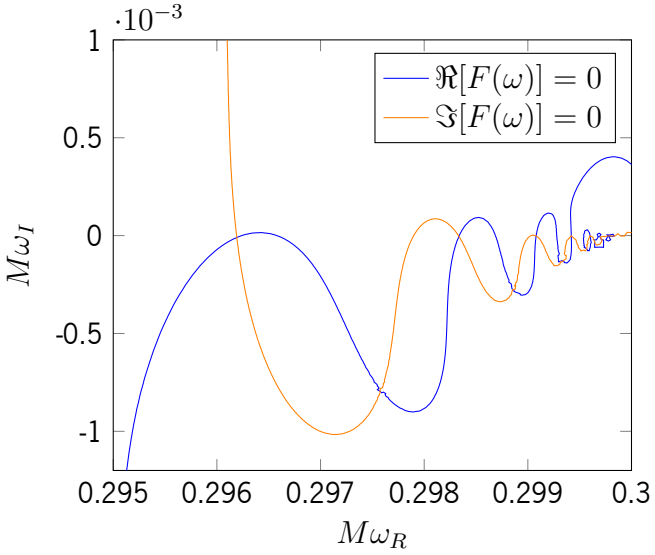

Figure 2.5: Plot of the solutions for equations (2.3.9) for $M\mu = 0.3$ and $\ell = 1$.

masses to be very small with huge wavelengths. For example, when $M\mu \sim 1$, the Compton wavelength of the field is about $1.5\,\mathrm{km}$ for a solar mass black hole and for a supermassive black hole with a mass around 10^8 solar masses the field's wavelength is $1.5\times10^{11}\,\mathrm{m} = 1\,\mathrm{AU}$ with a mass of $1.33\times10^{-10}\,\mathrm{eV}$ and $1.33 \times 10^{-18}\,\mathrm{eV}$ respectively. These masses are extremely small when compared to the masses of known elementary particles ($m_{\mathrm{neutrino}} < 0.120\,\mathrm{eV}$), but they play a major role in rotating black holes.

Since ω is a complex number, looking at equation (2.3.1) we see that the real part will make the field oscillate, while the imaginary part will correspond to the inverse of the lifetime of the particle of the field. Qualitatively, when $M\mu$ increases the real part of ω, which corresponds to the energy[4], must increase so that the field doesn't fall into the black hole since, if μ increases, the Compton wavelength becomes very small, meaning the particle gets "closer" (that is, more localized[5]) to the black hole and therefore the energy must increase (the field must oscillate more) in order to survive. Similarly if it is the mass of

[4]When $r \to \infty$ we get the flat space Klein-Gordon equation where we identify ω as the energy which is a purely real number.

[5]The Compton wavelength is a fundamental limitation on the measurement of a particle's position. According to the uncertainty principle, the uncertainty of the position of a relativistic particle must be $\Delta x \geq \lambda_C$. Then if we have a scalar particle around a black hole, its Compton wavelength shows how localized it is with respect to the black hole or how spread it is from it.

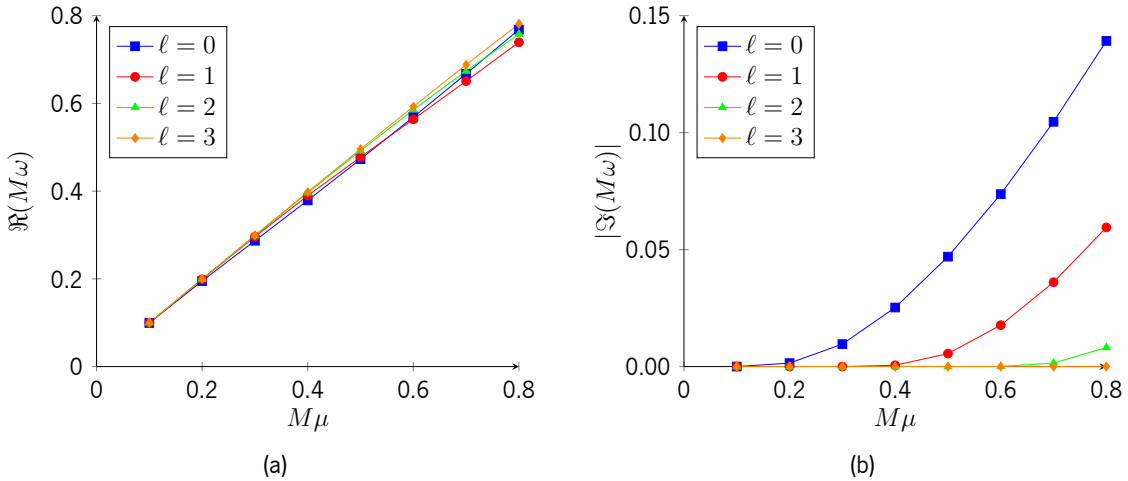

Figure 2.6: Frequency real and imaginary parts versus $M\mu$.

the hole M that increases then the energy increases again so that the particle doesn't fall into the hole. It can also be seen that the energy also increases with the angular momentum number ℓ, which can be explained by the fact that particles with higher angular momentum will have more energy. Lastly the imaginary part increases with $M\mu$, meaning that for small M or large wavelengths μ^{-1} the lifetime of the particle is much greater than for larger $M\mu$, which can be easily explained by the fact the field will barely be affected by small black holes or that fields with very large Compton wavelengths will be barely affected by the black hole, almost as if the particles were very far from it. That means that the lifetime of particles, from equation (2.1.8), far from the black hole (or for smaller black holes) will live much longer than the ones closer to it (or for more massive black holes).

The quasi-bound states of scalar fields around a black hole look similar to the bound states of the hydrogen atom, although there are some differences. Firstly in the hydrogen atom the bound states of the electron are stationary, whereas in our present situation our "bound" states are called quasi-bound since the wave function will decay. This is due to infalling modes into the black hole and that's why we get complex frequency values. Secondly in both problems we have different boundary conditions. In the hydrogen atom we require the wave function to vanish at the center, but in the present situation we have a different boundary condition not at the origin but at the event horizon where we chose infalling solutions

in (2.2.2) because no wave can come from the event horizon. It is because of this that we have states that decay in time instead of true stationary states.

We can check our numerical recursion coefficients values with analytic values calculated from Baumann *et al.* (2019), but this fails for the $\ell = 0$ case. The problem is in the method used to calculate the frequencies which can be seen in detail in Detweiler (1980). It consists in obtaining asymptotic solutions to equation (2.3.2) close to the horizon $r = 2M$ and at infinity $r \to \infty$. It is expected that these solutions overlap in some region and then we could in principle match both functions there. But this method only works when $M\omega, M\mu \ll \ell$, which when $\ell = 0$ it is an impossible condition to fulfill, meaning that we cannot be sure that the analytical results obtained for $\ell = 0$ are reliable. The analytical values in Baumann *et al.* (2019), except for $\ell = 0$, are given by

$$\omega_R \simeq \mu \left(1 - \frac{M^2\mu^2}{2k^2} - \frac{M^4\mu^4}{8k^4} + \frac{f_{k\ell}}{k^3} M^4\mu^4\right) \tag{2.3.10}$$

for the real part, where

$$f_{k\ell} = -\frac{6}{2\ell+1} + \frac{2}{k}$$

and

$$\omega_I = -4\omega\alpha^{4\ell+5} C_{k\ell} g_{\ell\omega} \tag{2.3.11}$$

for the imaginary part where

$$C_{k\ell} = \left(\frac{\ell!}{(2\ell)!(2\ell+1)!}\right)^2 \frac{\left(2^{4\ell+1}(\ell+k)!\right)}{k^{2\ell+4}(-\ell+k-1)!} \tag{2.3.12}$$

and

$$g_{\ell\omega} = \prod_{j=1}^{\ell} \left(j^2 + 16\omega^2\right) \tag{2.3.13}$$

where $k \in \mathbb{N}$. The fundamental mode is given for $k = \ell + 1$, analogous to the hydrogen atom. These expressions are only valid when $M\mu \ll 1$. In order to obtain values for ω_I we can consider that $\omega \approx \omega_R$ since the imaginary part is expected to be very small when compared to the real part. The plot and table showing the relative difference are given in figure 2.7 and in table 2.4.

In Figure 2.7 one can see that the relative differences increase when $M\mu$ which is expected since our analytical expressions are only valid for small values of $M\mu$, and it seems that the relative difference

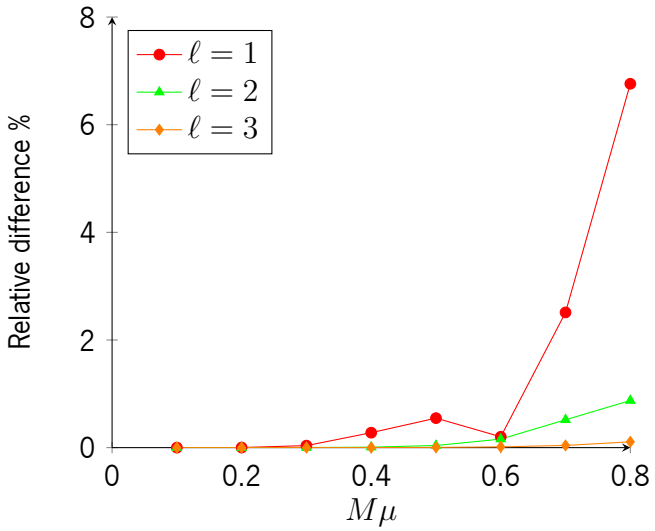

Figure 2.7: Real part relative difference $|[(M\omega_R)_{num} - (M\omega_R)_{analt}]\,/(M\omega_R)_{analt}| \times 100$ between numerical and analytic values Baumann *et al.* (2019).

decreases as ℓ increases. This might be because our analytical approximations must also satisfy the condition $M\mu \ll \ell$ so this might explain why the difference for the $\ell = 1$ situation is very large when compared to the remaining ones.

As for the imaginary part relative differences we see in Table 2.4 disparate values and in no way we can make an analysis like the one we have done for the real part. Since the imaginary part is very small, the numerical round offs can affect the accuracy of our values, therefore it is expected that the relative differences might be very large. Obviously since our values for small $M\mu$ are so small any difference in the order of magnitude will result in very large percentual differences (up to 10 orders of magnitude). For larger values of $M\mu$, although we have a somewhat large relative difference we can see in Table 2.3 that they are around the same order of magnitude (numerical values are sometimes 10 times greater than the analytical ones though), although for larger values of ℓ this isn't generally the case (where numerical values are 100 times greater). This is expected since the analytical expressions are only valid for small $M\mu$.

$M\mu$	$\ell = 1$		$\ell = 2$		$\ell = 3$	
	Analytical	Numerical	Analytical	Numerical	Analytical	Numerical
0.1	$9.65 \cdot 10^{-12}$	$1.34 \cdot 10^{-11}$	$8.71 \cdot 10^{-19}$	$5.70 \cdot 10^{-15}$	$1.90 \cdot 10^{-26}$	$6.37 \cdot 10^{-16}$
0.2	$1.39 \cdot 10^{-08}$	$4.06 \cdot 10^{-08}$	$2.24 \cdot 10^{-14}$	$3.46 \cdot 10^{-14}$	$8.26 \cdot 10^{-21}$	$5.84 \cdot 10^{-17}$
0.3	$1.17 \cdot 10^{-06}$	$9.46 \cdot 10^{-06}$	$1.13 \cdot 10^{-11}$	$4.90 \cdot 10^{-11}$	$2.29 \cdot 10^{-17}$	$5.13 \cdot 10^{-15}$
0.4	$2.94 \cdot 10^{-05}$	$5.63 \cdot 10^{-04}$	$1.10 \cdot 10^{-09}$	$1.17 \cdot 10^{-08}$	$7.84 \cdot 10^{-15}$	$3.10 \cdot 10^{-14}$
0.5	$3.67 \cdot 10^{-04}$	$5.54 \cdot 10^{-03}$	$4.17 \cdot 10^{-08}$	$1.23 \cdot 10^{-06}$	$8.25 \cdot 10^{-13}$	$1.24 \cdot 10^{-11}$
0.6	$2.87 \cdot 10^{-03}$	$1.77 \cdot 10^{-02}$	$8.54 \cdot 10^{-07}$	$7.00 \cdot 10^{-05}$	$4.03 \cdot 10^{-11}$	$1.55 \cdot 10^{-09}$
0.7	$1.59 \cdot 10^{-02}$	$3.61 \cdot 10^{-02}$	$1.12 \cdot 10^{-05}$	$1.50 \cdot 10^{-03}$	$1.14 \cdot 10^{-09}$	$1.19 \cdot 10^{-07}$
0.8	$6.72 \cdot 10^{-02}$	$5.95 \cdot 10^{-02}$	$1.05 \cdot 10^{-04}$	$8.15 \cdot 10^{-03}$	$2.12 \cdot 10^{-08}$	$6.19 \cdot 10^{-06}$

Table 2.3: Absolute value of the imaginary part of the frequency, comparison between numerical and analytical values.

$M\mu$	$\ell = 0$	$\ell = 1$	$\ell = 2$	$\ell = 3$
0.1	$9.28 \cdot 10^{01}$	$3.89 \cdot 10^{01}$	$6.54 \cdot 10^{05}$	$3.35 \cdot 10^{12}$
0.2	$1.98 \cdot 10^{02}$	$1.93 \cdot 10^{02}$	$5.43 \cdot 10^{01}$	$7.08 \cdot 10^{05}$
0.3	$7.88 \cdot 10^{01}$	$7.09 \cdot 10^{02}$	$3.34 \cdot 10^{02}$	$2.23 \cdot 10^{04}$
0.4	$5.39 \cdot 10^{00}$	$1.82 \cdot 10^{03}$	$9.65 \cdot 10^{02}$	$2.96 \cdot 10^{02}$
0.5	$3.91 \cdot 10^{01}$	$1.41 \cdot 10^{03}$	$2.84 \cdot 10^{03}$	$1.41 \cdot 10^{03}$
0.6	$3.08 \cdot 10^{01}$	$5.18 \cdot 10^{02}$	$8.09 \cdot 10^{03}$	$3.75 \cdot 10^{03}$
0.7	$5.28 \cdot 10^{01}$	$1.27 \cdot 10^{02}$	$1.33 \cdot 10^{04}$	$1.04 \cdot 10^{04}$
0.8	$9.34 \cdot 10^{01}$	$1.15 \cdot 10^{01}$	$7.67 \cdot 10^{03}$	$2.91 \cdot 10^{04}$

Table 2.4: Imaginary part relative difference $|(M\omega_I)_{num} - (M\omega_I)_{analt}/(M\omega_I)_{analt}| \times 100$ between numerical and analytic values Baumann *et al.* (2019).

2.4 Scalar quasi-normal modes

2.4.1 Recursion coefficients

For quasi-normal states we want solutions that behave as outgoing waves when $r \to \infty$. Looking back at equation (2.2.9) for quasi-normal modes we will pick the $A = 0$ solution and make $\mu = 0$ so that we get a wave behavior at $r \to \infty$. Our new ansatz to solve the Klein-Gordon equation

$$-\frac{\mathrm{d}^2 R(r)}{\mathrm{d}r^{*2}} + \left(1 - \frac{2M}{r}\right)\left[\frac{\ell\,(\ell+1)}{r^2} + \frac{2M}{r^3}\right] R(r) = \omega^2 R(r)$$

is given in Leaver (1985) as

$$R(r) = (r-2M)^{-2M\omega \mathrm{i}}\, r^{4M\omega \mathrm{i}} \mathrm{e}^{\mathrm{i}\omega(r-2M)} \sum_{n=0}^{\infty} a_n \left(1 - \frac{2M}{r}\right)^n \tag{2.4.1}$$

in order to get the expected asymptotic behavior. Just like before, making the replacement $x = 1 - 2M/r$ we have

$$R(x) = \mathrm{e}^{-\frac{2iMx\omega}{x-1}} \left(\frac{M}{1-x}\right)^{4iM\omega} \left(\frac{Mx}{2(1-x)}\right)^{-2iM\omega} \sum_{n=0}^{\infty} a_n x^n. \tag{2.4.2}$$

Now applying this in

$$\frac{x^2\,(1-x)^4}{4M^2} R''(x) + \frac{x\,(1-x)^3\,(1-3x)}{4M^2} R'(x) - \left[\frac{(1-x)^3}{4M^2} + \frac{\ell(\ell+1)\,(1-x)^2}{4M^2} - \omega^2\right] R(x) = 0$$

we have

$$-\left[\ell^2 + \ell - 32M^2\omega^2 + x(4M\omega + \mathrm{i})^2 - 8\mathrm{i}M\omega - 1\right] \sum_{n=0}^{\infty} a_n x^n + \left[x^2(3 - 8\mathrm{i}M\omega) + x(-4 + 16\mathrm{i}M\omega) - 4\mathrm{i}M\omega + 1\right] \sum_{n=0}^{\infty} n a_n x^{n-1} + x(x-1)^2 \sum_{n=0}^{\infty} n a_n \left(n x^{n-2} - x^{n-2}\right) = 0$$

and shifting the sums we get

$$\sum_{n=1}^{\infty}\Big[a_n x^n\left(-\ell^2-\ell+32M^2\omega^2+8\mathrm{i}M\omega-1\right)-(4M\omega+\mathrm{i})^2 a_{n-1}x^n+ \\ (n+1)a_{n+1}(1-4\mathrm{i}M\omega)x^n+(n-1)a_{n-1}(3-8\mathrm{i}M\omega)x^n+(n-1)(n-2)a_{n-1}x^n+ \\ -2n(n-1)a_n x^n+(n+1)na_{n+1}x^n+a_0\left(-\ell^2-\ell+32M^2\omega^2+8\mathrm{i}M\omega-1\right)+ \\ na_n(-4+16\mathrm{i}M\omega)x^n+a_1(1-4\mathrm{i}M\omega)\Big]=0. \quad (2.4.3)$$

Using the properties of the power series, we can now find the expansion coefficients which are given by

$$\begin{cases}\alpha_n=(n+1)(-4\mathrm{i}M\omega+n+1)\\ \beta_n=-\ell(\ell+1)+32M^2\omega^2+n(-2+16\mathrm{i}M\omega)+8\mathrm{i}M\omega-2n^2-1\\ \gamma_n=(n-4\mathrm{i}M\omega)^2\end{cases} \quad (2.4.4)$$

which is exactly what we have in Leaver (1985).

2.4.2 Quasi-Normal frequencies

Just like in section §2.3 we need to find solutions that satisfy the following equation

$$F(M\omega)\equiv\frac{\beta_0}{\alpha_0}-\cfrac{\gamma_1}{\beta_1-\cfrac{\alpha_1\gamma_2}{\beta_2-\cfrac{\alpha_2\gamma_3}{\beta_3-\ddots}}}=0. \quad (2.4.5)$$

The obtained values for the frequency can be seen in table 2.5 and in figure 2.9. The $k=0$ mode is called the fundamental mode since it is the longest lived mode and for that reason it is the most important one in this problem. One of the contour plots can be seen in figure 2.8. Just like in the quasi-bound states situation, the real part of the frequency corresponds to the "energy" of the field and it increases with the angular momentum number ℓ, which makes sense since we expect the energy to increase as the angular momentum increases. Moreover, it can be seen in figure 2.9 that there is a linear relationship between $M\omega_R$ and the angular momentum number ℓ.

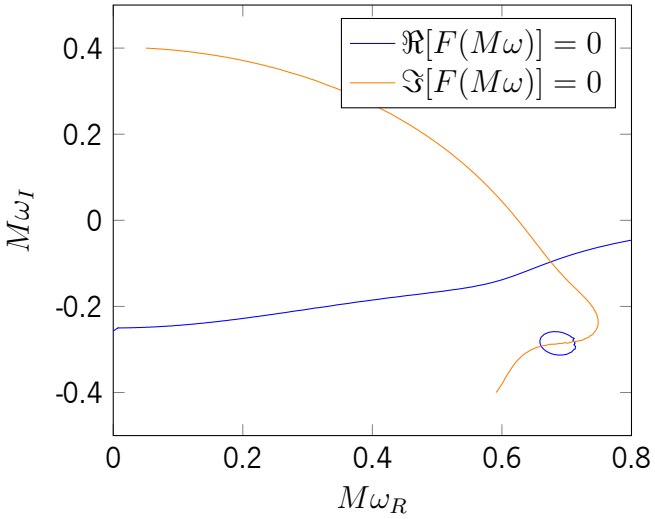

Figure 2.8: Contour plot for $\Re[F(M\omega)] = 0,\ \Im[F(M\omega)] = 0$ with $\ell = 3$.

k	$\ell = 0$		$\ell = 1$		$\ell = 2$		$\ell = 3$	
	$M\omega_R$	$-M\omega_I$	$M\omega_R$	$-M\omega_I$	$M\omega_R$	$-M\omega_I$	$M\omega_R$	$-M\omega_I$
0	0.11046	0.10490	0.29293	0.09766	0.48364	0.09676	0.67537	0.09650
1	0.08609	0.34806	0.26445	0.30626	0.46385	0.29560	0.66067	0.29229
2	0.07551	0.60076	0.22954	0.54013	0.43054	0.50856	0.63363	0.49601

Table 2.5: Quasi-normal frequencies and overtones (200 iterations).

Our results were calculated for 200 iterations of the infinite fraction (2.4.5). In table 2.6 we can see that the iteration number only affects the results of the smallest ℓ, namely $\ell = 0, 1$. As for the rest, the numerical results are very stable against the number of iterations at least up to the fifth decimal place, even on $k = 3$ since it is more difficult for the algorithm to find frequencies for higher values of k. It was important here though to calculate the terms up to 400 iterations for the simple reason that a more accurate approximation of the infinite fraction might help us detect some previously unknown overtones for a certain ℓ like, for example, $\ell = 0$. Then one just needs to use such a value as a starting guess and it's possible to find the desired root even with a lower number of iterations (e.g. 50).

Goebel (1972) realized that the real part of the fundamental frequency is related to waves in the

ℓ	50		100		200		400	
	$M\omega_R$	$-M\omega_I$	$M\omega_R$	$-M\omega_I$	$M\omega_R$	$-M\omega_I$	$M\omega_R$	$-M\omega_I$
0	0.07152	−0.59530	0.07574	−0.59912	0.07551	−0.60076	0.07574	−0.59912
1	0.22949	−0.54018	0.22954	−0.54013	0.22954	−0.54013	0.22954	−0.54013
2	0.43054	−0.50856	0.43054	−0.50856	0.43054	−0.50856	0.43054	−0.50856
3	0.63363	−0.49601	0.63363	−0.49601	0.63363	−0.49601	0.63363	−0.49601
10	2.00620	−0.48285	2.00620	−0.48285	2.00620	−0.48285	2.00620	−0.48285
15	2.97308	−0.48192	2.97308	−0.48192	2.97308	−0.48192	2.97308	−0.48192
20	3.93773	−0.48158	3.93773	−0.48158	3.93773	−0.48158	3.93773	−0.48158
30	5.86468	−0.48133	5.86468	−0.48133	5.86468	−0.48133	5.86468	−0.48133
40	7.79043	−0.48124	7.79043	−0.48124	7.79043	−0.48124	7.79043	−0.48124
50	9.71568	−0.48120	9.71568	−0.48120	9.71568	−0.48120	9.71568	−0.48120

Table 2.6: Frequency values for different iterations of the infinite fraction for $k = 2$ with five decimal places.

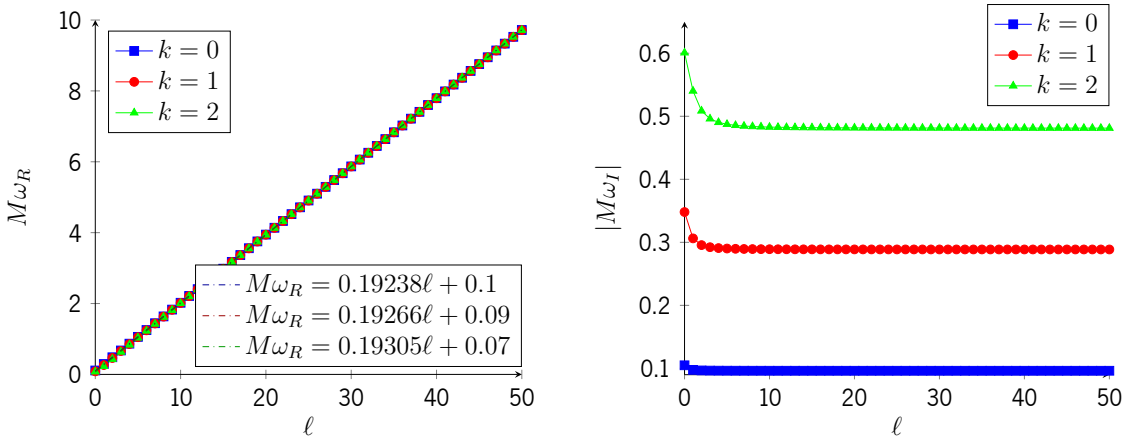

Figure 2.9: Quasi-normal frequencies.

unstable orbit $r = 3M$ in the Schwarzschild geometry, that is, there's a correspondence between the wave quantities like ω_R and ℓ to the classical geodesic quantities energy and angular momentum. In the geodesic approximation ($\ell \geq 20$), the energy of a massless test particle is

$$ME = \frac{L}{3 \times 3^{1/2}}. \tag{2.4.6}$$

Here E and L are, of course, the energy and angular momentum of a particle but a correspondence can be made between the frequency ω_R of a wave and the angular momentum number ℓ , where $L = \sqrt{\ell(\ell+1)} \approx \ell + 1/2$ so

$$M\omega_R = \frac{\ell + 1/2}{3 \times 3^{1/2}}. \tag{2.4.7}$$

In fact equation (2.4.7) corresponds exactly to the expression for the real part of the frequency obtained in Ferrari and Mashhoon (1984) using an analytical approximation the the wave equation directly.

When ℓ is very large, equation (2.1.12) has a maximum at $r = 3M$ just like in the classical Schwarzschild effective potential in equation (1.1.11). This is expected since when $\ell \gg 1$, V_{eff}^2 equals the geodesic potential. It is clear that there is a linear relationship between frequency and angular momentum, a relation that we can see too in Figure 2.9a. The slope of the line is $1/(3 \times 3^{1/2}) \approx 0.1925$, which is close to the obtained slopes for Figure 2.9a after adjusting a linear function to the results[6] which might justify our earlier comparison. Although Goebel (1972) has in mind gravitational perturbations of a black hole geometry, his analysis can be applied directly to massless scalar perturbations since they too travel on null geodesics in the geometrical optics limit. One thing that the analytical approximations, at least to this order, is that they don't take into account the fact that ω_R decreases slightly when k increases.

As for the imaginary part, the fact that our numerical results indicate that it does not change very much with ℓ (as it can be seen appendix D), but they do change with the overtone number. They are related with the population decay of particles near the unstable orbit near $r = 3M$. Goebel (1972) shows that such unstable orbits decay in time, meaning that their radius deviates from $r = 3M$ as

$$r \approx 3M + \text{const.} \times \mathrm{e}^{\gamma_L t}, \tag{2.4.8}$$

[6]The linear functions were fitted to 51 points with $\ell = 0, 1, \ldots, 50$ for each overtone k with an average correlation coefficient of $R^2 = 0.9999$.

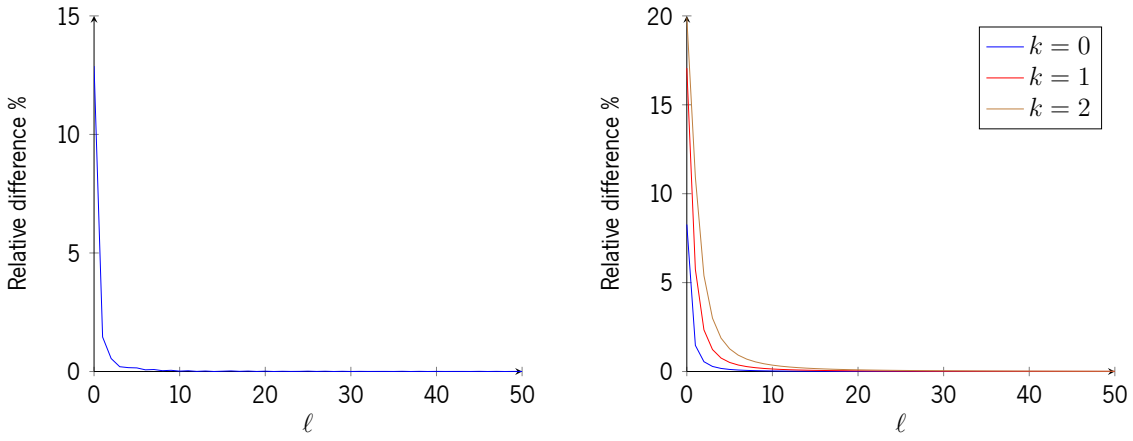

(a) Real part.

(b) Imaginary part.

Figure 2.10: Relative difference $|[(M\omega)_{\text{num}} - (M\omega)_{\text{analytic}}]/(M\omega)_{\text{analytic}}| \times 100$ between analytical and numerical values.

where $\gamma_L = 1/(3 \times 3^{1/2})$ and it is called the Lyapunov exponent. It is a measure of the rate at which a bundle of rays diverge or converge from the orbit radius. The imaginary part, given in Ferrari and Mashhoon (1984), can thus be written as

$$\omega_I = \gamma_L(k + 1/2) \tag{2.4.9}$$

where γ_L has the same numerical values as above.

This shows there is really a correspondence that can be made between quasi-normal modes and null geodesics in Schwarzschild, which closely fits our numerical data as seen in Figure 2.10.

3 Gravitational Modes on Schwarzschild

3.1 Theoretical considerations

3.1.1 Metric perturbations

Gravitational perturbations on black holes happen as the result of infalling matter or the collision of two black holes which results in a larger one. Just like a string of a violin when perturbed, the black hole geometry will "vibrate" in certain discrete modes, the so called gravitational quasi-normal modes, emitting gravitational radiation until it becomes a stationary black hole again.

In this chapter we will be interested in Schwarzschild black holes. However unlike the vibrations on an ideal string, the frequency of the modes is a complex number since it loses gravitational energy in the waves it radiates to infinity.

Assuming a small perturbation in Schwarzschild spacetime the metric can be written in generalized Schwarzschild coordinates as[1]

$$g_{\mu\nu} = g^{(0)}_{\mu\nu} + h_{\mu\nu}, \tag{3.1.1}$$

where $g^{(0)}_{\mu\nu}$ is the unperturbed metric which is

$$g^{(0)}_{\mu\nu}\mathrm{d}x^{\mu}\mathrm{d}x^{\nu} = -\left(1-\frac{2M}{r}\right)\mathrm{d}t^2 + \left(1-\frac{2M}{r}\right)^{-1}\mathrm{d}r^2 + r^2\left(\mathrm{d}\theta^2 + \sin\theta\mathrm{d}\phi^2\right) \tag{3.1.2}$$

[1] This section will be loosely based on Chapter 8 of Alcubierre (2012) and for that reason we will use the same notation, unless said otherwise.

and $h_{\mu\nu}$ is our metric perturbation which satisfies $|h_{\mu\nu}| \ll 1$.

We shall consider that our spacetime manifold $\mathcal{M}$ is actually the product of two other manifolds: $\mathcal{S}^2$ which is a two-sphere with coordinates (θ, ϕ) and $\mathcal{L}^2$ a Lorentzian submanifold with coordinates (t, r). We will also define that the indices in lower case Latin letters $(a, b, c, d, \ldots)$ refer to the submanifold $\mathcal{S}^2$, whereas for $\mathcal{L}^2$ we will use uppercase Latin letters $(A, B, C, D, \ldots)$. The indices on the whole manifold $\mathcal{M}$ will be indicated by Greek letters $(\alpha, \beta, \gamma, \delta, \ldots)$ as usual.

We will also define ∇_μ as the standard covariant derivative on $\mathcal{M}$, D_A as the covariant derivative on $\mathcal{L}^2$ and D_a as the covariant derivative on $\mathcal{S}^2$. The line element can be expressed as

$$\mathrm{d}s^2 = g_{AB}\mathrm{d}x^A\mathrm{d}x^B + r^2\Omega_{ab}\mathrm{d}x^a\mathrm{d}x^b, \tag{3.1.3}$$

where Ω_{ab} is the metric of $\mathcal{S}^2$ in spherical coordinates.

3.1.2 Multipole expansion

We can expand our perturbation in multipoles using the scalar, vector and tensor spherical harmonics, which only transform as tensors relative to changes of coordinates on the two-sphere, and divide them into odd and even harmonics, meaning they transform as $(-1)^{\ell+1}$ or as $(-1)^\ell$ respectively under a parity transformation. Spherical harmonics are defined as

$$\text{Scalar:} \quad Y^{\ell,m}(\theta,\phi) \tag{3.1.4a}$$

$$\text{Vector:} \begin{cases} Y_a^{\ell,m} = D_a Y^{\ell,m} & \text{Even} \\ X_a^{\ell,m} = -\epsilon_{ac}\Omega^{cb} D_b Y^{\ell,m} & \text{Odd} \end{cases} \tag{3.1.4b}$$

$$\text{Tensor:} \begin{cases} Z_{ab}^{\ell,m} = D_a D_b Y^{\ell,m} + \frac{1}{2} l(l+1)\Omega_{ab} Y^{\ell,m} & \text{Even} \\ X_{ab}^{\ell,m} = \frac{1}{2}\left(D_a X_a^{\ell,m} + D_b X_a^{\ell,m}\right), & \text{Odd} \end{cases} \tag{3.1.4c}$$

where ϵ_{ab} is the asymmetric Levi-Civita tensor on a sphere where $\epsilon_{\theta\phi} = \sin\theta$ and

$$Y^{\ell,m}(\theta,\phi) = \begin{cases} \dfrac{(-1)^\ell}{2^\ell \ell!}\sqrt{\dfrac{(2\ell+1)(\ell+m)!}{4\pi(\ell-m)!}}\mathrm{e}^{\mathrm{i}m\phi}\dfrac{1}{\sin^m\theta}\dfrac{\mathrm{d}^{\ell-m}\sin^{2\ell}\theta}{\mathrm{d}(\cos\theta)^{\ell-m}} & m \geq 0 \\ (-1)^m\left[Y^{\ell,m}(\theta,\phi)\right]^*. & m < 0 \end{cases} \tag{3.1.5}$$

It is easy to see that for $\ell = 0$ the vector harmonics vanish since $Y^{00} = \sqrt{1/4\pi}$ is a constant. It can also be shown that the tensor harmonics vanish for $\ell = 0$ and $\ell = 1$.

Our perturbation $h_{\mu\nu}$ can be written as

$$h_{\mu\nu} = h^{(e)}_{\mu\nu} + h^{(o)}_{\mu\nu}, \tag{3.1.6}$$

where $h^{(e)}_{\mu\nu}$, the even part of the perturbation, can be written as sum of terms in ℓ and m such as

$$\begin{aligned} \left(h^{\ell,m}_{AB}\right)^{(e)} &= H^{\ell,m}_{AB}Y^{\ell,m} \\ \left(h^{\ell,m}_{Ab}\right)^{(e)} &= H^{\ell,m}_{A}Y^{\ell,m}_{b} \\ \left(h^{\ell,m}_{ab}\right)^{(e)} &= r^2\left(K^{\ell,m}\Omega_{ab}Y^{\ell,m} + G^{\ell,m}Z^{\ell,m}_{ab}\right) \end{aligned} \tag{3.1.7}$$

and for $h^{(o)}_{\mu\nu}$, the odd part,

$$\begin{aligned} \left(h^{\ell,m}_{AB}\right)^{(o)} &= 0 \\ \left(h^{\ell,m}_{A}\right)^{(o)} &= h^{\ell,m}_{A}X^{\ell,m}_{b} \\ \left(h^{\ell,m}_{ab}\right)^{(o)} &= h^{\ell,m}X^{\ell,m}_{ab}, \end{aligned} \tag{3.1.8}$$

where $H^{\ell,m}_{AB}, H^{\ell,m}_{A}, K^{\ell,m}, G^{\ell,m}, h^{\ell,m}_{A}, h^{\ell,m}$ are functions of r and t. Under a coordinate transformation in $\mathcal{S}^2$ only we see that h_{AB} transform as scalars, h_{Ab} as vectors and h_{ab} as tensors. Therefore the total perturbation is

$$h_{AB} = \sum_{\ell,m} H^{\ell,m}_{AB}Y^{\ell,m} \tag{3.1.9a}$$

$$h_{Ab} = \sum_{\ell,m}\left[H^{\ell,m}_{A}Y^{\ell,m}_{b} + h^{\ell,m}_{A}X^{\ell,m}_{b}\right] \tag{3.1.9b}$$

$$h_{ab} = \sum_{\ell,m}\left[r^2\left(K^{\ell,m}\Omega_{ab}Y^{\ell,m} + G^{\ell,m}Z^{\ell,m}_{ab}\right) + h^{\ell,m}X^{\ell,m}_{ab}\right], \tag{3.1.9c}$$

where $\sum_m \equiv \sum_{m=-\ell}^{m=\ell}$ and $\sum_\ell \equiv \sum_{\ell=0}^{\infty}$.

3.1.3 Gauge transformations

One can perform a gauge transformation by an infinitesimal coordinate transformation

$$x^{\mu'} = x^{\mu} + \xi^{\mu} \quad (|\partial_{\rho}\xi^{\mu}| \ll 1) \tag{3.1.10}$$

and since the metric components transform as $g_{\mu'\nu'} = \Lambda^{\alpha}{}_{\mu'}\Lambda^{\beta}{}_{\nu'}g_{\alpha\beta}$ where $\Lambda^{\alpha}{}_{\mu'} = \delta^{\alpha}{}_{\mu} - \xi^{\alpha}{}_{,\mu}$ then equation (3.1.1) becomes

$$g_{\mu'\nu'} = g^{(0)}_{\mu\nu} + h_{\mu\nu} - \xi_{\mu;\nu} - \xi_{\nu;\mu}, \tag{3.1.11}$$

where $g^{(0)}_{\mu\nu}\xi^{\nu}{}_{;\sigma} \equiv \xi_{\mu;\sigma}$ where indices are raised using the unperturbed metric $g^{(0)}_{\mu\nu}$. We can now define that under a gauge transformation the perturbation transforms as $h^{\text{new}}_{\mu\nu} \equiv h^{\text{old}}_{\mu\nu} - \xi_{\mu;\nu} - \xi_{\nu;\mu}$.

Even gauge transformation We can also expand the gauge vector $\vec{\xi}$ in a multipole expansion. An even gauge transformation has components in $\mathcal{L}^2$

$$\xi_A = \sum_{\ell,m} E^{\ell,m}_A(t,r)Y^{\ell,m}(\theta,\phi) \tag{3.1.12}$$

and in $\mathcal{S}^2$

$$\xi_a = \sum_{\ell,m} E^{\ell,m}(t,r)Y^{\ell,m}_a(\theta,\phi). \tag{3.1.13}$$

Furthermore the components of $\nabla\vec{\xi}$ are given by

$$\nabla_A\xi_B = \sum_{\ell,m}\left(D_A E^{\ell,m}_B\right)Y^{\ell,m} \tag{3.1.14a}$$

$$\nabla_A\xi_b = \sum_{\ell,m}\left(D_A E^{\ell,m} - \frac{D_A r}{r}E^{\ell,m}\right)Y^{\ell,m}_b \tag{3.1.14b}$$

$$\nabla_a\xi_B = \sum_{\ell,m}\left(E^{\ell,m}_B - \frac{D_B r}{r}E^{\ell,m}\right)Y^{\ell,m}_a \tag{3.1.14c}$$

$$\nabla_a\xi_b = \sum_{\ell,m}\left[\left(D_a Y^{\ell,m}_b\right)E^{\ell,m} + r\Omega_{ab}\left(D^C r\right)E^{\ell,m}_C Y^{\ell,m}\right]. \tag{3.1.14d}$$

We shall now derive explicitly equation (3.1.14a):

$$\begin{aligned}
\nabla_A \xi_B &= \partial_A \xi_B - \xi_\alpha \Gamma^\alpha{}_{AB} \\
&= \partial_A \xi_B - \xi_C \Gamma^C{}_{AB} && \text{since mixed symbols vanish} \\
&= D_A \xi_B \\
&= D_A\big(\sum_{\ell,m} E^{\ell,m}_B Y^{\ell,m}\big) && \text{from (3.1.12)} \\
&= \sum_{\ell,m} \left(D_A E^{\ell,m}_B\right) Y^{\ell,m}
\end{aligned}$$

and by the same reasoning we can derive the rest of the components of $\nabla\xi$. The connection coefficients are those from the unperturbed metric since any corrections would result in second order changes. Under such gauge transformation, functions $H^{\ell,m}_{AB}, H^{\ell,m}_A, K^{\ell,m}, G^{\ell,m}$ will too be transformed. For example for $\left(h^{\ell,m}_{AB}\right)^{(e)}$ we have

$$\begin{aligned}
\left(h^{\ell,m}_{AB}\right)^{(e)} &\to \left(h^{\ell,m}_{AB}\right)^{(e)} - \nabla_A \xi_B - \nabla_B \xi_A \\
H^{\ell,m}_{AB} Y^{\ell,m} &\to H^{\ell,m}_{AB} Y^{\ell,m} - \left(D_A E^{\ell,m}_B\right) Y^{\ell,m} - \left(D_B E^{\ell,m}_A\right) Y^{\ell,m} \\
H^{\ell,m}_{AB} &\to H^{\ell,m}_{AB} - D_A E^{\ell,m}_B - D_B E^{\ell,m}_A
\end{aligned} \tag{3.1.15}$$

and following the same procedure for the other functions we get

$$H^{\ell,m}_{AB} \to H^{\ell,m}_{AB} - D_A E^{\ell,m}_B - D_B E^{\ell,m}_A \tag{3.1.16a}$$

$$H^{\ell,m}_A \to H^{\ell,m}_A - E^{\ell,m}_A - D_a E^{\ell,m} + \frac{2 D_A r}{r} E^{\ell,m} \tag{3.1.16b}$$

$$K^{\ell,m} \to K^{\ell,m} - \frac{2}{r}\left(D^A r\right) E^{\ell,m}_A + \frac{\ell(\ell+1)}{r^2} E^{\ell,m} \tag{3.1.16c}$$

$$G^{\ell,m} \to G^{\ell,m} - \frac{2}{r^2} E^{\ell,m}. \tag{3.1.16d}$$

We can also choose a $E^{\ell,m}$ and $E^{\ell,m}_A$ such that $G^{\ell,m}, H^{\ell,m}_A = 0$. This gauge is called the Regge-Wheeler gauge, from Regge and Wheeler (1957). Alternatively we can make gauge invariant combinations of the above functions as follows

$$\tilde{H}^{\ell,m}_{AB} = H^{\ell,m}_{AB} - D_A \varepsilon^{\ell,m}_B - D_B \varepsilon^{\ell,m}_A \tag{3.1.17}$$

and

$$\tilde{K}^{\ell,m} = K^{\ell,m} + \frac{1}{2}\ell(\ell+1)G^{\ell,m} - \frac{2}{r}\left(D^A r\right)\varepsilon_A^{\ell,m}, \tag{3.1.18}$$

where

$$\varepsilon_A^{\ell,m} = H_A^{\ell,m} - \frac{1}{2}r^2 D_A G^{\ell,m}.$$

In the Regge-Wheeler gauge, $\tilde{H}_{AB}^{\ell,m} = H_{AB}^{\ell,m}$ and $\tilde{K}^{\ell,m} = K^{\ell,m}$.

Odd gauge transformation Analogously we can have odd gauge transformations such as[2]

$$\begin{aligned} \xi_A &= 0 \\ \xi_a &= \sum_{\ell,m} E^{\ell,m} X_a^{\ell,m}. \end{aligned} \tag{3.1.19}$$

Here the components of $\nabla\vec{\xi}$ are

$$\nabla_A \xi_B = 0 \tag{3.1.20a}$$

$$\nabla_A \xi_b = \sum_{\ell,m}\left(D_A E^{\ell,m} - \frac{D_A r}{r}E^{\ell,m}\right)X_b^{\ell,m} \tag{3.1.20b}$$

$$\nabla_a \xi_B = -\sum_{\ell,m}\frac{D_B r}{r}E^{\ell,m}X_a^{\ell,m} \tag{3.1.20c}$$

$$\nabla_a \xi_b = \sum_{\ell,m}\left(D_a X_b^{\ell,m}\right)E^{\ell,m} \tag{3.1.20d}$$

and consequently functions $h_A^{\ell,m}, h^{\ell,m}$ become

$$\begin{aligned} h_a^{\ell,m} &\to h_A^{\ell,m} - D_A E^{\ell,m} + \frac{2D_A r}{r}E^{\ell,m} \\ h^{\ell,m} &\to h^{\ell,m} - 2E^{\ell,m}. \end{aligned} \tag{3.1.21}$$

We can make a gauge choice such that $h^{\ell,m} = 0$, the Regge-Wheeler gauge for odd gauge transformations.

The gauge invariant combinations are given by

$$\tilde{h}_A^{\ell,m} = h_A^{\ell,m} - \frac{1}{2}D_A h^{\ell,m} + \frac{D_A r}{r}h^{\ell,m}. \tag{3.1.22}$$

In the Regge-Wheeler gauge, $\tilde{h}_A^{\ell,m} = h_A^{\ell,m}$.

[2] Obviously we can't make something like $\xi_A = \sum_{\ell,m} E_A^{\ell,m} S^{\ell,m}$, where $S^{\ell,m}$ is a certain scalar spherical harmonic, since there is only one scalar spherical harmonic, $Y^{\ell,m}$, and it happens to be even under a parity transformation. For that reason the only possible choice for ξ_A is zero.

3.1.4 Perturbed Einstein equations

A perturbation of the metric like equation (3.1.1) perturbs all the quantities which depend on the metric tensor. Since $|h_{\mu\nu}| \ll 1$ we can find the variation of the Riemann and Ricci tensor up to first order. First we must find out how the Christoffel symbols

$$\Gamma^{\alpha}{}_{\mu\nu} = \frac{1}{2} g^{\alpha\beta} \left(g_{\beta\mu,\nu} + g_{\beta\nu,\mu} - g_{\mu\nu,\beta} \right)$$

change under a small change in the metric. It is easy to see that $g^{\mu\nu} = g^{(0)\mu\nu} - h^{\mu\nu}$ up to first order where $h^{\mu\nu} \equiv g^{(0)\mu\alpha} h_{\alpha\beta} g^{(0)\beta\nu}$. Under a small variation, up to first order, then

$$\delta\Gamma^{\alpha}{}_{\mu\nu} = \frac{1}{2} \delta g^{\alpha\beta} \left(g_{\beta\mu,\nu} + g_{\beta\nu,\mu} - g_{\mu\nu,\beta} \right) + \frac{1}{2} g^{\alpha\beta} \left(\partial_\nu \delta g_{\beta\mu} + \partial_\mu \delta g_{\beta\nu} - \partial_\beta g \delta g_{\mu\nu} \right), \tag{3.1.23}$$

where $\delta g_{\mu\nu}$ is the variation of the metric. Since equation (3.1.23) is a tensorial equation[3], then in a local Lorentzian frame at an arbitrary point $\mathcal{P}$ the derivatives of the metric vanish at the point so the first term in the previous equation vanishes as well and we get

$$\begin{aligned} \delta\Gamma^{\alpha}{}_{\mu\nu} &\overset{*}{=} \frac{1}{2} g^{\alpha\beta} \left(\partial_\nu \delta g_{\beta\mu} + \partial_\mu \delta g_{\beta\nu} - \partial_\beta g \delta g_{\mu\nu} \right) \\ &\overset{*}{=} \frac{1}{2} g^{\alpha\beta} \left(\nabla_\nu \delta g_{\beta\mu} + \nabla_\mu \delta g_{\beta\nu} - \nabla_\beta \delta g_{\mu\nu} \right) \end{aligned}$$

which implies that in any frame everywhere, since $\mathcal{P}$ is arbitrary,

$$\delta\Gamma^{\alpha}{}_{\mu\nu} = \frac{1}{2} g^{\alpha\beta} \left(\nabla_\nu \delta g_{\beta\mu} + \nabla_\mu \delta g_{\beta\nu} - \nabla_\beta \delta g_{\mu\nu} \right). \tag{3.1.24}$$

Now the Riemann tensor is given by

$$R^{\alpha}{}_{\beta\mu\nu} = \Gamma^{\alpha}{}_{\beta\nu,\mu} - \Gamma^{\alpha}{}_{\beta\mu,\nu} + \Gamma^{\alpha}{}_{\sigma\mu} \Gamma^{\sigma}{}_{\beta\nu} - \Gamma^{\alpha}{}_{\sigma\nu} \Gamma^{\sigma}{}_{\beta\mu}. \tag{3.1.25}$$

Therefore its variation is

$$\begin{aligned} \delta R^{\alpha}{}_{\beta\mu\nu} &= \delta \left(\Gamma^{\alpha}{}_{\beta\nu,\mu} - \Gamma^{\alpha}{}_{\beta\mu,\nu} + \Gamma^{\alpha}{}_{\sigma\mu} \Gamma^{\sigma}{}_{\beta\nu} - \Gamma^{\alpha}{}_{\sigma\nu} \Gamma^{\sigma}{}_{\beta\mu} \right) \\ &= \partial_\mu \delta\Gamma^{\alpha}{}_{\beta\nu} - \partial_\nu \delta\Gamma^{\alpha}{}_{\beta\mu} + \left(\delta\Gamma^{\alpha}{}_{\sigma\mu} \right) \Gamma^{\sigma}{}_{\beta\nu} \\ &\quad - \left(\delta\Gamma^{\alpha}{}_{\sigma\nu} \right) \Gamma^{\sigma}{}_{\beta\mu} + \Gamma^{\alpha}{}_{\sigma\mu} \delta\Gamma^{\sigma}{}_{\beta\nu} - \Gamma^{\alpha}{}_{\sigma\nu} \delta\Gamma^{\sigma}{}_{\beta\mu}. \end{aligned} \tag{3.1.26}$$

[3] Although $\Gamma^{\alpha}{}_{\mu\nu}$ is not a tensor, the difference between two connections is a tensor.

Since the $\Gamma\Gamma$ terms are zero in a local frame

$$\begin{aligned}\delta R^{\alpha}{}_{\beta\mu\nu} &\overset{*}{=} \partial_\mu \delta\Gamma^{\alpha}{}_{\beta\nu} - \partial_\nu \delta\Gamma^{\alpha}{}_{\beta\mu} \\ &\overset{*}{=} \nabla_\mu \delta\Gamma^{\alpha}{}_{\beta\nu} - \nabla_\nu \delta\Gamma^{\alpha}{}_{\beta\mu}\end{aligned}$$

then in any frame at any point

$$\delta R^{\alpha}{}_{\beta\mu\nu} = \nabla_\mu \delta\Gamma^{\alpha}{}_{\beta\nu} - \nabla_\nu \delta\Gamma^{\alpha}{}_{\beta\mu}. \tag{3.1.27}$$

By the same token, the variation of the Ricci tensor is

$$\delta R_{\mu\nu} = \delta R^{\alpha}{}_{\mu\alpha\nu} = \nabla_\alpha \delta\Gamma^{\alpha}{}_{\mu\nu} - \nabla_\nu \delta\Gamma^{\alpha}{}_{\mu\alpha} \tag{3.1.28}$$

and using (3.1.24)

$$\begin{aligned}\delta R_{\mu\nu} = &\frac{1}{2}\nabla_\alpha g^{\alpha\beta}\left(\nabla_\nu \delta g_{\beta\mu} + \nabla_\mu \delta g_{\beta\nu} - \nabla_\beta \delta g_{\mu\nu}\right) \\ &- \frac{1}{2}\nabla_\nu g^{\alpha\beta}\left(\nabla_\alpha \delta g_{\beta\mu} + \nabla_\mu \delta g_{\beta\alpha} - \nabla_\beta \delta g_{\mu\alpha}\right).\end{aligned} \tag{3.1.29}$$

Since we know that $\delta g_{\mu\nu} = h_{\mu\nu}$, then up to first order

$$\delta R_{\mu\nu} = \frac{1}{2}\left[\nabla_\alpha \nabla_\nu h^{\alpha}{}_{\mu} + \nabla_\alpha \nabla_\mu h^{\alpha}{}_{\nu} - \nabla_\alpha \nabla^\alpha h_{\mu\nu} - \nabla_\nu \nabla_\alpha h^{\alpha}{}_{\mu} + \nabla_\nu \nabla_\mu h^{\alpha}{}_{\alpha} - \nabla_\nu \nabla^\alpha h_{\mu\alpha}\right]. \tag{3.1.30}$$

Now the total Ricci tensor up to first order is

$$R_{\mu\nu} = R^{(0)}_{\mu\nu} + \delta R_{\mu\nu}, \tag{3.1.31}$$

where $R^{(0)}_{\mu\nu}$ is the unperturbed Ricci tensor. The vacuum Einstein equations

$$R_{\mu\nu} = 0 \tag{3.1.32}$$

become

$$R^{(0)}_{\mu\nu} + \delta R_{\mu\nu} = 0$$

and since $R^{(0)}_{\mu\nu} = 0$ for the Schwarzschild spacetime then

$$\delta R_{\mu\nu} = 0. \tag{3.1.33}$$

Therefore we have a second order differential equation for $h_{\mu\nu}$ which in principle can be solved. All we have to do now is replace $h_{\mu\nu}$ in equation (3.1.30) by its multipole expansion. The explicit formulas for the variation of the the components of the Ricci tensor for δR_{AB}, δR_{Ab}, δR_{ab} are given in Martel and Poisson (2005), although with a different notation.

We define the Zerilli-Moncrief master function as

$$\Psi^{\ell,m}_{\text{even}} = \frac{2r}{\ell(\ell+1)}\left[\tilde{K}^{\ell,m} + \frac{2}{\Lambda}\left(r^{,A}r^{,B}\tilde{H}^{\ell,m}_{AB} - rr^{,A}D_A\tilde{K}^{\ell,m}\right)\right] \tag{3.1.34}$$

and the Cunningham-Price-Moncrief master function as

$$\Psi^{\ell,m}_{\text{odd}} = \frac{2r}{(\ell-1)(\ell+2)}\epsilon^{AB}\left[D_A\tilde{h}^{\ell,m}_B - \frac{2r_{,A}}{r}\tilde{h}^{\ell,m}_B\right], \tag{3.1.35}$$

where $\Lambda = (\ell-1)(\ell+2)+6M/r$. These functions are important because from the Einstein equations we get a wave equation with respect to these functions, so for the even part we have

$$\frac{\partial}{\partial t^2}\Psi^{\ell,m}_{\text{even}} - \frac{\partial}{\partial r^{*2}}\Psi^{\ell,m}_{\text{even}} + V^{\ell,m}_{\text{even}}\Psi^{\ell,m}_{\text{even}} = S^{\ell,m}_{\text{even}}, \tag{3.1.36}$$

where r^* is the Regge-Wheeler coordinate defined in equation (2.1.15) and

$$V^{\ell,m}_{\text{even}} = \left(1-\frac{2M}{r}\right)\left\{\frac{1}{3}(l-1)(l+2)\frac{2(l-1)(l+2)\left(l^2+l+1\right)}{\left[\left(l^2+l-2\right)r+6M\right]^2} + \frac{1}{r^2} + \frac{2M}{r^3}\right\}. \tag{3.1.37}$$

For the odd part we have

$$\frac{\partial}{\partial t^2}\Psi^{\ell,m}_{\text{odd}} - \frac{\partial}{\partial r^{*2}}\Psi^{\ell,m}_{\text{odd}} + V^{\ell,m}_{\text{odd}}\Psi^{\ell,m}_{\text{odd}} = S^{\ell,m}_{\text{odd}}, \tag{3.1.38}$$

where

$$V^{\ell,m}_{\text{odd}} = \left(1-\frac{2M}{r}\right)\left[\frac{\ell(\ell+1)}{r^2} - \frac{6M}{r^3}\right]. \tag{3.1.39}$$

The wave equations (3.1.36) and (3.1.38) are called the Zerilli equation and the Regge-Wheeler equation respectively. The source terms $S^{\ell,m}_{\text{even(odd)}}$ are given explicitly in Martel and Poisson (2005), but in our case since we are solving the equations in the vacuum the source terms vanish since they are dependent of the components of the stress-energy tensor $\mathbf{T}$. Since our master functions depend on tensor harmonics, they are only non zero for $\ell \geq 2$, meaning that radiative phenomena can only happen for $\ell \geq 2$.

Both even and odd wave equations are isospectral[4], so they have the same spectrum of eigenvalues. Then we only need to calculate the eigenvalues for one of them, which we are going to do in section §3.2.

[4]See Chandrasekhar (1983)

3.1.5 Non-radiative modes

When $\ell = 0$ (monopole perturbations) all of the components of the perturbation that depend on either vector or tensor harmonics vanish, remaining only the following components

$$(h_{AB})^{(e)} = H^{0,0}_{AB} Y^{0,0}$$
$$(h_{ab})^{(e)} = r^2 \left(K^{0,0} \Omega_{ab} Y^{0,0} \right)$$

remain. Under a gauge transformation we see from equations (3.1.16) that

$$H^{0,0}_{AB} \to H^{0,0}_{AB} - D_A E^{0,0}_B - D_B E^{0,0}_A \tag{3.1.40}$$
$$K^{0,0} \to K^{0,0} - \frac{2}{r} \left(D^A r \right) E^{0,0}_A. \tag{3.1.41}$$

It is possible to choose a certain gauge such that $K^{0,0} = 0$, then our only perturbation components left are $(h_{AB})^{(e)}$ and the metric becomes

$$\mathrm{d}s^2 = \left[- \left(1 - \frac{2M}{r} \right) + (h_{tt})^{(e)} \right] \mathrm{d}t^2 + \left[\left(1 - \frac{2M}{r} \right)^{-1} + (h_{rr})^{(e)} \right] \mathrm{d}r^2 + r^2 \mathrm{d}\Omega^2 \tag{3.1.42}$$

which clearly describes a spherical symmetrical spacetime. Because of this, these perturbations can never produce gravitational waves since, due to Birkhoff's theorem[5], the resulting spacetime is still the Schwarzschild geometry (our perturbed spacetime is still spherically symmetric) which must be a static spacetime. Since the only free parameter in the metric is M then the effect of the perturbations is a change in the mass $M + \delta M$. The components become

$$(h_{tt})^{(e)} = \frac{2\delta M}{r} \tag{3.1.43}$$
$$(h_{rr})^{(e)} = \frac{2\delta M r}{(2M - r)(2(M + \delta M) - r)} \tag{3.1.44}$$

[5]The Birkhoff's theorem, Birkhoff (1923), states that any spherically symmetric solution to the Einstein equations must be the Schwarzschild geometry. This means that for example a pulsating star, which is still spherically symmetric, the geometry outside the star is still the Schwarzschild geometry.

When $\ell = 1$ (dipolar perturbations) all of the components of the perturbation that depend on tensor harmonics vanish so we just get

$$\left(h^{\ell,m}_{AB}\right)^{(e)} = H^{\ell,m}_{AB} Y^{\ell,m}$$
$$\left(h^{\ell,m}_{Ab}\right)^{(e)} = H^{\ell,m}_{A} Y^{\ell,m}_{b}$$
$$\left(h^{\ell,m}_{ab}\right)^{(e)} = r^2 K^{\ell,m} \Omega_{ab} Y^{\ell,m}$$

$$\left(h^{\ell,m}_{AB}\right)^{(o)} = 0$$
$$\left(h^{\ell,m}_{A}\right)^{(o)} = h^{\ell,m}_{A} X^{\ell,m}_{b}$$
$$\left(h^{\ell,m}_{ab}\right)^{(o)} = 0.$$

It is shown in Martel and Poisson (2005) that even dipolar perturbations can always be removed by choosing an appropriate gauge and that odd perturbations correspond to a slowly spinning black hole.

3.2 Gravitational quasi-normal modes

3.2.1 Recursion coefficients

We shall now proceed to calculate the eigenvalues for equation (3.1.38). It is trivial to separate the time and radial dependence of the equation, where the time part only contributes with a $\exp(-\mathrm{i}\omega t)$. Then if we consider $\Psi^{\ell,m}_{\text{odd}} = \eta(t) R^{\ell,m}(r^*)$ equation (3.1.38) becomes

$$-\frac{\mathrm{d}^2}{\mathrm{d}r^{*2}} R(r^*) + \left(1 - \frac{2M}{r}\right)\left[\frac{\ell(\ell+1)}{r^2} - \frac{6M}{r^3}\right] R(r^*) = \omega^2 R(r^*) \tag{3.2.1}$$

omitting ℓ, m for simplicity. The previous equation is very similar to equation (2.1.11) with $\mu = 0$. In fact equation (3.2.1) belongs to a general class of equations that can be written as

$$-\frac{\mathrm{d}^2}{\mathrm{d}r^{*2}} R(r^*) + \left(1 - \frac{2M}{r}\right)\left[\frac{\ell(\ell+1)}{r^2} + \frac{2M}{r^3}\left(1 - s^2\right)\right] R(r^*) = \omega^2 R(r^*), \tag{3.2.2}$$

where s is the spin of the field, 0 for scalar fields, -1 for vector fields like the electromagnetic one and -2 for tensor fields like a gravitational perturbation. By the chain rule we can set everything in terms of the Schwarzschild r coordinate so

$$-\frac{\mathrm{d}^2R(r)}{\mathrm{d}r^2}\left(1-\frac{2M}{r}\right)^2-\left(1-\frac{2M}{r}\right)\frac{\mathrm{d}R(r)}{\mathrm{d}r}\frac{2M}{r^2}+\left(1-\frac{2M}{r}\right)\left[\frac{\ell(\ell+1)}{r^2}-\frac{6M}{r^3}\right]=\omega^2R(r), \tag{3.2.3}$$

where $R(r)\equiv R\left(r^*(r)\right)$ which has the same form as the equation found for the quasi-normal modes in section §2.4.

In order to find the quasi-normal modes for this problem we must find the eigenvalues of the above equation. Again using the method found in Leaver (1985) and used in section 2.4.1 we make the change of variable $x=1-2M/r$ and our previous equation becomes

$$\frac{x^2\left(1-x\right)^4}{4M^2}R''(x)+\frac{x\left(1-x\right)^3\left(1-3x\right)}{4M^2}R'(x)-\left[\frac{-3\left(1-x\right)^3}{2M}+\frac{\ell(\ell+1)\left(1-x\right)^2}{4M^2}\right]R(x)= \\ =\omega^2R(x) \tag{3.2.4}$$

and we use the same ansatz as before, namely

$$R(x)=\mathrm{e}^{-\frac{2iMx\omega}{x-1}}\left(\frac{M}{1-x}\right)^{4iM\omega}\left(\frac{Mx}{2(1-x)}\right)^{-2iM\omega}\sum_{n=0}^{\infty}a(n)x^n. \tag{3.2.5}$$

The recursion coefficients are given by

$$\begin{cases}\alpha_n=(n+1)(n-4\mathrm{i}M\omega+1)\\ \beta_n=-\ell(\ell+1)-2n^2+n(16\mathrm{i}M\omega-2)+32M^2\omega^2+8\mathrm{i}M\omega+3\\ \gamma_n=n^2-8\mathrm{i}nM\omega-16M^2\omega^2-4.\end{cases} \tag{3.2.6}$$

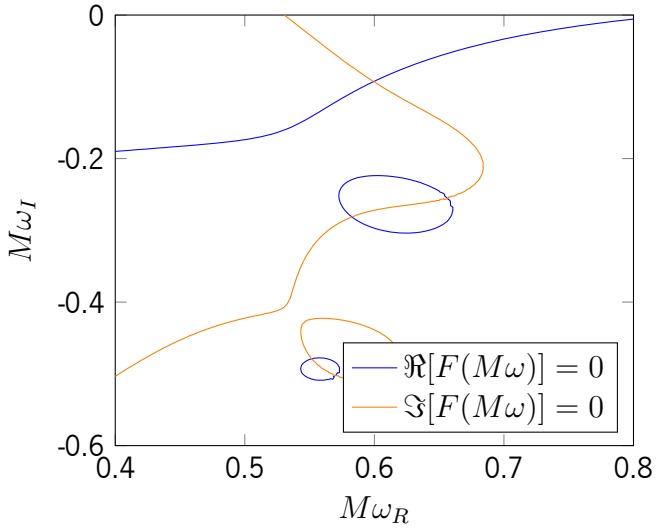

Figure 3.1: Contour plot for $\Re[F(M\omega)] = 0,\ \Im[F(M\omega)] = 0$ with $\ell = 3$.

3.2.2 Quasi-normal frequencies

From

$$F(M\omega) \equiv \frac{\beta_0}{\alpha_0} - \cfrac{\gamma_1}{\beta_1 - \cfrac{\alpha_1\gamma_2}{\beta_2 - \cfrac{\alpha_2\gamma_3}{\beta_3 - \ddots}}} = 0 \tag{3.2.7}$$

we can now obtain the values of ω as before, in table 3.1. A contour plot for equation $\Re[F(M\omega)] = 0$ and $\Im[F(M\omega)] = 0$ with $\ell = 3$ can be seen in figure 3.1. We too found solutions corresponding to the cases where $\ell = 0, 1$ but these solutions must be disregarded since, though $R(r)$ doesn't vanish for $\ell < 2$, equations (3.1.8) do vanish because the tensor harmonics vanish for such values of ℓ and we get no radiative perturbation for these modes.

A quick look into the data comparing gravitational and scalar quasi-normal modes shows that gravitational modes have less energy (ω_R) then scalar modes.

We have a similar situation to the quasi-normal modes found in section §2.4 which is expected since equation (3.2.3) is of the same form as equation (2.3.2), differing only on the spin term. A comparison

k	$\ell = 2$		$\ell = 3$		$\ell = 4$		$\ell = 5$	
	$M\omega_R$	$-M\omega_I$	$M\omega_R$	$-M\omega_I$	$M\omega_R$	$-M\omega_I$	$M\omega_R$	$-M\omega_I$
0	0.37367	0.08896	0.59944	0.09270	0.80918	0.09416	1.01230	0.09487
1	0.34671	0.27392	0.58264	0.28130	0.79663	0.28433	1.00222	0.28582
2	0.30105	0.47828	0.55169	0.47909	0.77271	0.47991	0.98270	0.48032

Table 3.1: Gravitational quasi-normal frequencies and overtones (200 iterations).

with the expressions obtained by Goebel (1972) is much more fitting now, since we are dealing with metric perturbations on a black hole geometry as well. Firstly we find there is a linear relationship between the angular momentum number ℓ and the frequency $M\omega_R$ as shown in figure 3.2a, whose slope[6] is close to the one predicted by Goebel (1972), $1/\left(3\sqrt{3}\right) \approx 0.1925$. If we just try to fit a linear function to points with $\ell \geq 20$ then we get the following equations

$$\begin{aligned} k = 0: &\quad M\omega_R = 0.19267\ell + 0.08 \\ k = 1: &\quad M\omega_R = 0.19273\ell + 0.08 \\ k = 2: &\quad M\omega_R = 0.19283\ell + 0.07, \end{aligned}$$

with $R^2 = 1$ up to the 6th decimal place. The slope is very close to $1/(3\sqrt{3})$, specially for the fundamental mode $k = 0$, in agreement with the analytical results.

Now since we are dealing with gravitational perturbations we can compare our numerical values of $M\omega_R$ for the fundamental mode $k = 0$ with the ones obtained using equation (2.4.7) in table 3.2. A plot showing the relative difference between the numerical and analytical values for the fundamental mode can be seen in figure 3.3. It must be kept in mind that equation (2.4.7) is only approximately valid in the geometrical optics limit, $\ell \geq 20$, so for small ℓ we expect greater differences between the numerical and analytical values. As we can see in Figure 3.3a, the relative difference decreases as ℓ increases which is expected because the approximation is only valid for $\ell \gg 1$. Yet even for values of ℓ close to $\ell = 2$, the difference is smaller than 25% decreasing abruptly for the next values of ℓ. For $\ell > 20$ the relative

[6]The linear functions were fitted to 49 points with $\ell = 2, 3, \ldots, 50$ for each overtone k with an average correlation coefficient of $R^2 = 0.99996$.

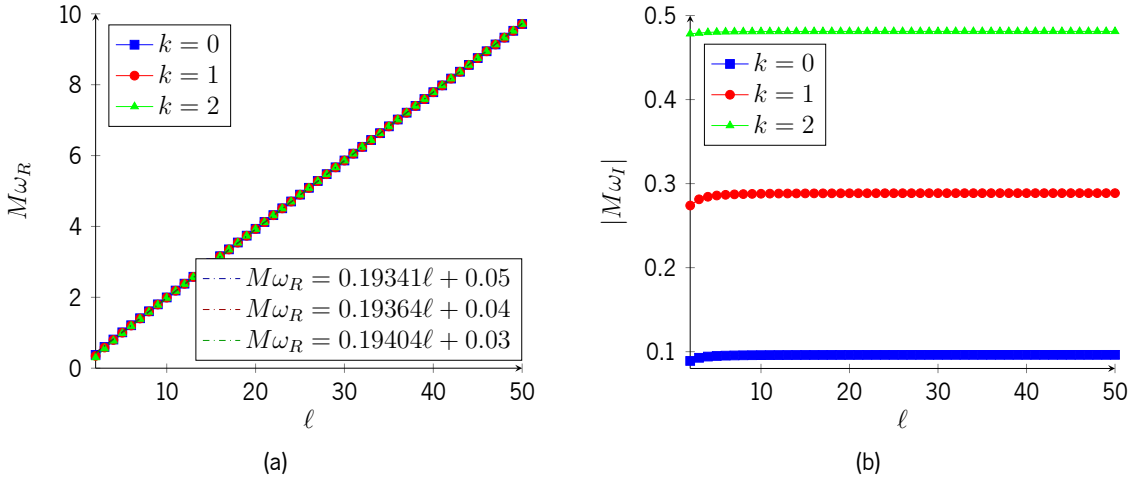

Figure 3.2: Gravitational quasi-normal frequencies

difference is already smaller than 0.3% meaning that our approximation is very good for large ℓ.

Comparing with section 2.4.2, we see that the scalar case has a slope value much closer to the theoretical prediction, $(3 \times 3^{1/2})^{-1} \approx 0.1925$. This may suggest that the spin of the gravitational perturbations produces another contribution not taken into account by standard trajectories equations. Perhaps due to the fact that here we have metric perturbations, the metric tensor here changes, unlike in the test scalar field case where the background geometry is indifferent to the the scalar field.

The imaginary part, Figure 3.3b, follows the same behavior as in the scalar case, which was discussed in section 2.4.2.

ℓ	Numerical	Analytical	Rel. Diff. (%)
2	0.374	0.481	22.266
3	0.599	0.674	11.072
4	0.809	0.866	6.585
5	1.012	1.058	4.391
10	1.997	2.021	1.174
15	2.967	2.983	0.536
20	3.933	3.945	0.310
30	5.862	5.870	0.132
40	7.788	7.794	0.080
50	9.714	9.719	0.049

Table 3.2: Relative difference $|((M\omega_R)_{\text{num}} - (M\omega_R)_{\text{analytic}})/(M\omega_R)_{\text{analytic}}| \times 100$ between analytical values, Goebel (1972), and numerical values for the fundamental mode.

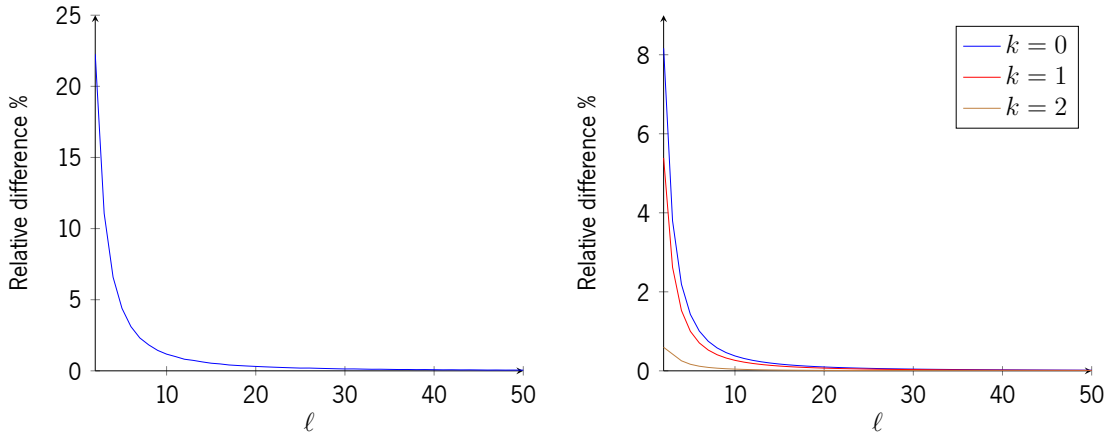

(a) Real part.

(b) Imaginary part.

Figure 3.3: Relative difference $|[(M\omega)_{\text{num}} - (M\omega)_{\text{analytic}}]/(M\omega)_{\text{analytic}}| \times 100$ between the numerical results for $k = 0$ and the obtained from the equations in Goebel (1972).

4 Test Scalar fields on Kerr Black Holes

4.1 The Klein-Gordon equation on Kerr spacetime

The metric of the Kerr geometry in Boyer-Lindquist (t, r, θ, ϕ) coordinates is given by

$$\mathrm{d}s^2 = -\frac{\Delta}{\rho^2}(\mathrm{d}t - a\sin^2\theta)^2 + \frac{\rho^2}{\Delta}\mathrm{d}r^2 + \frac{\sin^2\theta}{\rho^2}\left[a\mathrm{d}t - (r^2+a^2)\mathrm{d}\phi\right]^2 \tag{4.1.1}$$

where $\Delta \equiv r^2 - 2Mr + a^2$, $\rho^2 \equiv r^2 + a^2\cos^2\theta$ and $a \equiv J/M$ is the specific angular momentum, assuming the black hole rotates in the ϕ direction. We shall always consider that $a \geq 0$ no matter the sense of rotation of the black hole, since we just need to change coordinates $\phi \to -\phi$ which will result in the same line element as above. The inverse metric[1] is given by

$$\left(\frac{\partial}{\partial s}\right)^2 = -\frac{1}{\rho^2\Delta}\left[\left(r^2+a^2\right)\frac{\partial}{\partial t} + a\frac{\partial}{\partial\phi}\right]^2 + \frac{\Delta}{\rho^2}\left(\frac{\partial}{\partial r}\right)^2 + \frac{1}{\rho^2}\left(\frac{\partial}{\partial\theta}\right)^2 + \frac{1}{\rho^2\sin^2\theta}\left(\frac{\partial}{\partial\phi} + a\sin^2\theta\frac{\partial}{\partial t}\right)^2. \tag{4.1.2}$$

The d'Alembertian in these coordinates is given by

$$\Box = g^{tt}\frac{\partial^2}{\partial t^2} + 2g^{t\phi}\frac{\partial^2}{\partial t\partial\phi} + \frac{1}{\rho^2}\frac{\partial}{\partial r}\left(\rho^2 g^{rr}\frac{\partial}{\partial r}\right) + \frac{1}{\rho^2\sin\theta}\frac{\partial}{\partial\theta}\left(\rho^2\sin\theta g^{\theta\theta}\frac{\partial}{\partial\theta}\right) - g^{\phi\phi}\frac{\partial^2}{\partial\phi^2}. \tag{4.1.3}$$

Therefore the Klein-Gordon equation

$$\Box\Phi = \mu^2\Phi \tag{4.1.4}$$

[1] The symbol $\left(\frac{\partial}{\partial s}\right)^2$ is a shorthand notation for $\mathbf{g}^{-1} = g^{\mu\nu}\partial_\mu \otimes \partial_\nu$.

becomes

$$g^{tt}\frac{\partial^2\Phi}{\partial t^2}+2g^{t\phi}\frac{\partial^2\Phi}{\partial t\partial\phi}+\frac{1}{\rho^2}\frac{\partial}{\partial r}\left(\rho^2 g^{rr}\frac{\partial\Phi}{\partial r}\right)+\frac{1}{\rho^2\sin\theta}\frac{\partial}{\partial\theta}\left(\rho^2\sin\theta g^{\theta\theta}\frac{\partial\Phi}{\partial\theta}\right)-g^{\phi\phi}\frac{\partial^2\Phi}{\partial\phi^2}=\mu^2\Phi. \tag{4.1.5}$$

We can now separate the field as $\Phi(t,r,\theta,\phi)=\mathrm{e}^{-\mathrm{i}\omega t}\mathrm{e}^{\mathrm{i}m\phi}F(r,\theta)$, where $m\in\mathbb{Z}$, since the coordinate ϕ is defined between $\phi\in[0,2\pi[$, that is a cyclical coordinate, and if $\psi(\phi)=\mathrm{e}^{\mathrm{i}m\phi}$ then $\psi(0)=\psi(2\pi)$ meaning that

$$\begin{aligned}1&=\mathrm{e}^{\mathrm{i}m2\pi}\\ \Rightarrow 2\pi n&=2\pi m,\ n\in\mathbb{Z}.\end{aligned}$$

It then follows that m is a integer. Replacing our separated function in equation (4.1.5) then we get

$$\left(-g^{tt}\omega^2-g^{\phi\phi}m^2+2g^{t\phi}m\omega\right)\rho^2+\frac{1}{F}\frac{\partial}{\partial r}\left(\rho^2 g^{rr}\frac{\partial F}{\partial r}\right)+\frac{1}{F\sin\theta}\frac{\partial}{\partial\theta}\left(\rho^2\sin\theta g^{\theta\theta}\frac{\partial F}{\partial\theta}\right)=\mu^2\rho^2. \tag{4.1.6}$$

The equation can be again separated by making $F(r,\theta)=R(r)S(\theta)$ resulting in

$$\begin{aligned}&-a^2\sin^2\theta\,\omega^2-\frac{m^2}{\sin^2\theta}+\frac{1}{S(\theta)\sin\theta}\frac{\mathrm{d}}{\mathrm{d}\theta}\left(\sin\theta\frac{\mathrm{d}S(\theta)}{\mathrm{d}\theta}\right)-\mu^2a^2\cos^2\theta=\\ &\quad=-\frac{\left(r^2+a^2\right)^2}{\Delta}+2a\left(\frac{r^2+a^2}{\Delta}+1\right)m\omega-\frac{a^2}{\Delta}m^2-\frac{1}{R(r)}\left(\Delta\frac{\mathrm{d}R(r)}{\mathrm{d}r}\right)+\mu^2r\end{aligned} \tag{4.1.7}$$

and choosing $-\Lambda$ as a separation constant. In the end we have

$$\frac{1}{\sin\theta}\frac{\mathrm{d}}{\mathrm{d}\theta}\left(\sin\theta\frac{\mathrm{d}S(\theta)}{\mathrm{d}\theta}\right)+\left[a^2\cos^2\theta(\omega^2-\mu^2)-\frac{m^2}{\sin^2\theta}\right]S(\theta)=-\Lambda S(\theta) \tag{4.1.8}$$

$$\frac{\mathrm{d}}{\mathrm{d}r}\left(\Delta\frac{\mathrm{d}R(r)}{\mathrm{d}r}\right)+\left[\frac{\omega^2(r^2+a^2)^2+a^2m^2-4Mram\omega}{\Delta}-\omega^2a^2-\mu^2r^2\right]R(r)=\Lambda R(r). \tag{4.1.9}$$

4.2 Asymptotic solutions and boundary conditions

4.2.1 Near the horizon

Let us rewrite equation (4.1.9) as

$$\frac{\mathrm{d}}{\mathrm{d}r}\left(\Delta\frac{\mathrm{d}R(r)}{\mathrm{d}r}\right)+\left[\frac{\left(\omega(r^2+a^2)-am\right)^2+\Delta 2am\omega}{\Delta}-\omega^2a^2-\mu^2r^2-\Lambda\right]R(r)=0. \quad (4.2.1)$$

Let us define a new coordinate,

$$\mathrm{d}r^*=\left[\left(r^2+a^2\right)/\Delta\right]\mathrm{d}r \quad (4.2.2)$$

or explicitly

$$r^*=r+M\ln\Delta+\frac{M^2}{\sqrt{M^2-a^2}}\ln\left(\frac{r-r_+}{r-r_-}\right), \quad (4.2.3)$$

as a generalization of the Regge-Wheeler coordinate in Kerr spacetime, Teukolsky (1973). Then multiplying by Δ and performing the required chain rules on equation (4.2.1) we get

$$(r^2+a^2)^2\frac{\mathrm{d}^2R(r^*)}{\mathrm{d}r^{*2}}+\Delta 2r\frac{\mathrm{d}R(r^*)}{\mathrm{d}r^*}+\Big[\left(\omega(r^2+a^2)-am\right)^2+\Delta\left(2am\omega-\omega^2a^2-\mu^2r^2-\Lambda\right)\Big]R(r^*)=0. \quad (4.2.4)$$

In Kerr black holes the event horizon corresponds to the hypersurface of "radius"[2] $r_+=M+\sqrt{M^2-a^2}$, also known as the outer horizon. Now very close to the event horizon the previous equation becomes

$$4M^2r_+^2\frac{\mathrm{d}^2R(r^*)}{\mathrm{d}r^{*2}}\simeq-(am-2M\omega r_+)^2R(r^*) \quad (4.2.5)$$

which implies that

$$R(r^*)\sim\exp\left[-\mathrm{i}\left(\omega-\frac{am}{2Mr_+}\right)r^*\right] \quad (4.2.6)$$

[2] In Schwarzschild geometry a hypersurface of constant t and r coordinates has surface area equal to $4\pi r^2$, then we can associate r with the radius of such hypersurface which is a 2-sphere. In Kerr we don't have spherical symmetry and therefore the area of a hypersurface is $A(r)=\iint\sqrt{(r^2+a^2)^2-a^2\Delta\sin^2\theta}\sin\theta\,\mathrm{d}\phi\,\mathrm{d}\theta$ which at the horizon is $A(r_+)=4\pi\sqrt{(r_+^2+a^2)}$, meaning we cannot attach the same meaning of r as in the previous case. It can also be seen that in the limit $M\to 0$, the metric in (4.1.1) becomes Minkowski spacetime in ellipsoidal coordinates further strengthening the fact that r is not the radius of a surface. Nevertheless we shall keep referring it as the radial coordinate for lack of a better name.

where the minus solution was chosen since we want to impose that no waves come from the event horizon. Expanding r^* this results in

$$R(r) \sim (r - r_+)^{i\left[r_+\omega - \frac{am}{2M}\right]}$$

4.2.2 Far from source

Rewriting equation (4.2.1) as

$$\frac{\mathrm{d}^2R(r)}{\mathrm{d}r^2} + \frac{2(r-M)}{\Delta}\frac{\mathrm{d}R(r)}{\mathrm{d}r} + \left[\frac{\left(\omega(r^2+a^2) - am\right)^2 + \Delta 2am\omega}{\Delta^2} + \frac{-\omega^2a^2 - \mu^2r^2 - \Lambda}{\Delta}\right] R(r) = 0. \tag{4.2.7}$$

Bound states Far from the black hole at zeroth order the previous equation becomes

$$\frac{\mathrm{d}^2R(r)}{\mathrm{d}r^2} + (\omega^2 - \mu^2)R(r) \simeq 0 \tag{4.2.8}$$
$$\Rightarrow R(r) \sim \mathrm{e}^{-\sqrt{\mu^2-\omega^2}r}$$

where the minus solution was chosen since we want the state's wave function to decay at infinity. Also we make $\omega^2 < \mu^2$ in order to get bound states. At first order we have

$$\frac{\mathrm{d}^2R(r)}{\mathrm{d}r^2} + \frac{2}{r}\frac{\mathrm{d}R(r)}{\mathrm{d}r} + \left[\left(\omega^2 - \mu^2\right) + \frac{4M\omega^2 - 2\mu^2M}{r}\right] R(r) \simeq 0 \tag{4.2.9}$$

which results in

$$R(r) \sim \mathrm{e}^{-\sqrt{\mu^2-\omega^2}r} r^{-1-\chi} \tag{4.2.10}$$

where $\chi = (\mu^2M - 2M\omega^2)/\sqrt{\mu^2 - \omega^2}$.

Normal modes In order to get normal modes we must have a wave like behavior when $r \to \infty$ and thus we must impose $\omega^2 > \mu^2$. We will also consider $\mu = 0$. Then at infinity we get

$$R(r) \sim \mathrm{e}^{\mathrm{i}\omega r} r^{-1+\mathrm{i}2M\omega} \tag{4.2.11}$$

where we choose the positive sign in the exponential since we want outgoing waves.

4.3 Super-radiance

Let's consider a scalar field Φ with Lagrangian density

$$\mathcal{L} = \frac{1}{2}\partial_\mu \Phi \partial^\mu \Phi + \frac{1}{2}\mu^2 \Phi^2 \tag{4.3.1}$$

which must extremize the following action

$$S = \int \mathrm{d}^4x \sqrt{-g}\mathcal{L}. \tag{4.3.2}$$

Varying the action with respect to the field and setting $\delta S = 0$, it's easy to see from the Euler-Lagrange equations we get the usual Klein-Gordon equation

$$\Box\Phi = \mu^2\Phi.$$

Varying the action with respect to the metric we obtain the stress-energy tensor of the field whose components are given by

$$T_{\mu\nu} = \frac{-2}{\sqrt{-g}}\frac{\delta(\sqrt{-g}\mathcal{L})}{\delta g^{\mu\nu}} = \frac{1}{2}g_{\mu\nu}\left(\partial_\alpha\Phi\partial^\alpha\Phi + \mu^2\Phi^2\right) - \partial_\mu\Phi\partial_\nu\Phi. \tag{4.3.3}$$

By the local conservation of energy and momentum the stress-energy tensor $\mathbf{T}$ must obey the condition

$$\nabla\mathbf{T} = 0. \tag{4.3.4}$$

Contracting $\mathbf{T}$ with the timelike Killing vector $\vec{k} = \partial/\partial t$ we get an energy current[3] given by

$$j^\mu = T^\mu{}_\nu k^\nu = \frac{1}{2}k^\mu\left(\partial_\alpha\Phi\partial^\alpha\Phi + \mu^2\Phi^2\right) - \partial^\mu\Phi\partial_\nu\Phi k^\nu \tag{4.3.5}$$

which is conserved

$$\nabla_\mu j^\mu = \nabla_\mu\left(T^\mu{}_\nu\right)k^\nu + T^{\mu\nu}\nabla_\mu k_\nu = 0 \tag{4.3.6}$$

since the first term vanishes due to equation (4.3.4) and the second term vanishes as well, since $\vec{k}$ is a Killing vector, by Killing's equation $\nabla\vec{k}$ is anti-symmetric which when contracted with a symmetric tensor

[3] We can interpret j^0 as the energy density and j^i as the energy flux through a spacelike hypersurface with normal one-form $\tilde{\mathrm{d}}x^i$ far from the black hole.

gives zero. We can now integrate over the shaded region $\mathcal{S}$ in figure 4.1, bounded by the event horizon $\mathcal{N}$ (null hypersurface), by two spacelike hypersurfaces Σ_1 and Σ_2 and by a timelike surface at i_0 (unseen in the picture). Let's work out the special case where the Σs are Cauchy surfaces (basically an instant of time t). We have

$$\int_{\mathcal{S}} \mathrm{d}^4x\sqrt{-g}\nabla_\mu j^\mu = 0 \tag{4.3.7}$$

by Gauss' theorem

$$\int_{\partial\mathcal{S}} \mathrm{d}^3S\sqrt{-g}n_\mu j^\mu = 0$$

and since Σs are Cauchy surfaces

$$\underbrace{\int_{\Sigma_2} \mathrm{d}^3S\sqrt{-g}j^0}_{\text{density of energy} \times \text{volume} = \text{energy}} - \int_{\Sigma_1} \mathrm{d}^3S\sqrt{-g}j^0 + \underbrace{\int_{\text{at}\,\infty} \mathrm{d}^3S\sqrt{-g}\, n_\mu j^\mu}_{\text{energy that escaped to } \infty \text{ between } t=1 \text{ and } t=2} = -\int_{\mathcal{N}} \mathrm{d}^3S\sqrt{-g}n_\mu j^\mu \tag{4.3.8}$$

$$E_2 - E_1 + E_{\text{escaped}} = -\int_{\mathcal{N}} \mathrm{d}^3S\sqrt{-g}n_\mu j^\mu \tag{4.3.9}$$

where $E_1$and E_2 are the energies of the field at $t = t_1$ and $t = t_2$ respectively and $\vec{n}$ is the normal vector field to the hypersurfaces. As for $\int_{\mathcal{N}} \mathrm{d}^3S\sqrt{-g}n_\mu j^\mu$ it can be interpreted as the energy that went through the horizon. In the general case where the hypersurfaces Σs are generic spacelike surfaces we get

$$\int_{\Sigma_2} \mathrm{d}^3S\sqrt{-g}n_\mu j^\mu - \int_{\Sigma_1} \mathrm{d}^3S\sqrt{-g}n_\mu j^\mu + \int_{\text{at}\,\infty} \mathrm{d}^3S\sqrt{-g}\, n_\mu j^\mu = -\int_{\mathcal{N}} \mathrm{d}^3S\sqrt{-g}n_\mu j^\mu \tag{4.3.10}$$

$$E_2 - E_1 + E_{\text{escaped}} = -\int_{\mathcal{N}} \mathrm{d}^3S\sqrt{-g}n_\mu j^\mu \tag{4.3.11}$$

where in this case E_i is called the energy at Σ_i with $i = 1, 2$.

We can calculate the power lost to the black hole horizon. Let's consider that the points of our two spacelike surfaces are separated by a very small Δt. For simplicity, lets consider that Σ_i are Cauchy surfaces and that at infinity Φ and $\partial\Phi$ vanish so that $E_{\text{escaped}} = 0$. Then according to equation (4.3.9)

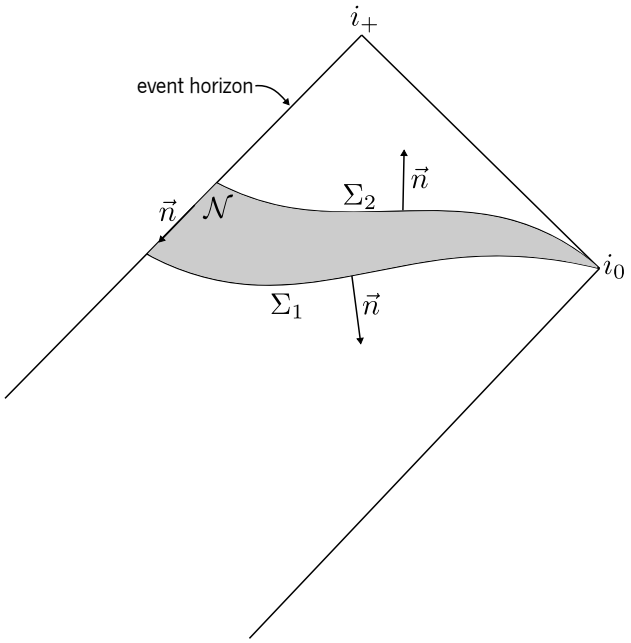

Figure 4.1: Conformal spacetime diagram of a piece of the Kerr geometry, adapted from Townsend (1997).

the power (energy by unit time) lost during Δt is

$$P = \lim_{\Delta t \to 0} \frac{E_{t+\Delta t} - E_t}{\Delta t} = \frac{\mathrm{d}E}{\mathrm{d}t} = -\frac{\mathrm{d}}{\mathrm{d}t} \int_{\mathcal{N}} \underbrace{\mathrm{d}^3 S \sqrt{-g}}_{\mathrm{d}A\,\mathrm{d}t} n_\mu j^\mu \tag{4.3.12}$$

$$\Rightarrow P = -\int_{\partial \mathcal{N}} \mathrm{d}A\, n_\mu j^\mu$$

where at the horizon $n_\mu = \xi_\mu$ defined by $\vec{\xi} = \partial_t + \Omega_H \partial_\phi$, where Ω_H is the angular velocity of the black hole given by $\Omega_H = a/(r_+^2 + a^2)$, see Townsend (1997). Then

$$P = -\int_{\partial \mathcal{N}} \mathrm{d}A\, \xi_\mu j^\mu \tag{4.3.13}$$

and since $\xi_\mu k^\mu = 0$ at the horizon

$$\begin{aligned} &= \int_{\partial \mathcal{N}} \mathrm{d}A\, k^\nu \xi_\mu \partial^\mu \Phi \partial_\nu \Phi \\ &= \int_{\partial \mathcal{N}} \mathrm{d}A \left(\frac{\partial \Phi}{\partial t} + \Omega_H \frac{\partial \Phi}{\partial \phi} \right) \frac{\partial \Phi}{\partial t}. \end{aligned} \tag{4.3.14}$$

Given a field like in section §4.1 of the form $\Phi = \Re\left[F(r,\theta)\mathrm{e}^{-\mathrm{i}\omega t}\mathrm{e}^{\mathrm{i}m\phi}\right] = F(r,\theta)\cos(\omega t - m\phi)$

we have

$$P = \omega(\omega - m\Omega_H) \int_{\partial\mathcal{N}} \mathrm{d}A\, F^2(r,\theta) \sin^2(\omega t - m\phi). \tag{4.3.15}$$

The time average of the power lost is given by

$$\begin{aligned} \langle P \rangle &= \omega(\omega - m\Omega_H) \frac{\omega}{2\pi} \int_0^{2\pi/\omega} \int_{\partial\mathcal{N}} \mathrm{d}t\, \mathrm{d}A\, F^2(r,\theta) \sin^2(\omega t - m\phi) \\ &= \frac{1}{2}\omega(\omega - m\Omega_H) \underbrace{\int_{\partial\mathcal{N}} \mathrm{d}A\, F^2(r,\theta)}_{>0}. \end{aligned} \tag{4.3.16}$$

Therefore there are situations where $\langle P \rangle < 0$ which we call super-radiant modes of the field. This happens when

$$0 < \omega < m\Omega_H, \tag{4.3.17}$$

meaning that states with $m = 0$ can't be super-radiant modes of a scalar field.

We will see below that our boundary conditions will force our scalar field to have a complex frequency $\omega = \omega_R + \mathrm{i}\omega_I$

$$\Phi(x^\mu) = F(r,\theta)\mathrm{e}^{-\mathrm{i}\omega_R t}\mathrm{e}^{\omega_I t}\mathrm{e}^{\mathrm{i}m\phi}. \tag{4.3.18}$$

If we also generalize our field to be complex (for the sake of generality), its stress energy tensor is given by

$$T_{\mu\nu} = -\partial_{(\mu}\Phi^*\partial_{\nu)}\Phi + \frac{1}{2}g_{\mu\nu}(\partial_\alpha\Phi^*\partial^\alpha\Phi - m^2\Phi^*\Phi). \tag{4.3.19}$$

The conserved current is

$$j^\mu = -\frac{1}{2}(\partial^\mu\Phi^*\partial_\nu\Phi + \partial_\nu\Phi^*\partial^\mu\Phi)k^\nu + \frac{1}{2}k^\mu(\partial_\alpha\Phi^*\partial^\alpha\Phi - m^2\Phi^*\Phi). \tag{4.3.20}$$

Then the power lost becomes

$$\begin{aligned} P &= \int_{\partial\mathcal{N}} \left[\partial_0\Phi^*\partial_0\Phi + \frac{1}{2}\Omega_H\left(\partial_\phi\Phi^*\partial_0\Phi + \partial_0\Phi^*\partial_\phi\Phi\right)\right] \mathrm{d}A \\ &= \int_{\partial\mathcal{N}} \underbrace{|F(r,\theta)|^2\mathrm{e}^{2\omega_I t}}_{>0}[\omega_I^2 + \omega_R(-m\Omega_H + \omega_R)]\, \mathrm{d}A. \end{aligned} \tag{4.3.21}$$

In order to get $P < 0$ we must have

$$\omega_I^2 + \omega_R(-m\Omega_H + \omega_R) < 0$$

or

$$0 < \frac{|\omega|^2}{\omega_R} < m\Omega_H. \tag{4.3.22}$$

When $|\omega_I| \ll \omega_R$ the previous condition reduces to (4.3.17).

We can solve equation (4.3.13) for the values of ω instead of solving an inequality. Let's obtain an expression for the first term assuming Σ is a Cauchy surface

$$\begin{aligned} P \equiv \frac{\mathrm{d}E}{\mathrm{d}t} &= \frac{\mathrm{d}}{\mathrm{d}t}\int_\Sigma \mathrm{d}^3x\sqrt{-g}j^0 \\ &= \frac{\mathrm{d}}{\mathrm{d}t}\int_\Sigma \mathrm{d}^3x\sqrt{-g}(g^{00}j_0 + g^{0\phi}j_\phi) \end{aligned} \tag{4.3.23}$$

the derivative becomes ∂_0 inside the integral by Leibniz's integral rule and commutes with all other ∂ so

$$= \int_\Sigma \mathrm{d}^3x\sqrt{-g}\partial_0 \mathrm{e}^{2\omega_I t}\,[\cdots]$$

taking the exponential out of the derivatives from both Φ and Φ^*

$$= 2\omega_I \int_\Sigma \mathrm{d}^3x\sqrt{-g}j^0 \tag{4.3.24}$$

where $\mathrm{d}^3x \equiv \mathrm{d}r\,\mathrm{d}\theta\,\mathrm{d}\phi$. Now equation (4.3.13) can be written as

$$\begin{aligned} 2\omega_I \int_\Sigma \mathrm{d}^3x\sqrt{-g}j_0 &= [\omega_I^2 + \omega_R(-m\Omega_H + \omega_R)] \int_{\partial\mathcal{N}} \underbrace{|F(r,\theta)|^2 \mathrm{e}^{2\omega_I t}}_{>0}\,\mathrm{d}A \\ \omega_I &= [\omega_I^2 + \omega_R(-m\Omega_H + \omega_R)] \frac{\int_{\partial\mathcal{N}} |F(r,\theta)|^2 \mathrm{e}^{2\omega_I t}\,\mathrm{d}A}{2\int_\Sigma \mathrm{d}^3x\sqrt{-g}j^0}. \end{aligned} \tag{4.3.25}$$

It follows from equation (4.3.25) that ω_I is positive every time the condition $-m\Omega_H + \omega_R < 0$ is obeyed (when $\omega_I \ll \omega_R$). There will be a super-radiant scalar field mode, where the mode grows exponentially. A word must be said about the integral terms. The integral $\int_{\partial\mathcal{N}} |F(r,\theta)|^2 \mathrm{e}^{2\omega_I t}\,\mathrm{d}A$ is proportional to $R(r_+)$ since the angular integral only contributes with an overall constant factor and we know that $F(r,\theta) = R(r)S(\theta)$ and it is always positive. . But the R function which will be integrated in $\int_\Sigma \mathrm{d}^3x\sqrt{-g}j_0$, for bound and normal states differ in the normalization of the functions, namely the normal modes radial function is not normalizable[4] whereas in the bound state case that indeed is the case. Also the integral $\int_\Sigma \mathrm{d}^3x\sqrt{-g}j^0$ must be greater than zero and such is the case, shown in Dolan (2007).

[4]Similar to the fact that in elementary quantum mechanics a free wave is not normalizable.

Could this super-radiant instability cause the Kerr black hole to be unstable against scalar perturbations as the field grows? In our test field approximation our scalar field is very weak ($\Phi(x^\mu) = \epsilon\Xi(x^\mu),\ \epsilon \ll 1$, where Ξ is a scalar function) so its contribution to the stress-energy tensor (4.3.19) is of order $\mathcal{O}(\epsilon^2)$, which implies that for a test scalar field the vacuum Einstein equation is a very good approximation. But as the field grows the test field approximation breaks down and we must take the stress-energy tensor of the field into consideration. Such back-reaction of the field on the geometry will eventually slow down the black hole, until we get a stationary situation accompanied by emission of gravitational waves. Such waves could then be detected on Earth by detectors like LIGO, offering evidence of the existence of such scalar fields around Kerr black holes. If the scalar field is complex, however, there are exact (albeit numerical) solutions of the Einstein-complex-Klein Gordon system describing stationary black holes in equilibrium with the scalar cloud without emission of gravitational waves, Herdeiro and Radu (2014).

4.4 Quasi-bound states

4.4.1 Recursion coefficients

Let us begin with the angular equation. Making $u = \cos\theta$ we get

$$(1-u^2)\frac{\mathrm{d}^2S(u)}{\mathrm{d}u^2} - 2u\frac{\mathrm{d}S(u)}{\mathrm{d}u} + \left[a^2u^2(\omega^2-\mu^2) + \Lambda - \frac{m^2}{1-u^2}\right]S(u) = 0. \tag{4.4.1}$$

Furthermore we demand that $S(u)$ is finite at the singular points $u = \pm 1$, that is when $\theta = 0, \pi$ so we propose the ansatz given in Leaver (1985)

$$S(u) = \mathrm{e}^{au\sqrt{\omega^2-\mu^2}}(1+u)^k(1-u)^k\sum_{n=0}^{\infty} b_n(1+u)^n \tag{4.4.2}$$

where $k = \frac{1}{2}|m|$. Again, making the replacement $x = 1+u$, we can now replace $S(u)$ in equation (4.4.1) where we find that our series coefficients must satisfy the following conditions

$$\alpha_0^\theta b_1 + \beta_0^\theta a_0 = 0 \tag{4.4.3}$$

and

$$\alpha_n^\theta b_{n+1} + \beta_n^\theta b_n + \gamma_n^\theta b_{n-1} = 0, \quad n \geq 1 \tag{4.4.4}$$

where

$$\begin{cases} \alpha_n^\theta = 2(n+1)(2k+n+1) \\ \beta_n^\theta = k(4a\sqrt{\omega^2-\mu^2} - 4n - 2) + n(4a\sqrt{\omega^2-\mu^2} - 1) + \\ \qquad a\sqrt{\omega^2-\mu^2}(a\sqrt{\omega^2-\mu^2} + 2) - 4k^2 + \Lambda - n^2 \\ \gamma_n^\theta = -2a\sqrt{\omega^2-\mu^2}(2k+n) \end{cases} \tag{4.4.5}$$

where $\gamma_0 = 0$.

For the radial equation we propose the following ansatz found in Dolan (2007)

$$R(r) = (r-r_+)^{-\mathrm{i}\sigma}(r-r_-)^{-\mathrm{i}\sigma+\chi-1}\mathrm{e}^{-r\sqrt{\mu^2-\omega^2}} \sum_{n=0}^{\infty} d_n \left(\frac{r-r_+}{r-r_-}\right)^n, \tag{4.4.6}$$

where $\sigma = (2M\omega r_+ - am)/b$, with $b = 2\sqrt{M^2-a^2}$ and $\chi = -(\mu^2 - 2\omega^2)M/\sqrt{\mu^2-\omega^2}$, which obeys the required boundary conditions. We again find that our series coefficients must satisfy the following

$$\alpha_0^r d_1 + \beta_0^r d_0 = 0 \tag{4.4.7}$$

$$\alpha_n^r d_{n+1} + \beta_n^r d_n + \gamma_n^r d_{n-1} = 0, \quad n \geq 1. \tag{4.4.8}$$

where

$$\begin{cases} \alpha_0^r = \dfrac{2iam + b - 2iM\omega(b+2M)}{b} \\ \beta_0^r = \dfrac{4M^2\omega(2M\omega+i)}{b} - \dfrac{1}{\sqrt{\mu^2-\omega^2}}\Big[M^2\left(\mu^2\left(\sqrt{\mu^2-\omega^2} - 6i\omega\right) + \omega^2\left(-7\sqrt{\mu^2-\omega^2} + 8i\omega\right)\right) \\ \quad +M\left(-2i\omega\sqrt{\mu^2-\omega^2} + \mu^2 - 2\omega^2\right) + \sqrt{\mu^2-\omega^2}(\Lambda+1)\Big] \end{cases} \tag{4.4.9}$$

$$
\begin{cases}
\alpha_n^r = \dfrac{(n+1)(2iam+bn+b)-2iM\omega(bn+b+2M+n)}{b} \\
\beta_n^r = \dfrac{4M^2\omega(2M\omega+i)}{b} - \dfrac{1}{\sqrt{\mu^2-\omega^2}}\left[M^2\left(\mu^2\left(\sqrt{\mu^2-\omega^2}-6i\omega\right)+\omega^2\left(-7\sqrt{\mu^2-\omega^2}+8i\omega\right)\right)+\right. \\
\quad \left. M(2n+1)\left(-2i\omega\sqrt{\mu^2-\omega^2}+\mu^2-2\omega^2\right)+\sqrt{\mu^2-\omega^2}(\Lambda+2n(n+1)+1)\right] \\
\gamma_n^r = \dfrac{1}{b(\mu^2-\omega^2)^{3/2}}\left[2am(\mu^2-\omega^2)\left(iM\left(\mu^2-2\omega^2\right)+2M\omega\sqrt{\mu^2-\omega^2}+in\sqrt{\mu^2-\omega^2}\right)+\right. \\
\quad b\left\{12i\mu^2M^3\omega^3+M^2\left(-4\mu^2\omega^2\sqrt{\mu^2-\omega^2}+\mu^4\left(\sqrt{\mu^2-\omega^2}-2i\omega\right)+4\omega^4\left(\sqrt{\mu^2-\omega^2}-i\omega\right)\right)+\right. \\
\quad 2Mn(\mu^2-\omega^2)\left(\mu^2+\omega\left(-2\omega-i\sqrt{\mu^2-\omega^2}\right)\right)+n^2(\mu^2-\omega^2)^{3/2}\Big\}+ \\
\quad 2M\omega\left\{M^2\left(-4\mathrm{i}\omega^4+2\mu^2\omega\left(-2\sqrt{\mu^2-\omega^2}+3i\omega\right)-2i\mu^4\right)+\right. \\
\quad \left.\left.\omega^3\sqrt{\mu^2-\omega^2}-2iMn(\mu^2-\omega^2)^{3/2}\right\}\right].
\end{cases}
\tag{4.4.10}
$$

4.4.2 Quasi-bound frequencies

Just like in the previous chapters, we want the quasi-bound frequencies ω of our states. So again we use Leaver's continued fraction method. In the present case, however, the situation is different because the angular equation depends on ω and that gives rise to a coupled system between Λ and ω which we must solve for the two parameter at the same time.

From the conditions (4.4.3) and (4.4.4) we can write

$$
\frac{\beta_0^\theta}{\alpha_0^\theta} = -\frac{b_1}{b_0} \tag{4.4.11}
$$

which allows us to write

$$
F(\Lambda,\omega) \equiv \frac{\beta_0^\theta}{\alpha_0^\theta} - \cfrac{\gamma_1^\theta}{\beta_1^\theta - \cfrac{\alpha_1^\theta\gamma_2^\theta}{\beta_2^\theta - \cfrac{\alpha_2^\theta\gamma_3^\theta}{\beta_3^\theta - \ddots}}} = 0. \tag{4.4.12}
$$

Similarly we can also write a continued fraction for the coefficients of the radial equation (4.4.4)

$$G(\Lambda,\omega)\equiv\frac{\beta_0^r}{\alpha_0^r}-\cfrac{\gamma_1^r}{\beta_1^r-\cfrac{\alpha_1^r\gamma_2^r}{\beta_2^r-\cfrac{\alpha_2^r\gamma_3^r}{\beta_3^r-\ddots}}}=0. \tag{4.4.13}$$

We can in principle solve the system of equations above by using numerical root finding methods. The values of the frequency are given in tables 4.1, 4.2 and 4.4. The values were obtained with 200 iterations of the infinite continued fraction.

Just like in the Schwarzschild case, ω_R increases with $M\mu$ since, as the distance from the black hole decreases, the particle must rotate faster in order to avoid being swallowed by the black hole. However here $M\mu$ isn't the ratio of the particle's Compton wavelength with the black hole radius (divided by two), since the radius of the black hole is $r_+ = M + \sqrt{M^2 - a^2}$. However considering $r_+ = r_+(M)$ we can see that the function $r_+(M)$ is monotonically increasing, so qualitatively the same considerations given in section 2.3.2 apply, namely that the energy increases with $M\mu$, see Table 4.1. The energy also increases with the angular momentum number ℓ as expected. Just like before, for small black holes or large Compton wavelengths ω_I will decrease in absolute value, meaning that the field will survive longer. Physically it corresponds to a loosely bound field, barely affected by the gravitational field.

In Table 4.2 we see that the frequency increases with m so we get a larger value for energy ω_R when $m = \ell$. This is expected because the particle travels in the same directions as the rotation of the black hole and its velocity is increased due to the dragging caused by the black hole, increasing the particle's energy. As for ω_I, it decreases as m increases. This is probably due to a particle traveling in the opposite direction of the black hole's rotation, is dragged by the black hole rotating in the opposite direction. Thus the particle slows down and it is more difficult for it not to fall in the hole. Therefore it won't remain in orbit for a very long time, quickly being absorbed by the black hole.

As seen in section §4.3 in order to have super-radiant modes their frequency must obey inequality (4.3.22). In fact since the values of our imaginary parts of the frequency are so small we are well justified in using inequality (4.3.17) as a very good approximation to (4.3.22) so we can use it to check if a mode

$M\mu$	$\ell = 0$		$\ell = 1$		$\ell = 2$		$\ell = 3$	
	$M\omega_R$	$-M\omega_I$	$M\omega_R$	$-M\omega_I$	$M\omega_R$	$-M\omega_I$	$M\omega_R$	$-M\omega_I$
0.1	0.09945	$1.51 \cdot 10^{-05}$	0.09987	$1.10 \cdot 10^{-11}$	0.09994	$7.18 \cdot 10^{-16}$	0.09998	$4.84 \cdot 10^{-18}$
0.2	0.19506	$1.51 \cdot 10^{-03}$	0.19895	$3.49 \cdot 10^{-08}$	0.19955	$3.45 \cdot 10^{-14}$	0.19984	$5.03 \cdot 10^{-15}$
0.3	0.28697	$9.79 \cdot 10^{-03}$	0.29619	$8.52 \cdot 10^{-06}$	0.29844	$3.73 \cdot 10^{-11}$	0.29914	$-2.18 \cdot 10^{-14}$
0.4	0.37933	$2.56 \cdot 10^{-02}$	0.38956	$5.37 \cdot 10^{-04}$	0.39619	$9.36 \cdot 10^{-09}$	0.39793	$3.45 \cdot 10^{-14}$
0.5	0.47388	$4.74 \cdot 10^{-02}$	0.47750	$5.51 \cdot 10^{-03}$	0.49220	$1.03 \cdot 10^{-06}$	0.49588	$8.83 \cdot 10^{-12}$
0.6	0.57112	$7.39 \cdot 10^{-02}$	0.56360	$1.78 \cdot 10^{-02}$	0.58543	$6.16 \cdot 10^{-05}$	0.59269	$1.15 \cdot 10^{-09}$
0.7	0.67930	$2.94 \cdot 10^{-02}$	0.65055	$3.64 \cdot 10^{-02}$	0.67387	$1.41 \cdot 10^{-03}$	0.68798	$9.28 \cdot 10^{-08}$
0.8	0.77550	$4.21 \cdot 10^{-02}$	0.73925	$6.02 \cdot 10^{-02}$	0.75774	$8.00 \cdot 10^{-03}$	0.78118	$5.05 \cdot 10^{-06}$

Table 4.1: Quasi-bound frequencies for $a = 0.4M$ with $m = 0$.

m	$\ell=0$		$\ell=1$		$\ell=2$		$\ell=3$	
	$M\omega_R$	$-M\omega_I$	$M\omega_R$	$-M\omega_I$	$M\omega_R$	$-M\omega_I$	$M\omega_R$	$-M\omega_I$
-3	——	——	——	——	——	——	0.29914	$1.29 \cdot 10^{-13}$
-2	——	——	——	——	0.29844	$-2.86 \cdot 10^{-10}$	0.29914	$1.30 \cdot 10^{-13}$
-1	——	——	0.29614	$2.14 \cdot 10^{-5}$	0.29844	$1.10 \cdot 10^{-10}$	0.29914	$-8.93 \cdot 10^{-14}$
0	0.28697	$9.79 \cdot 10^{-3}$	0.29619	$8.52 \cdot 10^{-6}$	0.29844	$3.79 \cdot 10^{-11}$	0.29914	$6.07 \cdot 10^{-16}$
1	——	——	0.29624	$2.66 \cdot 10^{-6}$	0.29845	$1.08 \cdot 10^{-11}$	0.29945	$5.94 \cdot 10^{-16}$
2	——	——	——	——	0.29845	$2.48 \cdot 10^{-12}$	0.29914	$2.08 \cdot 10^{-17}$
3	——	——	——	——	——	——	0.29945	$-1.66 \cdot 10^{-15}$

Table 4.2: Quasi-bound frequencies for $a = 0.4M$ with and $M\mu = 0.3$.

a/M	0.2	0.4	0.6	0.8	0.9	0.99
$M\Omega_H$	0.06758	0.14119	0.23077	0.36364	0.48083	0.77215

Table 4.3: Maximum real frequency for a mode to be super-radiant.

is supposed to be super-radiant. Physically, if $\omega_I > 0$, we have a super-radiant instability, where the field grows exponentially (positive ω_I) which won't happen for normal modes. In Table 4.4 we can see that when $\omega_R < m\Omega_H$ the imaginary part of the frequency is indeed positive, confirming our theoretical expectations. We must remark that although we can see two or three positive values for ω_I in tables 4.1 and 4.2 those values must be due to numerical inaccuracies, since there are no super-radiant modes for $m = 0$. We shall point out these unexpected results by using a different color. For reference in Table 4.3, we give the value of $m\Omega_H$ as a function of a for better comparison with the values of Table 4.4[5] and Table 4.5.

Let's now see if such instabilities can be detected at our time scale. From Table 4.5 we see that the strongest instability happens when $M\mu = 0.4$, $a = 0.99M$ and $\ell = 1 = m$. That corresponds to an e-folding time of $\tau = 7.58 \times 10^6 GM/c^3\,\mathrm{s}$. For a solar mass black hole we have $\tau \approx 18\,\mathrm{s}$, which means that we should see such instabilities developing in astrophysical black holes. However, there is a price to pay. For solar mass black holes we had to find a particle with a mass around $10^{-10}\,\mathrm{eV}$ which is much smaller than the lightest know particle ($m_{\mathrm{neutrino}} \lesssim 0.120\,\mathrm{eV}$). Obviously, for supermassive black holes the situation is even worse since we needed a field with $m_{\mathrm{particle}} \sim 10^{-20}\,\mathrm{eV}$. But could there be stronger instabilities for $M\mu \gg 1$? According to Zouros and Eardley (1979), for $M\mu \gg 1$

$$M\omega_I = 10^{-7}\exp(-1.84M\mu) \tag{4.4.14}$$

which results in very large e-folding times. In fact the maximum instability is located around $M\mu \approx 0.42$ for $\ell = m = 1$, see Dolan (2007).

Let's consider a light boson like the π_0, which has a mass of $134.97\,\mathrm{MeV}$. In order to have $M\mu = 0.4$ we have two alternatives: either we find a black hole with $M \sim 10^{11}\,\mathrm{kg}$, (which is around the mass

[5] It was not possible to obtain accurate values for $M\mu < 0.4$ due to problems in the root finding algorithm.

a	$M\mu = 0.4$		$M\mu = 0.5$	
	$M\omega_R$	$M\omega_I$	$M\omega_R$	$M\omega_I$
0	0.39619	$1.1704 \cdot 10^{-08}$	0.49220	$1.2271 \cdot 10^{-06}$
$0.2M$	0.39620	$-3.67 \cdot 10^{-09}$	0.49225	$-4.11 \cdot 10^{-07}$
$0.4M$	0.39621	$-7.73 \cdot 10^{-10}$	0.49230	$-9.68 \cdot 10^{-08}$
$0.6M$	0.39622	$-6.22 \cdot 10^{-11}$	0.49235	$-1.12 \cdot 10^{-08}$
$0.8M$	0.39624	$2.33 \cdot 10^{-11}$	0.49240	$5.35 \cdot 10^{-11}$
$0.9M$	0.39624	$3.13 \cdot 10^{-11}$	0.49242	$3.04 \cdot 10^{-10}$
$0.99M$	0.39624	$3.49 \cdot 10^{-11}$	0.49244	$3.64 \cdot 10^{-10}$

a	$M\mu = 0.6$		$M\mu = 0.7$		$M\mu = 0.8$	
	$M\omega_R$	$M\omega_I$	$M\omega_R$	$M\omega_I$	$M\omega_R$	$M\omega_I$
0	0.58542	$-7.00 \cdot 10^{-05}$	0.67386	$-1.50 \cdot 10^{-03}$	0.75789	$-8.15 \cdot 10^{-03}$
$0.2M$	0.58568	$-2.58 \cdot 10^{-05}$	0.67462	$-7.58 \cdot 10^{-04}$	0.75805	$-5.83 \cdot 10^{-03}$
$0.4M$	0.58591	$-6.83 \cdot 10^{-06}$	0.67549	$-2.70 \cdot 10^{-04}$	0.75886	$-3.40 \cdot 10^{-03}$
$0.6M$	0.58612	$-9.77 \cdot 10^{-07}$	0.67631	$-5.16 \cdot 10^{-05}$	0.76053	$-1.24 \cdot 10^{-03}$
$0.8M$	0.58629	$-2.42 \cdot 10^{-08}$	0.67698	$-2.20 \cdot 10^{-06}$	0.76281	$-1.16 \cdot 10^{-04}$
$0.9M$	0.58638	$1.44 \cdot 10^{-09}$	0.67726	$-5.06 \cdot 10^{-08}$	0.76380	$-6.15 \cdot 10^{-06}$
$0.99M$	0.58645	$2.06 \cdot 10^{-09}$	0.67748	$7.84 \cdot 10^{-09}$	0.76450	$2.15 \cdot 10^{-08}$

Table 4.4: Quasi-bound frequencies as a approaches the extreme limit $a \to M$, with $\ell = 2$ and $m = 2$.

a	$M\mu = 0.4$		$M\mu = 0.5$	
	$M\omega_R$	$M\omega_I$	$M\omega_R$	$M\omega_I$
0	0.38956	$5.6274 \cdot 10^{-04}$	0.47759	$5.5442 \cdot 10^{-03}$
$0.2M$	0.38972	$-3.78 \cdot 10^{-04}$	0.47738	$-4.68 \cdot 10^{-03}$
$0.4M$	0.38991	$-2.20 \cdot 10^{-04}$	0.47727	$-3.68 \cdot 10^{-03}$
$0.6M$	0.39012	$-9.80 \cdot 10^{-05}$	0.47734	$-2.52 \cdot 10^{-03}$
$0.8M$	0.39033	$-2.25 \cdot 10^{-05}$	0.47777	$-1.20 \cdot 10^{-03}$
$0.9M$	0.39044	$-4.41 \cdot 10^{-06}$	0.47824	$-5.14 \cdot 10^{-04}$
$0.99M$	0.39052	$1.32 \cdot 10^{-07}$	0.47895	$-1.97 \cdot 10^{-05}$

a	$M\mu = 0.6$		$M\mu = 0.7$		$M\mu = 0.8$	
	$M\omega_R$	$M\omega_I$	$M\omega_R$	$M\omega_I$	$M\omega_R$	$M\omega_I$
0	0.56381	$-1.77 \cdot 10^{-02}$	0.65075	$-3.61 \cdot 10^{-02}$	0.73930	$-5.95 \cdot 10^{-02}$
$0.2M$	0.56238	$-1.66 \cdot 10^{-02}$	0.64778	$-3.53 \cdot 10^{-02}$	0.73466	$-5.98 \cdot 10^{-02}$
$0.4M$	0.56081	$-1.51 \cdot 10^{-02}$	0.64426	$-3.44 \cdot 10^{-02}$	0.72906	$-6.03 \cdot 10^{-02}$
$0.6M$	0.55905	$-1.32 \cdot 10^{-02}$	0.63984	$-3.30 \cdot 10^{-02}$	0.72182	$-6.09 \cdot 10^{-02}$
$0.8M$	0.55699	$-1.02 \cdot 10^{-02}$	0.63361	$-3.08 \cdot 10^{-02}$	0.71121	$-6.23 \cdot 10^{-02}$
$0.9M$	0.55580	$-7.93 \cdot 10^{-03}$	0.62889	$-2.93 \cdot 10^{-02}$	0.70322	$-6.46 \cdot 10^{-02}$
$0.99M$	0.55429	$-4.56 \cdot 10^{-03}$	0.62219	$-2.87 \cdot 10^{-02}$	0.76237	$-2.79 \cdot 10^{-02}$

Table 4.5: Quasi-bound frequencies as a approaches the extreme limit $a \to M$, with $\ell = 1$ and $m = 1$.

proposed for the hypothetical primordial black holes) or we find an ultralight boson in nature and detect its gravitational wave imprint caused by its back-reaction on the black hole.

Now we just need to see how the algorithm behaves as a and the number of iterations change, since in the previous chapters we have seen how it behaved for different values of ℓ and μ, see Table 4.6. Once again it is the imaginary part of the frequency that is most affected by the number of iterations of the infinite continued fraction. Yet now we see that when $a \to M$ our values become more dependent on the number of iterations. This happens because the term $\sum_n d_n \left[(r - r_+)/(r - r_-)\right]^n$ in equation (4.4.6) becomes $\sum_n d_n$ yielding a meaningless solution to the differential equation, since both horizons become one at the extreme limit $r_+ = r_-$. More recursions help getting more precise values at the cost of a longer computational time.

4.4.2.1 Comparison with analytical approximations

From Baumann *et al.* (2019) we have the following analytical expressions for the real and imaginary parts of the frequency given by

$$M\omega_R = M\mu\left[1 - \frac{a^2}{2n^2} - \frac{a^4}{8n^4} + \frac{f_{n\ell}}{n^3}(M\mu)^4 + \frac{h_\ell}{n^3}\frac{a}{M}m(M\mu)^5\right] \tag{4.4.15}$$

where

$$f_{n\ell} = -\frac{6}{2\ell+1} + \frac{2}{n}, \text{ and} \qquad\qquad h_\ell = \frac{16}{2\ell(2\ell+1)(2\ell+2)}.$$

For the imaginary part we have

$$M\omega_I = 2\left(1 - \sqrt{1-(a/M)^2}\right) C_{n\ell} g_{\ell m}(Mm\Omega_H - \omega)(M\mu)^{4\ell+5} \tag{4.4.16}$$

where

$$C_{n\ell} = \frac{2^{4\ell+1}(n+\ell)!}{n^{2\ell+4}(n-\ell-1)!}\left[\frac{\ell!}{(2\ell)!(2\ell+1)!}\right]^2$$

and

$$g_{\ell m} = \prod_{k=1}^{\ell}\left[k^2(1-(a/M)^2 + \left(\frac{a}{M} - 2r_+\omega^2\right)\right].$$

a	50		100	
	$M\omega_R$	$M\omega_I$	$M\omega_R$	$M\omega_I$
$0.2M$	0.492251	$-4.1129 \cdot 10^{-07}$	0.492251	$-4.1129 \cdot 10^{-07}$
$0.4M$	0.492304	$-9.6844 \cdot 10^{-08}$	0.492304	$-9.6844 \cdot 10^{-08}$
$0.6M$	0.492353	$-1.1243 \cdot 10^{-08}$	0.492353	$-1.1243 \cdot 10^{-08}$
$0.8M$	0.492399	$5.3525 \cdot 10^{-11}$	0.492399	$5.3551 \cdot 10^{-11}$
$0.9M$	0.492421	$2.9619 \cdot 10^{-10}$	0.492421	$3.0411 \cdot 10^{-10}$
$0.99M$	0.492441	$-4.3061 \cdot 10^{-08}$	0.492441	$-1.4873 \cdot 10^{-10}$

a	200		400	
	$M\omega_R$	$M\omega_I$	$M\omega_R$	$M\omega_I$
$0.2M$	0.492251	$-4.1129 \cdot 10^{-07}$	0.492251	$-4.1129 \cdot 10^{-07}$
$0.4M$	0.492304	$-9.6844 \cdot 10^{-08}$	0.492304	$-9.6844 \cdot 10^{-08}$
$0.6M$	0.492353	$-1.1243 \cdot 10^{-08}$	0.492353	$-1.1243 \cdot 10^{-08}$
$0.8M$	0.492399	$5.3551 \cdot 10^{-11}$	0.492399	$5.3551 \cdot 10^{-11}$
$0.9M$	0.492421	$3.0413 \cdot 10^{-10}$	0.492421	$3.0413 \cdot 10^{-10}$
$0.99M$	0.492441	$3.6373 \cdot 10^{-10}$	0.492441	$3.6651 \cdot 10^{-10}$

Table 4.6: Numerical precision with the number of iterations $M\mu = 0.5$, $\ell = 2$, $m = 2$.

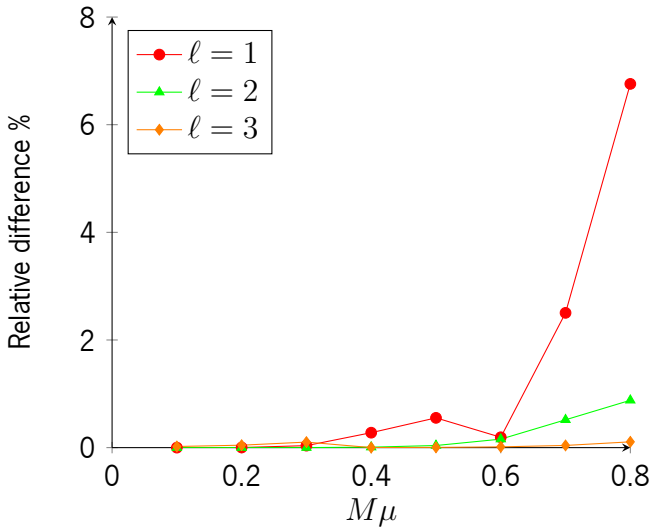

Figure 4.2: Relative differences between analytical and numerical values for the real part, with $m = 0$ and $a = 0.2M$.

The fundamental mode is given by $n = \ell + 1$.

In this analysis we again didn't include the $\ell = 0$ case since the analytical approximations only make sense when $M\mu \ll \ell$.

When a/M is fixed the differences between the numerical and analytical values follow the same pattern as in the Schwarzschild case, that is, the analytical approximation becomes worse with increasing $M\mu$, as seen in figure 4.2 since the approximation is only valid when $M\mu \ll \ell$. As for the imaginary part, in Table 4.7, the relative difference is very large for small values of $M\mu$. Again this is due to the fact that the imaginary part is very close to zero, so any difference at all will translate in a great relative difference. In some cases for large $M\mu$ the relative difference increases due to the fact that the approximation is only valid for $M\mu \ll \ell$.

As for the decreasing relative differences as a/M increases between analytical and numerical values in Table 4.8, probably this is due to the numerical method itself, since the approximation is no way dependent on a, as it works for every value of a.

$M\mu$	$\ell = 1$			$\ell = 2$			$\ell = 3$		
	Num.	Analt.	Rel. diff.	Num.	Analt.	Rel. diff.	Num.	Analt.	Rel. diff.
0.1	$1.28 \cdot 10^{-11}$	$9.20 \cdot 10^{-12}$	$3.86 \cdot 10$	$7.12 \cdot 10^{-18}$	$7.98 \cdot 10^{-19}$	$9.93 \cdot 10^{2}$	$8.88 \cdot 10^{-18}$	$1.67 \cdot 10^{-26}$	$5.31 \cdot 10^{10}$
0.2	$3.92 \cdot 10^{-8}$	$1.33 \cdot 10^{-8}$	$1.95 \cdot 10^{2}$	$4.41 \cdot 10^{-14}$	$2.07 \cdot 10^{-14}$	$1.13 \cdot 10^{2}$	$1.29 \cdot 10^{-15}$	$7.32 \cdot 10^{-21}$	$1.76 \cdot 10^{7}$
0.3	$9.22 \cdot 10^{-6}$	$1.12 \cdot 10^{-6}$	$7.20 \cdot 10^{2}$	$4.60 \cdot 10^{-11}$	$1.05 \cdot 10^{-11}$	$3.38 \cdot 10^{2}$	$7.60 \cdot 10^{-14}$	$2.05 \cdot 10^{-17}$	$3.71 \cdot 10^{5}$
0.4	$5.56 \cdot 10^{-4}$	$2.83 \cdot 10^{-5}$	$1.86 \cdot 10^{3}$	$1.11 \cdot 10^{-8}$	$1.03 \cdot 10^{-9}$	$9.82 \cdot 10^{2}$	$4.65 \cdot 10^{-14}$	$7.06 \cdot 10^{-15}$	$5.58 \cdot 10^{2}$
0.5	$5.54 \cdot 10^{-3}$	$3.54 \cdot 10^{-4}$	$1.46 \cdot 10^{3}$	$1.18 \cdot 10^{-6}$	$3.91 \cdot 10^{-8}$	$2.91 \cdot 10^{3}$	$1.15 \cdot 10^{-11}$	$7.47 \cdot 10^{-13}$	$1.44 \cdot 10^{3}$
0.6	$1.77 \cdot 10^{-2}$	$2.77 \cdot 10^{-3}$	$5.40 \cdot 10^{2}$	$6.79 \cdot 10^{-5}$	$8.03 \cdot 10^{-7}$	$8.35 \cdot 10^{3}$	$1.44 \cdot 10^{-9}$	$3.66 \cdot 10^{-11}$	$3.85 \cdot 10^{3}$
0.7	$3.62 \cdot 10^{-2}$	$1.54 \cdot 10^{-2}$	$1.35 \cdot 10^{2}$	$1.48 \cdot 10^{-3}$	$1.06 \cdot 10^{-5}$	$1.39 \cdot 10^{4}$	$1.12 \cdot 10^{-7}$	$1.04 \cdot 10^{-9}$	$1.07 \cdot 10^{4}$
0.8	$5.97 \cdot 10^{-2}$	$6.50 \cdot 10^{-2}$	8.23	$8.11 \cdot 10^{-3}$	$9.90 \cdot 10^{-5}$	$8.10 \cdot 10^{3}$	$5.89 \cdot 10^{-6}$	$1.94 \cdot 10^{-8}$	$3.03 \cdot 10^{4}$

Table 4.7: Relative differences in percentage $|[(M\omega_I)_{\text{num}} - (M\omega_I)_{\text{analytic}}]/(M\omega_I)_{\text{analytic}}| \times 100$ between analytical and numerical values for the absolute value of $M\omega_I$, with $m = 0$ and $a = 0.2$.

a	$M\mu = 0.4$			$M\mu = 0.5$		
	Num.	Ana.	Rel. diff.	Num.	Ana.	Rel. diff.
$0.2M$	0.39620	0.39623	0.00782	0.49225	0.49242	0.03452
$0.4M$	0.39621	0.39624	0.00732	0.49230	0.49245	0.03005
$0.6M$	0.39622	0.39625	0.00681	0.49235	0.49248	0.02640
$0.8M$	0.39624	0.39626	0.00606	0.49240	0.49251	0.02335
$0.9M$	0.39624	0.39626	0.00580	0.49242	0.49253	0.02193
$0.99M$	0.39624	0.39627	0.00555	0.49244	0.49254	0.02071

a	$M\mu = 0.6$			$M\mu = 0.7$			$M\mu = 0.8$		
	Num.	Ana.	Rel. diff.	Num.	Ana.	Rel. diff.	Num.	Ana.	Rel. diff.
$0.2M$	0.58568	0.58644	0.12874	0.67462	0.67760	0.43935	0.75805	0.76510	0.92028
$0.4M$	0.58591	0.58652	0.10468	0.67549	0.67783	0.34551	0.75886	0.76561	0.88204
$0.6M$	0.58612	0.58662	0.08592	0.67631	0.67806	0.25794	0.76053	0.76613	0.73081
$0.8M$	0.58629	0.58671	0.07141	0.67698	0.67830	0.19328	0.76281	0.76665	0.50075
$0.9M$	0.58638	0.58676	0.06544	0.67726	0.67841	0.16966	0.76380	0.76691	0.40526
$0.99M$	0.58645	0.58680	0.06050	0.67748	0.67852	0.15224	0.76450	0.76714	0.34361

Table 4.8: Relative difference in percentage $|[(M\omega_R)_{\rm num} - (M\omega_R)_{\rm analytic}]/(M\omega_R)_{\rm analytic}| \times 100$ between real quasi-bound frequencies as a approaches the extreme limit $a \to M$, with $\ell = 2$ and $m = 2$.

a	$M\mu = 0.4$			$M\mu = 0.5$		
	Num.	Ana.	Rel. diff.	Num.	Ana.	Rel. diff.
$0.2M$	$-3.67 \cdot 10^{-9}$	$-1.18 \cdot 10^{-9}$	$2.11 \cdot 10^{2}$	$-4.11 \cdot 10^{-7}$	$-4.16 \cdot 10^{-8}$	$8.88 \cdot 10^{2}$
$0.4M$	$-7.73 \cdot 10^{-10}$	$-8.29 \cdot 10^{-10}$	6.78	$-9.68 \cdot 10^{-8}$	$-2.82 \cdot 10^{-8}$	$2.43 \cdot 10^{2}$
$0.6M$	$-6.22 \cdot 10^{-11}$	$-4.72 \cdot 10^{-10}$	$8.68 \cdot 10$	$-1.12 \cdot 10^{-8}$	$-1.38 \cdot 10^{-8}$	$1.87 \cdot 10$
$0.8M$	$2.33 \cdot 10^{-11}$	$-5.94 \cdot 10^{-10}$	$1.04 \cdot 10^{2}$	$5.35 \cdot 10^{-11}$	$-7.78 \cdot 10^{-9}$	$1.01 \cdot 10^{2}$
$0.9M$	$3.13 \cdot 10^{-11}$	$8.94 \cdot 10^{-10}$	$9.65 \cdot 10$	$3.04 \cdot 10^{-10}$	$6.60 \cdot 10^{-9}$	$9.54 \cdot 10$
$0.99M$	$3.49 \cdot 10^{-11}$	$2.38 \cdot 10^{-10}$	$8.53 \cdot 10$	$3.64 \cdot 10^{-10}$	$1.74 \cdot 10^{-9}$	$7.91 \cdot 10$

a	$M\mu = 0.6$			$M\mu = 0.7$			$M\mu = 0.8$		
	Num.	Ana.	Rel. diff.	Num.	Ana.	Rel. diff.	Num.	Ana.	Rel. diff.
$0.2M$	$-2.58 \cdot 10^{-5}$	$-8.22 \cdot 10^{-7}$	$3.04 \cdot 10^{3}$	$-7.58 \cdot 10^{-4}$	$-1.06 \cdot 10^{-5}$	$7.05 \cdot 10^{3}$	$-5.83 \cdot 10^{-3}$	$-9.84 \cdot 10^{-5}$	$5.82 \cdot 10^{3}$
$0.4M$	$-6.83 \cdot 10^{-6}$	$-5.61 \cdot 10^{-7}$	$1.12 \cdot 10^{3}$	$-2.70 \cdot 10^{-4}$	$-7.38 \cdot 10^{-6}$	$3.55 \cdot 10^{3}$	$-3.40 \cdot 10^{-3}$	$-7.02 \cdot 10^{-5}$	$4.74 \cdot 10^{3}$
$0.6M$	$-9.77 \cdot 10^{-7}$	$-2.74 \cdot 10^{-7}$	$2.56 \cdot 10^{2}$	$-5.16 \cdot 10^{-5}$	$-3.77 \cdot 10^{-6}$	$1.27 \cdot 10^{3}$	$-1.24 \cdot 10^{-3}$	$-3.78 \cdot 10^{-5}$	$3.18 \cdot 10^{3}$
$0.8M$	$-2.42 \cdot 10^{-8}$	$-1.07 \cdot 10^{-7}$	$7.75 \cdot 10$	$-2.20 \cdot 10^{-6}$	$-1.47 \cdot 10^{-6}$	$4.99 \cdot 10$	$-1.16 \cdot 10^{-4}$	$-1.64 \cdot 10^{-5}$	$6.03 \cdot 10^{2}$
$0.9M$	$1.44 \cdot 10^{-9}$	$3.58 \cdot 10^{-8}$	$9.60 \cdot 10$	$-5.06 \cdot 10^{-8}$	$2.78 \cdot 10^{-7}$	$1.18 \cdot 10^{2}$	$-6.15 \cdot 10^{-6}$	$3.07 \cdot 10^{-6}$	$3.00 \cdot 10^{2}$
$0.99M$	$2.06 \cdot 10^{-9}$	$6.17 \cdot 10^{-9}$	$6.67 \cdot 10$	$7.84 \cdot 10^{-9}$	$1.14 \cdot 10^{-8}$	$3.11 \cdot 10$	$2.15 \cdot 10^{-8}$	$1.08 \cdot 10^{-8}$	$9.88 \cdot 10$

Table 4.9: Relative difference in percentage $|[(M\omega_I)_{\rm num} - (M\omega_I)_{\rm analytic}]/(M\omega_I)_{\rm analytic}| \times 100$ between imaginary quasi-bound frequencies as a approaches the extreme limit $a \to M$, with $l = 2$ and $m = 2$.

4.5 Scalar quasi-normal modes

4.5.1 Recursion coefficients

We have again to calculate the recursion coefficients for the angular and radial equations

$$\frac{1}{\sin\theta}\frac{\mathrm{d}}{\mathrm{d}\theta}\left(\sin\theta\frac{\mathrm{d}S(\theta)}{\mathrm{d}\theta}\right)+\left[a^2\cos^2\theta\omega^2-\frac{m^2}{\sin^2\theta}\right]S(\theta)=-\Lambda S(\theta) \tag{4.5.1}$$

$$\frac{\mathrm{d}}{\mathrm{d}r}\left(\Delta\frac{\mathrm{d}R(r)}{\mathrm{d}r}\right)+\left[\frac{\omega^2(r^2+a^2)^2+a^2m^2-4Mram\omega}{\Delta}-\omega^2a^2\right]=\Lambda R(r). \tag{4.5.2}$$

The coefficients for the angular equation are practically the same as before differing in setting $\mu=0$. They are given by

$$\begin{cases}\alpha_n^\theta=2(n+1)(2k+n+1)\\ \beta_n^\theta=k(4a\omega-4n-2)+n(4a\omega-1)+a\omega(a\omega+2)-4k^2+\Lambda-n^2,\ n\geq 1\\ \gamma_n^\theta=-2a\omega(2k+n)\end{cases}$$

where $\gamma_0=0$.

As for the radial equation we have the following ansatz

$$R(r)=\mathrm{e}^{\mathrm{i}\omega r}(r-r_-)^{-1+2\mathrm{i}\omega M+\mathrm{i}\sigma}(r-r_+)^{-\mathrm{i}\sigma}\sum_{n=0}^{\infty}d_n\left(\frac{r-r_+}{r-r_-}\right)^n, \tag{4.5.3}$$

where $\sigma=\left(2M\omega r_+-am\right)/b$, and $b=2\sqrt{M^2-a^2}$. Making $x=\frac{r-r_+}{r-r_-}$, we can find the conditions

$$\alpha_0^r d_1+\beta_0^r d_0=0 \tag{4.5.4}$$

$$\alpha_n^r d_{n+1}+\beta_n^r d_n+\gamma_n^r d_{n-1}=0,\quad n\geq 1. \tag{4.5.5}$$

Just like before, using the continued fraction method we obtain

$$\begin{cases}\alpha_0^r=\dfrac{-2Mb\mathrm{i}\omega+b+2\mathrm{i}am-4M^2\mathrm{i}\omega}{b}\\ \beta_0^r=\dfrac{-2am\left[\left(b+4M\right)\omega+\mathrm{i}\right]-a^2\omega\left[\left(b+16M\right)\omega+4\mathrm{i}\right]+8M^2\omega\left[2\omega\left(b+2M\right)+\mathrm{i}\right]}{b}\\ \qquad -\Lambda+4M\mathrm{i}\omega-1\end{cases} \tag{4.5.6}$$

$$\begin{cases} \alpha_n^r = \dfrac{(n+1)\left(b(n-2M\mathrm{i}\omega)+b+2\mathrm{i}am-4M^2i\omega\right)}{b} \\ \beta_n^r = \dfrac{2am\left[-(b+4M)\,\omega-2\mathrm{i}n-\mathrm{i}\right]-2bn^2-a^2\omega\left[(b+16M)\,\omega+8\mathrm{i}n+4\mathrm{i}\right]}{b}+ \\ \qquad \dfrac{8M\mathrm{i}n\omega\,(b+2M)+8M^2\omega\left[2\omega\,(b+2M)+\mathrm{i}\right]}{b}-\Lambda-2n+4M\mathrm{i}\omega-1 \\ \gamma_n^r = \dfrac{(n-4M\mathrm{i}\omega)\left(b(n-2M\mathrm{i}\omega)+2\mathrm{i}am-4M^2\mathrm{i}\omega\right)}{b} \end{cases}, \; n \geq 1. \tag{4.5.7}$$

4.5.2 Quasi-normal frequencies

Using Leaver's continued fraction method, we obtained some quasi-normal frequencies, given in Tables 4.10, 4.11 and 4.12. The values were obtained with 200 iterations of the infinite continued fraction.

As in the quasi-bound situation, the energy increases with m due to the particle moving in the same direction as the black hole. Also, the modes with smaller m are also more damped than modes with greater m, which could be interpreted as slower rotating modes, which don't have the required energy to keep them away from the black hole, thus having a shorter lifetime.

In table 4.12 the energies increase with the rotation parameter. Since we are considering fields with $m = \ell$ they are accelerated by the black hole's rotation and the faster the black hole rotates, that is, the higher the value of a/M the faster will particles orbit the hole, thus increasing their energies (except for $\ell = 0$ which corresponds to a polar orbit). For the same reason their life time is also longer since it will take longer for the field to be absorbed by the black hole.

Looking at (4.2.11), the radial function that describes quasi-normal modes can't be normalized which in turn will invalidate equation (4.3.25) meaning that there cannot be any super-radiant instability[6] for quasi-normal modes. Such conclusion is supported by the data in Table 4.12.

In Table 4.12, the imaginary part of the frequency goes to zero as $a \to M$. Although, as Leaver noted, the recursion coefficients are singular at $a = M$, this can be avoided if $M\omega_R = m/2$ and $M\omega_I = 0$. This is coincidentally the maximum value of the super-radiance frequency for an extreme

[6] However there is super-radiance in massless fields, since they can extract energy form the black hole. It just doesn't make the field grow exponentially.

k	$m=-2$		$m=-1$		$m=0$		$m=1$		$m=2$	
	$M\omega_R$	$-M\omega_I$	$M\omega_R$	$-M\omega_I$	$M\omega_R$	$-M\omega_I$	$M\omega_R$	$-M\omega_I$	$M\omega_R$	$-M\omega_I$
0	0.43306	0.09598	0.45932	0.09577	0.48886	0.09547	0.52214	0.09515	0.55965	0.09493
1	0.40907	0.29477	0.43805	0.29314	0.47013	0.29132	0.50578	0.28955	0.54541	0.28821
2	0.36942	0.51188	0.40248	0.50604	0.43844	0.50018	0.47775	0.49479	0.52071	0.49048

Table 4.10: Quasi-normal frequencies and first three overtones for $\ell = 2$ and $a = 0.4M$.

m	$\ell = 0$		$\ell = 1$		$\ell = 2$		$\ell = 3$	
	$M\omega_R$	$-M\omega_I$	$M\omega_R$	$-M\omega_I$	$M\omega_R$	$-M\omega_I$	$M\omega_R$	$-M\omega_I$
-3	———	———	———	———	———	———	0.60029	0.09571
-2	———	———	———	———	0.43306	0.09598	0.62548	0.09561
-1	———	———	0.2669	0.0969	0.45932	0.09577	0.65285	0.09544
0	0.11170	0.10325	0.29608	0.09626	0.48886	0.09547	0.68265	0.09523
1	———	———	0.33157	0.09579	0.52214	0.09515	0.71512	0.09501
2	———	———	———	———	0.55965	0.09493	0.75053	0.09481
3	———	———	———	———	———	———	0.78909	0.09468

Table 4.11: Quasi-normal frequencies for $a = 0.4$, fundamental mode.

black hole. These modes are called zero damped modes. However near the extreme limit there are modes that are still damped (for example $\ell = 0$). Although Leaver's method fails when $a = M$, the value for the near extreme case is a good approximation to the real values (see Richartz (2016) and references therein).

We can see in Table 4.13 how the values change with the number of iterations of the continued fraction. We chose $\ell = 0$ as we have seen before it is at lower angular momentum numbers that we see any difference in the values of the frequencies with the iteration number. Both the real and imaginary part are stable at lower values of a (mostly a change in the last digit), but precision gets worse as a increases. Even the real part changes considerably for $a = 0.99M$ even for the higher iterations. This is probably a symptom of our recursion coefficients being singular when $a = M$, so for even higher values of a, more recursions would be recommended.

4.5.2.1 Comparison with analytical approximations

We can obtain an analytical[7] approximation to the quasi-normal modes by using a WKB approximation as done in Yang *et al.* (2012). We shall present here the relevant equations, valid only in the eikonal limit

[7] In fact it is a semi-analytical approximation, because although we get formulas to obtain the frequencies, they can only be obtained by numerical root finding of a polynomial equation.

a	$\ell=0$		$\ell=1$		$\ell=2$		$\ell=3$		$\ell=4$	
	$M\omega_R$	$-M\omega_I$	$M\omega_R$	$-M\omega_I$	$M\omega_R$	$-M\omega_I$	$M\omega_R$	$-M\omega_I$	$M\omega_R$	$-M\omega_I$
0	0.11045	0.10490	0.29294	0.09766	0.48364	0.09676	0.67537	0.09650	0.86742	0.09639
$0.2M$	0.11077	0.10451	0.31004	0.09725	0.51712	0.09638	0.72531	0.09614	0.93388	0.09603
$0.4M$	0.11170	0.10325	0.33157	0.09579	0.55965	0.09493	0.78909	0.09468	1.01902	0.09458
$0.6M$	0.11317	0.10070	0.36028	0.09224	0.61736	0.09125	0.87632	0.09096	1.13594	0.09084
$0.8M$	0.11454	0.09570	0.40327	0.08313	0.70682	0.08152	1.01333	0.08107	1.32090	0.08088
$0.9M$	0.11385	0.09157	0.43723	0.07185	0.78164	0.06929	1.13011	0.06863	1.47998	0.06838
$0.99M$	0.11038	0.08950	0.49342	0.03671	0.92803	0.03106	1.36863	0.03024	1.81106	0.03003

Table 4.12: Quasi-normal real frequencies as a gets close to the extreme limit for $m=\ell$.

a	50		100		200		400	
	$M\omega_R$	$-M\omega_I$	$M\omega_R$	$-M\omega_I$	$M\omega_R$	$-M\omega_I$	$M\omega_R$	$-M\omega_I$
0	0.11044	0.10489	0.11046	0.10490	0.11045	0.10490	0.11045	0.10490
$0.2M$	0.11076	0.10451	0.11077	0.10451	0.11077	0.10451	0.11077	0.10451
$0.4M$	0.11169	0.10324	0.11170	0.10325	0.11170	0.10325	0.11170	0.10325
$0.6M$	0.11319	0.10068	0.11317	0.10070	0.11317	0.10070	0.11317	0.10070
$0.8M$	0.11452	0.09575	0.11454	0.09570	0.11454	0.09570	0.11454	0.09570
$0.9M$	0.11381	0.09143	0.11386	0.09156	0.11385	0.09157	0.11385	0.09157
$0.99M$	0.10892	0.08794	0.11075	0.08990	0.11038	0.08950	0.11044	0.08949

Table 4.13: Numerical precision with the number of iterations for scalar quasi-normal modes for $\ell = m = 0$.

$\ell \gg 1$ and $a\omega_R/(\ell+1/2) \ll 1$, in order to compare with our numerical values

$$M\omega_R = \frac{M(1-xM)\mu a(\ell+1/2)}{M^2(x-3)x^2+(x+1)a^2} \tag{4.5.8}$$

where, on this subsection only, $\mu = m/(\ell+1/2)$ and x obeys the following equation

$$2x^4(x-3)^2 + 4x^2[(1-\mu^2)x^2 - 2x - 3(1-\mu^2)](a/M)^2 + (1-\mu^2)[(2-\mu^2)x^2 + 2(2+\mu^2)x + (2-\mu^2)](a/M)^4 = 0 \tag{4.5.9}$$

which is approximately true when $a\omega_R/(\ell+1/2)$ is small, which is usually the case even when $a = M$. Here $x = r_0/M$, where r_0 is the maximum of the radial potential of the Teukolsky equation. As for the imaginary part, we have

$$M\omega_I = -(k+1/2)\gamma_L \tag{4.5.10}$$

where k is the mode's overtone number and $\Omega_R = \omega_R/(\ell+1/2)$ and

$$\gamma_L \equiv \frac{(x^2-2x+a^2)\sqrt{4(6x^2M^2\Omega_R^2-1)+2a^2\Omega_R(3-\mu^2)}}{2x^4M^2\Omega_R - 4ax\mu + a^2x\Omega_R[x(3-\mu^2)+2(1+\mu^2)] + a^4\Omega_R(1-\mu^2)/M^2}.$$

which is the Lyapunov exponent. For $m = 0$, equation (4.5.8) is not valid and must be replaced with

$$M\omega_R(m=0) = \frac{\pi\sqrt{x^2-2x+(a/M)^2}(\ell+1/2)}{(x^2+(a/M)^2)\mathrm{EllipE}\left[\frac{a^2(x^2-2x+(a/M)^2)}{M^2(x^2+a^2)^2}\right]}, \tag{4.5.11}$$

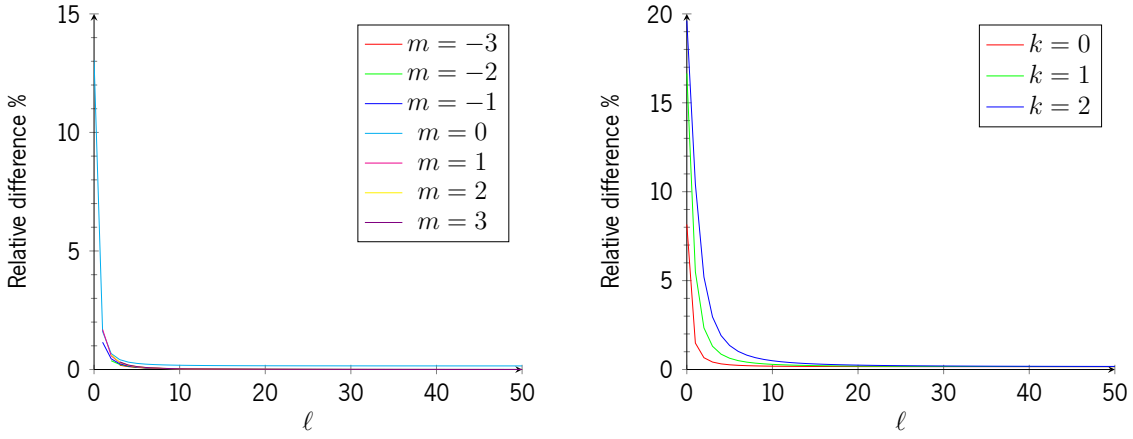

(a) Real part.

(b) Imaginary part for $m = 0$.

Figure 4.3: Relative difference $|[(M\omega)_{\rm num} - (M\omega)_{\rm analytic}]/(M\omega)_{\rm analytic}| \times 100$ between numerical and analytical quasi-normal frequencies for $a = 0.4M$.

where EllipE is the elliptic integral of second kind and x is given by

$$(x-3)M^3x^2 + (x+1)Ma^2 = 0.$$

Although these expressions are only valid in the limit $a\omega_R/(\ell+1/2) \ll 1$, even for $a = 1$ the expressions above are still a good approximation since $\omega_R/(\ell+1/2)$ is smaller than one. For example, for $\ell = 4, m = 4, a = 0.99M$, $a\omega_R/(\ell + 1/2) \approx 0.39$. It is even better for larger values of ℓ.

In Figure 4.3 we compare the numerical and analytical values of the real and imaginary parts of the frequencies. For the real part, as expected for large ℓ, our numerical values are very close to the analytical ones differing in about 0.15% for $\ell > 20$, so the method agrees with the theoretical predictions. Even for $\ell = 0$ the difference is around 13%, meaning the analytical prediction is very good even outside the domain of validity. For the imaginary part we find a similar behavior as before. However, the relative difference increases with the overtone number even for large values of ℓ.

Looking at Figure 4.4 we find the expected behavior when ℓ increases, that is $a\omega_R/(\ell + 1/2)$ decreases and the relative difference decreases as expected. However for a fixed value of ℓ the relative difference decreases for large values of a, although it begins by following the expected behavior of increasing with a, which is not expected since as a increases the approximation should, in principle, become

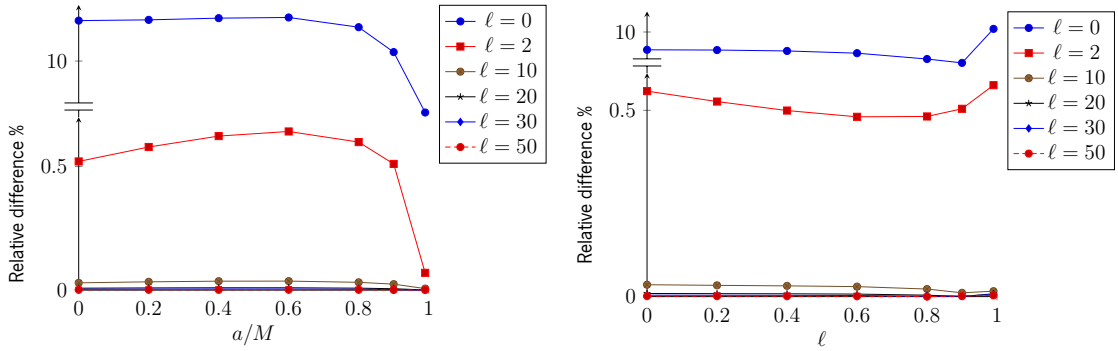

(a) Real part.

(b) Imaginary part.

Figure 4.4: Relative difference $|[(M\omega)_{\text{num}} - (M\omega)_{\text{analytic}}]/(M\omega)_{\text{analytic}}| \times 100$ between numerical and analytical quasi-normal frequencies for $a/M = 0, \ldots, 1$ with $m = 0$.

worse. We don't know the cause of such behavior, though it could have something to do with being near the extreme limit where we cannot be sure that the numerical algorithm behaves as expected, and a combination of some factors could cause such a decrease in the relative difference. But again we offer no solution to this problem.

4.5.2.2 Geometric interpretation

Just as the Schwarzschild quasi-normal modes in the eikonal limit, there also exists here a correspondence between them and the trajectories of null rays in Kerr spacetime, as shown by Yang *et al.* (2012), which can give us a picture of how those modes orbit black holes.

The equations of motion for a null particle in Kerr spacetime are given in Misner *et al.* (2017) as

$$\rho^2 \frac{\mathrm{d}\theta}{\mathrm{d}\lambda} = \sqrt{\Theta} \tag{4.5.12}$$

$$\rho^2 \frac{\mathrm{d}r}{\mathrm{d}\lambda} = \sqrt{\mathcal{R}} \tag{4.5.13}$$

$$\rho^2 \frac{\mathrm{d}\phi}{\mathrm{d}\lambda} = -(aE - L_z/\sin^2\theta) + \frac{a}{\Delta}(E(r^2+a^2) - aL_z) \equiv \mathcal{F}(r,\theta) \tag{4.5.14}$$

$$\rho^2 \frac{\mathrm{d}t}{\mathrm{d}\lambda} = -a(aE\sin^2\theta - L_z) + (r^2+a^2)\Delta^{-1}(E(r^2+a^2) - aL_z) \equiv \mathcal{T}(r,\theta), \tag{4.5.15}$$

where

$$\mathcal{R} = (E(r^2 + a^2) - aL_z)^2 - \Delta\left[(L_z - aE)^2 + Q\right] \tag{4.5.16}$$

$$\Theta = Q - \cos^2\theta\left[-a^2E^2 + L_z^2/\sin^2\theta\right]. \tag{4.5.17}$$

Here the conserved quantities of Kerr spacetime (E energy, L_z azimuthal angular momentum and Q Carter's constant) are identified with the wave quantities of the quasi-normal modes (ω_R, m, and $\Lambda - m^2$, respectively). It is shown in Yang *et al.* (2012) the boundary conditions for the existence of quasi-normal modes imply the following: the orbits must be "spherical", that is, with constant r, with radius given by the equations

$$\mathcal{R}(r) = \mathcal{R}'(r) = 0, \tag{4.5.18}$$

where $'$ denotes $\mathrm{d}/\mathrm{d}r$, and must satisfy a Bohr-Sommerfeld condition

$$\int_{\theta_-}^{\theta_+} \sqrt{\Theta}\mathrm{d}\theta = \pi(L - |L_z|), \tag{4.5.19}$$

where $\theta_\pm$ are the roots of $\Theta(\theta) = 0$, which quantizes Carter's constant and the azimuthal angular momentum. The Carter's constant can then be written as

$$Q \approx L^2 - m^2 - \frac{a\omega_R}{2}\left(1 - \frac{m^2}{L^2}\right). \tag{4.5.20}$$

From equation (4.5.18) we can solve simultaneously for both r (the radius of the orbit) and E which results in

$$Q/E^2 = \frac{r^3(r^3 - 6Mr^2 + 9M^2r - 4a^2M)}{a^2(r - M)^2} \tag{4.5.21}$$

$$L_z/E = -\frac{r^3 - 3Mr^2 + a^2r + a^2M}{a(r - M)}. \tag{4.5.22}$$

Comparing equation (4.5.22) with equation (4.5.8), we see, after a trivial algebraic manipulation, that both expressions are identical, if we make the previous identification of the wave quantities with the geodesic quantities.

It is shown in that the imaginary part of the frequency corresponds to the following geometric quantity

$$\omega_I = (k + 1/2)\frac{\sqrt{2\mathcal{R}''(r_{\mathrm{orbit}})}\Delta(r_{\mathrm{orbit}})}{\frac{\partial}{\partial E}\mathcal{R}(r_{\mathrm{orbit}}) + \left(\frac{\partial}{\partial Q}\mathcal{R}\frac{\mathrm{d}Q}{\mathrm{d}E}\right)\Big|_{r=r_{\mathrm{orbit}}}}, \tag{4.5.23}$$

where we identify

$$\gamma_L = \frac{\sqrt{2\mathcal{R}''(r_{\rm orbit})}\Delta(r_{\rm orbit})}{\frac{\partial}{\partial E}\mathcal{R}(r_{\rm orbit}) + \left(\frac{\partial \mathcal{R}}{\partial Q}\frac{\mathrm{d}Q}{\mathrm{d}E}\right)\Big|_{r=r_{\rm orbit}}}$$

as the Lyapunov constant, therefore establishing a connection with equation (4.5.10).

Using only geometrical quantities the real part of quasi-normal modes frequencies can be obtained using the following formula in Li *et al.* (2021), evaluated at the orbit's radius,

$$\omega_R = (\ell + 1/2)\omega_{\rm orb} + m\omega_{\rm prec}, \tag{4.5.24}$$

where

$$\omega_{\rm orb} = 2\pi\left(2\int_{\theta_-}^{\theta_+}\frac{\mathcal{T}(r,\theta)}{\sqrt{\Theta(\theta)}}\mathrm{d}\theta\right)^{-1}$$

and

$$\omega_{\rm prec} = \Delta\phi_{\rm prec}\left(2\int_{\theta_-}^{\theta_+}\frac{\mathcal{T}(r,\theta)}{\sqrt{\Theta(\theta)}}\mathrm{d}\theta\right)^{-1}$$

where

$$\Delta\phi_{\rm prec} = 2\int_{\theta_-}^{\theta^+}\frac{\mathcal{F}(r,\theta)}{\sqrt{\Theta}}\mathrm{d}\theta - \mathrm{sgn}m.$$

It is important to note that equation (4.5.24) is an *implicit* equation for ω_R since one can easily see that $\omega_{\rm orb}$ and $\omega_{\rm prec}$ have ω_R dependent terms. We just wrote the equation in this form to compare directly with equation (2.4.6).

Different values of m will correspond to different types of orbits. By equation (4.5.20) we see Q becomes $Q = L^2 - a\omega_R/2$ when $m = 0$ (polar orbits) and $Q = 0$ when $L = \pm m$ for $\ell \gg 1$ since $L \to \sqrt{\ell(\ell+1)} \approx \ell + 1/2$ (equatorial orbits).

For slowly rotating black holes the previous formula can be written as

$$\omega_R = \frac{L}{\sqrt{27}M} + m\frac{2a}{27M^2}. \tag{4.5.25}$$

This is very similar to the expression obtained by Goebel (1972) and used in section 2.4.2, except for an extra term $\Omega_{\rm prec}$ which comes from the frame dragging effects of the Kerr black hole. For slowly rotating black holes, polar orbits have the same energy as in a Schwarzschild black hole.

5 Gravitational Perturbations on Kerr

5.1 The Teukolsky equation

The gravitational perturbations for Schwarzschild black holes were obtained in chapter 3. It important from a theoretical point of view, since it can be thought as a toy model of a black hole, because obtained results for Schwarzschild black holes are qualitatively similar for rotating black holes and can be used as approximations for slowly rotating black holes, although they don't take into account the change of ω with the azimuthal angular momentum number m. However, in order to get accurate results to compare with the observations of astrophysical black holes, which are expected to have a non-zero angular momentum[1], which can be quite close to the extreme Kerr limit. Therefore these black holes can only be described by the full Kerr metric which will make the problem of perturbations on such geometry considerably more complicated.

Unlike the Schwarzschild geometry, one cannot perturb the metric just like in chapter 3 due to the increased complexity of the Kerr metric. One way to solve the problem is through the Newman-Penrose formalism, but the derivation of a master equation for the gravitational perturbations is very long and falls outside the scope of this thesis. The interested reader may refer to the original article by Teukolsky (1973) or to the classical book of Chandrasekhar (1983). We will just present here the perturbation master equation which goes by the name of Teukolsky equation, valid for scalar, vector, tensorial and massless $\frac{1}{2}$

[1] For information about the mass and the angular momentum of some astrophysical black holes see Bambi (2020).

spin particles,

$$\left[\frac{(r^2+a^2)^2}{\Delta}-a^2\sin^2\theta\right]\frac{\partial^2\Phi}{\partial t^2}+\left[\frac{a^2}{\Delta}-\frac{1}{\sin^2\theta}\right]\frac{\partial^2\Phi}{\partial\phi^2}-\Delta^{-s}\frac{\partial}{\partial r}\left(\Delta^{s+1}\frac{\partial\Phi}{\partial r}\right)+$$
$$-\frac{1}{\sin\theta}\frac{\partial}{\partial\theta}\left(\sin\theta\frac{\partial\Phi}{\partial\phi}\right)-2s\left[\frac{a(r-M)}{\Delta}+\frac{\mathrm{i}\cos\theta}{\sin^2\theta}\right]\frac{\partial\Phi}{\partial\phi}+\frac{4Mar}{\Delta}\frac{\partial^2\Phi}{\partial t\partial\phi}+$$
$$-2s\left[\frac{M(r^2-a^2)}{2\Delta}-r-\mathrm{i}a\cos\theta\right]\frac{\partial\Phi}{\partial t}+(s^2\cot^2\theta-s)\Phi=0. \quad (5.1.1)$$

We can separate the field as $\Phi(x^\mu)=\mathrm{e}^{-\mathrm{i}\omega t+\mathrm{i}m\phi}R(r)S(\theta)$ which results in an angular and radial equations

$$\frac{\mathrm{d}}{\mathrm{d}u}\left[\left(1-u^2\right)\frac{\mathrm{d}S}{\mathrm{d}u}\right]+\left[a^2\omega^2u^2-2a\omega su+s+\Lambda-\frac{(m+su)^2}{1-u^2}\right]S=0 \quad (5.1.2)$$

where $u=\cos\theta$ and Λ is a separation constant, and

$$\Delta\frac{\mathrm{d}^2R}{\mathrm{d}r^2}+2(s+1)(r-M)R+V(a,\omega,s,m,M,\Lambda;r)R=0 \quad (5.1.3)$$

where

$$V(a,\omega,s,m,M,\Lambda;r)=\frac{(r^2+a^2)^2\omega^2-4Mam\omega r+a^2m^2+\mathrm{i}s[2am(r-M)-2M\omega(r^2-a^2)]}{\Delta}+$$
$$2\mathrm{i}s\omega r-a^2\omega^2-\Lambda. \quad (5.1.4)$$

5.2 Gravitational quasi-normal modes

5.2.1 Recursion coefficients

The separated Teukolsky equations, with $s=-2$, become

$$\frac{\mathrm{d}}{\mathrm{d}u}\left(\left(1-u^2\right)\frac{\mathrm{d}S(u)}{\mathrm{d}u}\right)+\left(a^2\omega^2u^2+4a\omega u-2+\Lambda-\frac{(m-2u)^2}{1-u^2}\right)S(u)=0 \quad (5.2.1)$$

and

$$\Delta\frac{\mathrm{d}^2R(r)}{\mathrm{d}r^2}+(2r-M)R(r)+\Bigg(\frac{(r^2+a^2)^2\omega^2-4Mam\omega r+a^2m^2-2\mathrm{i}[2am(r-M)-2M\omega(r^2-a^2)]}{\Delta}$$
$$-4\mathrm{i}\omega r-a^2\omega^2-\Lambda\Bigg)R(r)=0, \quad (5.2.2)$$

where Λ is a separation constant.

Just like in the scalar field case we shall now propose the following ansatzs found in Leaver (1985)

$$S(u) = \mathrm{e}^{a\omega u}(1+u)^{k_1}(1-u)^{k_2}\sum_{n=0}^{\infty} a_n(1+u)^n, \tag{5.2.3}$$

where $k_{1,2} = \frac{1}{2}|m \pm 2|$, and

$$R(r) = \mathrm{e}^{\mathrm{i}\omega r}(r-r_-)^{-1+2+\mathrm{i}\omega+\mathrm{i}\sigma}(r-r_+)^{2-\mathrm{i}\sigma}\sum_{n=0}^{\infty} d_n\left(\frac{r-r_+}{r-r_-}\right)^n. \tag{5.2.4}$$

Again we need to solve a system of two infinite fraction equations to obtain the recursion coefficients for both angular and radial equations (see section §B.4). The angular recursion coefficients are given by

$$\begin{cases} \alpha_n^\theta = 2(n+1)(2k_1+n+1) \\ \beta_n^\theta = -\left[a^2\omega^2 - 2(\Lambda-2+1)\right] + 2n(-2a\omega+k_1+k_2+1)+ \\ \quad -\left[2a\omega(2k_1-2+1) - (k_1+k_2)(k_2+k_2+1)\right] + (n-1)n \\ \gamma_n^\theta = -2a\omega(n+k_1+k_2-2), \end{cases} \tag{5.2.5}$$

whereas the radial coefficients are given by

$$\begin{cases} \alpha_n^r = n^2 + (c_0+1)n + c_0 \\ \beta_n^r = -2n^2 + (c_1+2)n + c_3 \\ \gamma_n^r = n^2 + (c_2-3)n + c_4 - c_2 + 2 \end{cases} \tag{5.2.6}$$

where

$$\begin{aligned} c_0 &= -\frac{2\mathrm{i}}{b}\left(\frac{4M^2\omega}{2} - am\right) + 2 - 2\mathrm{i}M\omega + 1 \\ c_1 &= \frac{4\mathrm{i}}{b}\left(\frac{4M^2\omega}{2} - am\right) + 2\mathrm{i}(b+4M)\omega - 4 \\ c_2 &= -\frac{2\mathrm{i}}{b}\left(\frac{4M^2\omega}{2} - am\right) - 2 - 6\mathrm{i}M\omega + 3 \\ c_3 &= -\Lambda + \omega^2(4Mb - a^2 + 16M^2) + \frac{(8M\omega+2\mathrm{i})}{b}\left(\frac{4M^2\omega}{2} - am\right) + \\ &\quad - 2am\omega + \mathrm{i}(b+4M)\omega + 2 - 1 \\ c_4 &= -\frac{(8M\omega+2\mathrm{i})}{b}\left(\frac{4M^2\omega}{2} - am\right) + 2\mathrm{i}M\omega - 2 - 8M^2\omega^2 + 1. \end{aligned} \tag{5.2.7}$$

Like in the scalar case, we must solve a system of equations with two different infinite continued fractions

$$F(\Lambda,\omega) \equiv \frac{\beta_0^\theta}{\alpha_0^\theta} - \cfrac{\gamma_1^\theta}{\beta_1^\theta - \cfrac{\alpha_1^\theta\gamma_2^\theta}{\beta_2^\theta - \cfrac{\alpha_2^\theta\gamma_3^\theta}{\beta_3^\theta - \ddots}}} = 0, \quad G(\Lambda,\omega) \equiv \frac{\beta_0^r}{\alpha_0^r} - \cfrac{\gamma_1^r}{\beta_1^r - \cfrac{\alpha_1^r\gamma_2^r}{\beta_2^r - \cfrac{\alpha_2^r\gamma_3^r}{\beta_3^r - \ddots}}} = 0. \tag{5.2.8}$$

5.2.2 Quasi-normal frequencies

Our numerical results for the gravitational quasi-normal frequencies on the Kerr background can be found in Tables 5.1, 5.2 and 5.3. The values were obtained with 200 iterations of the infinite continued fraction.

The same considerations we made regarding quasi-normal modes for scalar fields apply here, since qualitatively, the values of the frequency follow the same pattern. However the real values of the frequency and the absolute value of the imaginary part are smaller than the obtained frequencies for the scalar case due to the coupling of the spin with the metric.

In this case we again don't have super-radiant instabilities, since our perturbations are massless, which makes the radial wave function non-normalizable (compare with equation (4.3.25)).

More over, as in the scalar case we see that, as $a \to M$, the imaginary part becomes closer to zero, which agrees with the predictions for an extreme Kerr black hole. In fact for the presented modes, we always get zero damped modes, where $M\omega \to m/2$.

We can see in Table 5.4 how the values change with the number of iterations of the continued fraction. We found it was needed to check the accuracy of our method since the inclusion of spin makes the equations mode difficult to solve. We chose $\ell = m = 2$ because it is the lowest possible angular momentum number. Both the real and imaginary part are stable at lower values of a, but precision gets worse as for $a > 0.9M$. Even the real part changes in its last two digits for $a = 0.99M$ even for the higher iterations. Again this is probably a symptom of our recursion coefficients being singular when

k	$m=-2$		$m=-1$		$m=0$		$m=1$		$m=2$	
	$M\omega_R$	$-M\omega_I$	$M\omega_R$	$-M\omega_I$	$M\omega_R$	$-M\omega_I$	$M\omega_R$	$-M\omega_I$	$M\omega_R$	$-M\omega_I$
1	0.33246	0.08913	0.35463	0.08848	0.37968	0.08783	0.40798	0.08726	0.43984	0.08688
2	0.29888	0.27693	0.32564	0.27343	0.35467	0.27001	0.38631	0.26699	0.42085	0.26473
3	0.24327	0.49253	0.27715	0.48084	0.31238	0.47008	0.34922	0.46069	0.38778	0.45326

Table 5.1: Gravitational quasi-normal frequencies and first three overtones for $\ell = 2$ and $a = 0.4M$.

m	$\ell = 2$		$\ell = 3$		$\ell = 4$		$\ell = 5$	
	$M\omega_R$	$-M\omega_I$	$M\omega_R$	$-M\omega_I$	$M\omega_R$	$-M\omega_I$	$M\omega_R$	$-M\omega_I$
-5	———	———	———	———	———	———	0.89373	0.09441
-4	———	———	———	———	0.71617	0.09385	0.91713	0.09432
-3	———	———	0.53233	0.09265	0.73946	0.09370	0.94179	0.09420
-2	0.33246	0.08913	0.55529	0.09235	0.76429	0.09350	0.96779	0.09405
-1	0.35463	0.08848	0.58024	0.09197	0.79078	0.09326	0.99522	0.09387
0	0.37968	0.08783	0.60737	0.09154	0.81907	0.09298	1.02418	0.09367
1	0.40798	0.08726	0.63687	0.09107	0.84928	0.09268	1.05474	0.09346
2	0.43984	0.08688	0.66892	0.09062	0.88152	0.09237	1.08699	0.09324
3	———	———	0.70365	0.09022	0.91590	0.09208	1.12102	0.09303
4	———	———	———	———	0.95250	0.09183	1.15690	0.09284
5	———	———	———	———	———	———	1.19467	0.09267

Table 5.2: Gravitational quasi-modes with $a = 0.4M$ on the fundamental mode.

$a = M$, so we need more iterations if we wish to obtain values for $a > 0.99M$.

5.2.2.1 Comparison with analytical values

Like in section 4.5.2.1, we will compare our numerical values with the values of the WKB method of the mentioned section. For gravitational perturbations the relative differences for the real part of the frequency are much greater than for the scalar case, especially for small ℓ for which we get differences around 30%. Even for large ℓ we get differences for gravitational modes around 40 times greater than for scalar modes (although for both cases the relative difference is below 1%). This happens because of the coupling between the spin of the graviton and the metric, which in first order is ignored by the WKB method used by Yang *et al.* (2012). Besides the mentioned reason, since the obtained expressions can be identified with the trajectory equations for null rays in Kerr, gravitational perturbations are perturbations of the very metric itself which introduces another source of error when we use the trajectory equations. For example,

a	$\ell=2$		$\ell=3$		$\ell=4$		$\ell=5$		$\ell=6$	
	$M\omega_R$	$-M\omega_I$	$M\omega_R$	$-M\omega_I$	$M\omega_R$	$-M\omega_I$	$M\omega_R$	$-M\omega_I$	$M\omega_R$	$-M\omega_I$
0	0.37367	0.08896	0.59944	0.09270	0.80918	0.09416	1.01230	0.09487	1.21201	0.09527
$0.2M$	0.40215	0.08831	0.64479	0.09197	0.87172	0.09354	1.09194	0.09432	1.30866	0.09477
$0.4M$	0.43984	0.08688	0.70365	0.09022	0.95250	0.09183	1.19467	0.09267	1.43327	0.09316
$0.6M$	0.49405	0.08377	0.78622	0.08638	1.06498	0.08791	1.33734	0.08876	1.60617	0.08927
$0.8M$	0.58602	0.07563	0.92189	0.07700	1.24755	0.07813	1.56774	0.07883	1.88475	0.07928
$0.9M$	0.67161	0.06487	1.04464	0.06546	1.41042	0.06616	1.77188	0.06664	2.13071	0.06697
$0.99M$	0.87089	0.02939	1.32308	0.02940	1.77314	0.02947	2.22168	0.02954	2.66919	0.02960

Table 5.3: Gravitational quasi-normal real frequencies as a gets close to the extreme limit for $m=\ell$.

a	50		100		200		400	
	$M\omega_R$	$-M\omega_I$	$M\omega_R$	$-M\omega_I$	$M\omega_R$	$-M\omega_I$	$M\omega_R$	$-M\omega_I$
0	0.37367	0.08896	0.37367	0.08896	0.37367	0.08896	0.37367	0.08896
$0.2M$	0.40215	0.08831	0.40215	0.08831	0.40215	0.08831	0.40215	0.08831
$0.4M$	0.43984	0.08688	0.43984	0.08688	0.43984	0.08688	0.43984	0.08688
$0.6M$	0.49405	0.08377	0.49405	0.08377	0.49405	0.08377	0.49405	0.08377
$0.8M$	0.58602	0.07563	0.58602	0.07563	0.58602	0.07563	0.58602	0.07563
$0.9M$	0.67162	0.06487	0.67162	0.06487	0.67161	0.06487	0.67162	0.06487
$0.99M$	0.87090	0.02939	0.87090	0.02939	0.87089	0.02939	0.87090	0.02939

Table 5.4: Numerical precision with the number of iterations for scalar quasi-normal modes for $\ell = m = 2$.

in the Christoffel symbols for the geodesic equation, we ignore $\mathcal{O}(\delta g_{\mu\nu}^2)$ terms.

For the imaginary part of the frequency, comparing from $\ell = 2$ onwards we see peculiar differences from the scalar case. Unlike the scalar case, here the error increases as the overtone number decreases, and for larger ℓ the error for gravitational perturbations is slightly smaller (1.1 times) than the error for the scalar case. In fact something similar also happens with the scalar and gravitational modes for the Schwarzschild background. It seems then, that the spin of the wave is responsible for increasing its lifetime.

In Figure 5.2 we see a similar behavior in gravitational as the one we've seen in the scalar case. The differences are greater than in the scalar case as expected. Yet we see here the same problem as in the scalar case where the relative difference goes to zero when $a \to M$, which is contrary to which we had expected. Again we cannot offer any explanation to this behavior.

These modes have, just like scalar fields, a geometrical interpretation as spherical orbits of null rays in Kerr spacetime that obey the conditions

$$\int_{\theta_-}^{\theta_+} \sqrt{\Theta}\mathrm{d}\theta = \pi(L - |L_z|)$$

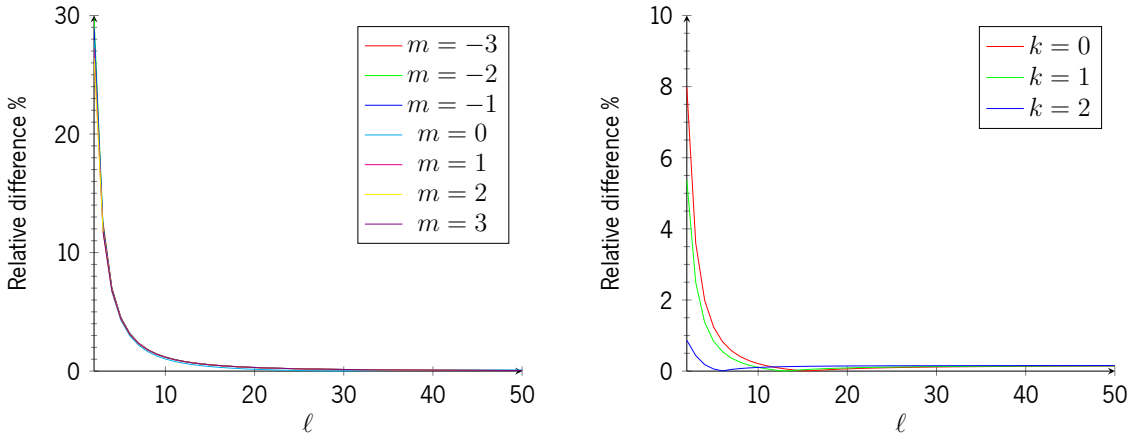

(a) Real part.

(b) Imaginary part for $m = 0$.

Figure 5.1: Relative difference $|[(M\omega)_{\text{num}} - (M\omega)_{\text{analytic}}]/(M\omega)_{\text{analytic}}| \times 100$ between numerical and analytical quasi-normal frequencies for $a = 0.4M$.

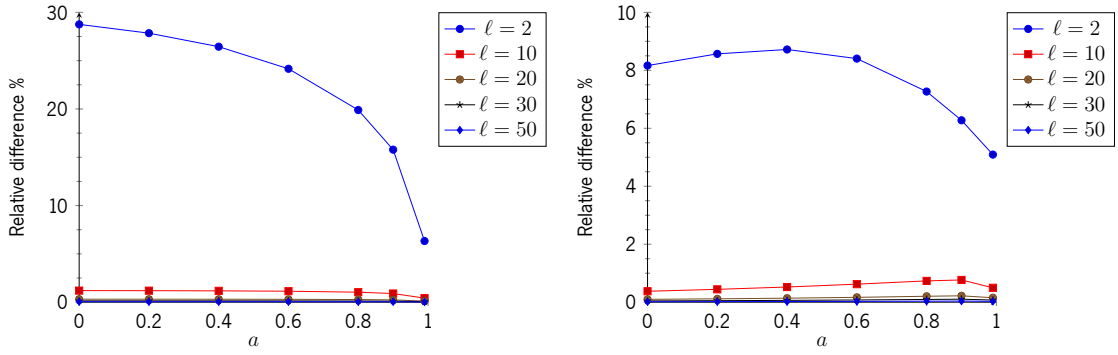

(a) Real part.

(b) Imaginary part.

Figure 5.2: Relative difference $|[(M\omega)_{\text{num}} - (M\omega)_{\text{analytic}}]/(M\omega)_{\text{analytic}}| \times 100$ between numerical and analytical quasi-normal frequencies for $a/M = 0, \ldots, 1$ with $m = 0$.

and

$$\mathcal{R}(r) = \mathcal{R}'(r) = 0.$$

However just like in the static case we expect deviations from the geodesic behavior due to the fact that gravitational perturbations are changes in the background itself, whereas scalar perturbations move in an unperturbed metric, at least in the test field approximation.

In the next chapter we will apply our results to a particular detection of gravitational waves and see if our obtained values are in agreement with the experimental data.

6 Comparison with Event GW190521

6.1 The GW190521 event

The GW190521 event, Abbott *et al.* (2020), was detected on the 21st May 2019 by LIGO and VIRGO detectors. It consisted of the gravitational waves emitted by the merger of two black holes 17 billion light-years away, with masses of 85 and 66 solar masses resulting in an intermediate mass black hole with $M = 142M_\odot$, with an estimated spin $a/M \approx 0.72$.[1] The remaining $9M_\odot$ were radiated away as gravitational waves. It was the event with largest progenitor masses of black holes detected so far. The signal from the LIGO detector in Hanford can be seen in Figure 6.1a.

In order to apply our previous results to this situation we must analyze only the ringdown part of the wave-form, which corresponds to the signal after the central peak in Figure 6.1a. The central peak happens when the two black holes merge which results in a perturbed black hole geometry which will vibrate in discrete quasi-normal frequencies until it becomes stationary. Following Abbott *et al.* (2020) we shall consider as ringdown all the signal that comes $12.7\,\mathrm{ms}$ after the time of the maximum peak in Figure 6.1a. The resulting waveform is in Figure 6.2.

[1] We shall not present the uncertainties associated with these measurements since they are not important for the analysis we are going to perform.

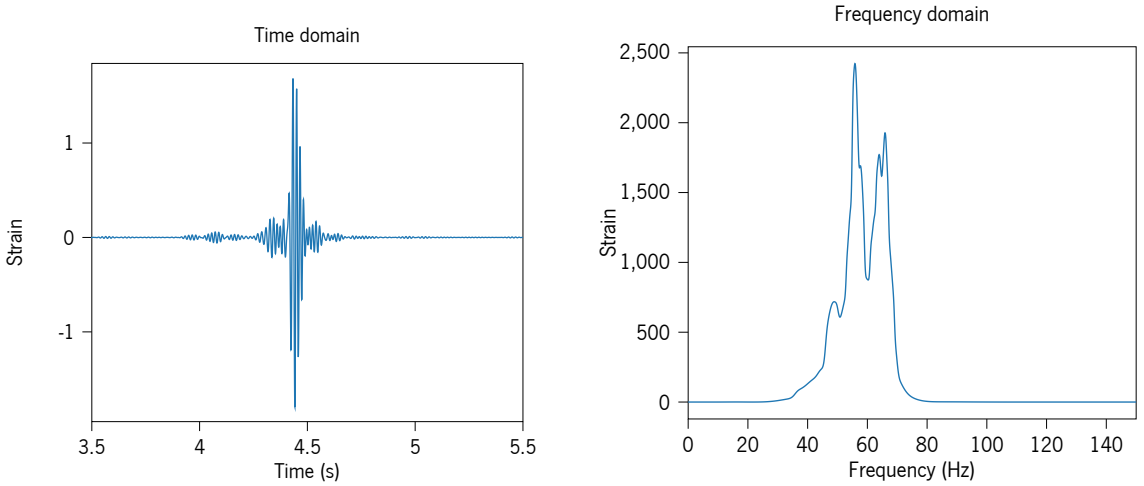

Figure 6.1: Wave-form of the signal in the time and frequency domain.

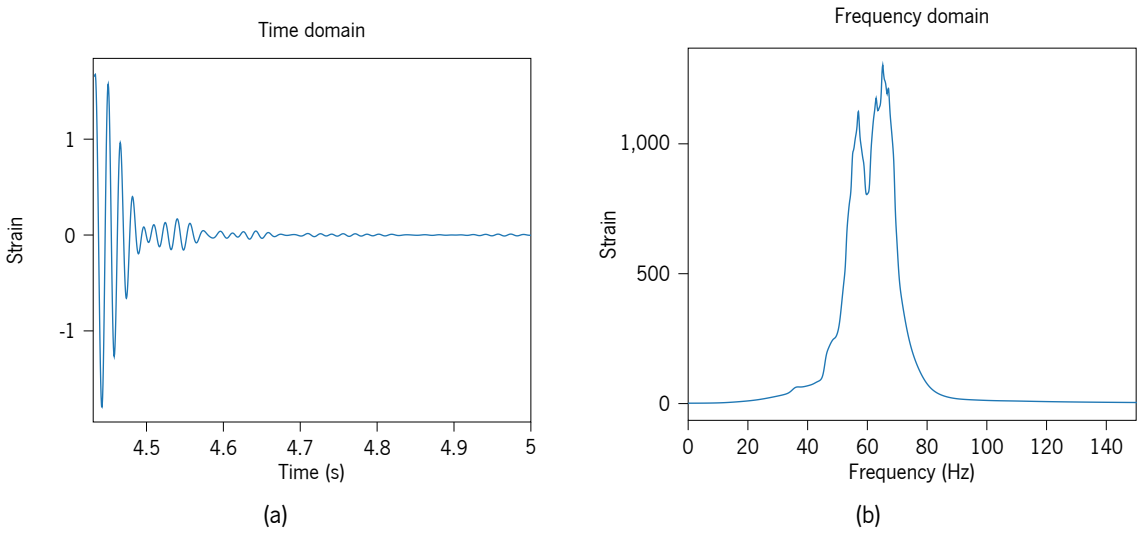

Figure 6.2: Ringdown wave-form in the time and frequency domain.

m	$\ell = 2$		$\ell = 3$		$\ell = 4$	
	$M\omega_R$	$-M\omega_I$	$M\omega_R$	$-M\omega_I$	$M\omega_R$	$-M\omega_I$
-4	———	———	———	———	1.34346	0.18625
-3	———	———	1.00073	0.18416	1.41284	0.18557
-2	0.62646	0.17761	1.07024	0.18284	1.49022	0.18444
-1	0.69565	0.17449	1.15054	0.18076	1.57690	0.18285
0	0.78181	0.17059	1.24391	0.17799	1.67441	0.18085
1	0.88994	0.16693	1.35291	0.17483	1.78436	0.17855
2	1.02394	0.16492	1.47984	0.17182	1.90831	0.17620
3	———	———	1.62611	0.16964	2.04753	0.17411
4	———	———	———	———	2.20263	0.17257

Table 6.1: Gravitational quasi-normal frequencies for $a = 0.65M$, geometric units.

6.2 Fitting of the data with quasi-normal frequencies

In order to fit[2] our data to the detected signals we cannot use the mass and spin of the black hole without adjusting those values with the value of the redshift ($z = 0.82$) due to the expansion of the universe. Taking that into account the effective mass and spin of the black hole are $M^* = 252M_\odot$ and $a^* = 0.65M^*$, respectively, as given by Abbott *et al.* (2020). Since our effective spin is $a^* = 0.65M^*$ we need to obtain data for that parameter. We just need to obtain the frequencies for low values of ℓ since our frequency domain is between 30 to $90\,\mathrm{Hz}$. Using a WKB approximation, like the one in section 4.5.2.1 one can have an idea of the modes that lie in this range, however due to large differences between the analytical and numerical methods for small ℓ we must use Leaver's method to obtain more precise frequencies. We list their values in Tables 6.1 and 6.2.

The wave-function of a gravitational perturbation for a given mode is given by

$$\Phi_{k,\ell,m}(x^\mu) = \mathrm{e}^{-\mathrm{i}\omega_{k,\ell,m}t+\mathrm{i}m\phi} R_{k,\ell,m}(r) S_{k,\ell,m}(\theta) \tag{6.2.1}$$

[2]Fit parameters can be found in appendix C.

m	$\ell = 2$		$\ell = 3$		$\ell = 4$	
	$f(\mathrm{Hz})$	$-\omega_I(\mathrm{s}^{-1})$	$f(\mathrm{Hz})$	$-\omega_I(\mathrm{s}^{-1})$	$f(\mathrm{Hz})$	$-\omega_I(\mathrm{s}^{-1})$
-4	———	———	———	———	85.63263	74.59338
-3	———	———	63.78685	73.75365	90.05528	74.32063
-2	39.93118	71.13454	68.21798	73.22475	94.98722	73.86857
-1	44.34097	69.88375	73.33585	72.39362	100.5129	73.23183
0	49.83299	68.32064	79.28773	71.28554	106.7283	72.42732
1	56.72509	66.85561	86.23506	70.01734	113.7364	71.50694
2	65.26643	66.0509	94.32575	68.81432	121.6371	70.56516
3	———	———	103.6494	67.9408	130.5106	69.72801
4	———	———	———	———	140.3969	69.11483

Table 6.2: Gravitational quasi-normal frequencies for a black hole with $M^* = 252M_\odot$ and $a^* = 0.65M^*$, where $f = \omega_R/2\pi$. We used Hz and s^{-1} here to emphasize the fact that ω_I is not a frequency, but an inverse lifetime $1/\tau$.

which can be written as

$$\Phi_{k,\ell,m}(x^\mu) = G_{k,\ell,m}(r,\theta,\phi)\mathrm{e}^{-\mathrm{i}\omega_{k,\ell,m}t}, \tag{6.2.2}$$

where k, ℓ, m denotes the overtone number, the angular momentum number and the azimuthal angular momentum number, respectively and G is a complex valued function. The complete wave-function of a general perturbation is the sum of all the modes

$$\Phi(x^\mu) = \sum_{k,\ell,m} G_{k,\ell,m}(r,\theta,\phi)\mathrm{e}^{-\mathrm{i}\omega_{k,\ell,m}t}. \tag{6.2.3}$$

We are only interested in the real part of the wave-function because it is the one with physical significance so (6.2.3) becomes

$$\Psi(x^\mu) \equiv \Re[\Phi(x^\mu)] = \sum_{k,\ell,m} A_{k,\ell,m}(r,\theta,\phi)\cos(\omega_{k,\ell,m}t + \varrho_{k,\ell,m}), \tag{6.2.4}$$

where $\varrho_{k,\ell,m}$ is the phase of the respective mode and A is now a real valued function. Obviously we don't need all the modes since our frequencies are constrained in the range 30 to $90\,\mathrm{Hz}$, a few modes should be enough to obtain a good fit to the wave-form.

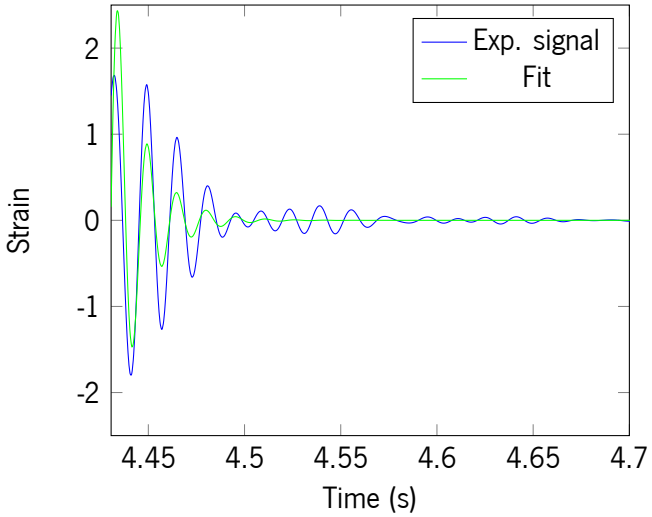

Figure 6.3: Ringdown wave-form and adjusted function for the fundamental mode $\ell = m = 2$ with fit parameter $R^2 = 0.734$.

The mode with $\ell = m = 2$ is the longest lived mode, and this is valid for all the values of a of gravitational perturbations, as one can verify in the previous chapters. Then one expects the mode $\ell = m = 2$ to be the strongest mode present in the waveform since it's the least damped one. In Figure 6.3 we see the fitted wave and the ringdown waveform. Although it follows the general behavior of the wave-form, it is clear than only one wave mode isn't enough.

If we fit the ringdown waveform to all the wave modes with $\ell = 2, 3$ and $m = -\ell, \ldots, \ell$, we are able to capture a wide range of frequencies in the 30–$90\,\mathrm{Hz}$ wave range. The fit is plotted, alongside the original wave-form, in Figure 6.4. The fitted plot almost overlaps the original signal, showing a very good agreement with the experimental data. A deeper analysis of the wave form should include other wave modes and even the overtones, which are very important describing the behavior of the wave function close to the peak, as indicated by Isi *et al.* (2019).

To conclude, this means that our analysis of black hole perturbations payed off, since we have showed, for a real life scenario, that our theoretical results are in close agreement with the experimental data.

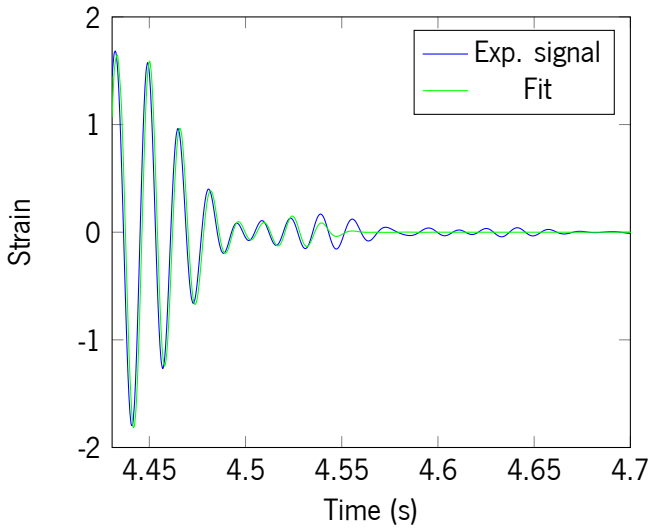

Figure 6.4: Ringdown wave-form and adjusted function for the fundamental mode with $\ell = 2, 3$ and $m = -\ell, \ldots, \ell$ with fit parameter $R^2 = 0.9946$.

7 Conclusion

We have seen that the existence of scalar fields on black hole geometries quantizes the field's frequencies, and, depending on the relation between their mass and frequencies, might give rise to quasi-bound states or quasi-normal modes. As for gravitational perturbations we are only able to obtain quasi-normal modes since they have no mass. Both kinds of quasi-normal modes correspond to spherical orbits around black holes in the geometrical limit $\ell \gg 1$. We too found that for rotating black holes, scalar fields with very small masses, of the order of $10^{-10}\,\mathrm{eV}$, are responsible for the strongest super-radiant instabilities, where the field grows exponentially in the test field approximation. The method used (Leaver's infinite continued fraction method) has been successful in obtaining the expected frequency values, based on physical arguments, and it agreed with analytical approximations in their respective domain of validity.

We have shown the importance of perturbation theory on black holes which allows us to describe phenomena on such geometries, which would be much more difficult to do with the full field equations. It allowed us to obtain non-trivial phenomena on black holes such as the instability of super-radiant modes, and to successfully relate the obtained frequencies of gravitational quasi-normal modes on Kerr to a specific gravitational wave signal, GW190521, with a goodness of fit of $R^2 = 0.994619$, concluding that our theoretical predictions match with sufficient accuracy, for the purposes of this thesis, with the observational data. This shows that considering only linear gravitational perturbations is enough to obtain a good correlation with experimental data.

As for what else could have been done, one could further explore vector perturbations as well as the

influence of bosonic fields during the merge of binary black holes and predict their gravitational imprint on a wave signal, useful for future searches for these particles which are candidates to dark matter. It would be interesting to calculate quasi-normal modes for other black hole solutions, like Kerr AdS, and obtain super-radiant instabilities with gravitational perturbations. This may happen because particles can never reach spatial infinity in such geometries, acting effectively as "bound" states or as a field trapped between mirrors, confining gravitational fields inside which are continuously amplified by the black hole. The methods studied in this thesis could in principle be applied to even more exotic black holes. With these theoretical predictions, in the future, new data from the gravitational wave detectors might allow us to detect the phenomena caused by possible ultralight bosonic fields and to confirm to an even greater precision the predictions of General Relativity, or even disprove it.

Appendices

A Klein-Gordon equation on Schwarzschild geometry

The Klein-Gordon equation for a scalar field on the Schwarzschild background is

$$\left[-\left(1-\frac{2M}{r}\right)^{-1}\frac{\partial^2}{\partial t^2}+\frac{1}{r^2}\hat{\boldsymbol{L}}^2+\frac{1}{r^2}\frac{\partial}{\partial r}\left(r^2\left(1-\frac{2M}{r}\right)\frac{\partial}{\partial r}\right)\right]\Phi=\mu^2\Phi \tag{A.0.1}$$

where

$$\left(\frac{1}{\sin^2\theta}\frac{\partial^2}{\partial\phi^2}+\cot\theta\frac{\partial}{\partial\theta}+\frac{\partial^2}{\partial\theta^2}\right)=\hat{\boldsymbol{L}}^2. \tag{A.0.2}$$

To solve equation (A.0.1) one can use the separation of variables method making $\Phi(t,r,\theta,\phi)=\eta(t)\psi(r,\theta,\phi)$ and we can try out this solution

$$\left\{-\frac{1}{f(r)}\frac{\partial^2}{\partial t^2}+\frac{1}{r^2}\hat{\boldsymbol{L}}^2+\frac{1}{r^2}\frac{\partial}{\partial r}\left[r^2f(r)\frac{\partial}{\partial r}\right]\right\}\eta(t)\psi\left(r,\theta,\phi\right)=\mu^2\eta(t)\psi\left(r,\theta,\phi\right) \tag{A.0.3}$$

$$-\frac{1}{f}\frac{\partial^2\eta}{\partial t^2}\psi+\frac{1}{r^2}\eta\hat{\boldsymbol{L}}^2\psi+\eta\frac{1}{r^2}\frac{\partial}{\partial r}\left[r^2f\frac{\partial\psi}{\partial r}\right]=\mu^2\eta\psi \tag{A.0.4}$$

where $f(r)\equiv 1-2M/r$. We hide the coordinate dependence of the functions to unclutter the expression. Dividing by both $\eta(t)$ and $\psi(r,\theta,\phi)$ we get

$$-\frac{1}{f}\frac{1}{\eta}\frac{\partial^2\eta}{\partial t^2}+\frac{1}{r^2\psi}\hat{\boldsymbol{L}}^2\psi+\frac{1}{\psi r^2}\frac{\partial}{\partial r}\left[r^2f\frac{\partial\psi}{\partial r}\right]=\mu^2 \tag{A.0.5}$$

$$-\frac{1}{\psi}f\left\{\frac{1}{r^2}\frac{\partial}{\partial r}\left[r^2f\frac{\partial\psi}{\partial r}\right]+\frac{\hat{\boldsymbol{L}}^2}{r^2}\psi-\mu^2\psi\right\}=-\frac{1}{\eta}\frac{\mathrm{d}^2\eta}{\mathrm{d}t^2}. \tag{A.0.6}$$

Now both sides can only be equal only if they are equal to a constant, let's say ω^2. Then

$$-\frac{1}{\eta}\frac{\mathrm{d}^2\eta}{\mathrm{d}t^2}=\omega^2$$

$$-\frac{1}{\psi}f\left\{\frac{1}{r^2}\frac{\partial}{\partial r}\left[r^2 f\frac{\partial\psi}{\partial r}\right]+\frac{\hat{\boldsymbol{L}}^2}{r^2}\psi-\mu^2\psi\right\}=\omega^2.$$

Solving for the first equation we get

$$\eta(t)=A\mathrm{e}^{-\mathrm{i}\omega t}+B\mathrm{e}^{\mathrm{i}\omega t} \tag{A.0.7}$$

where we chose the negative exponent solution.

As for the second equation let's define the operator

$$\hat{H}\equiv\frac{1}{r^2}\frac{\partial}{\partial r}\left[r^2 f\frac{\partial}{\partial r}\right]+\frac{\hat{\boldsymbol{L}}^2}{r^2}-\mu^2. \tag{A.0.8}$$

It is easy to see that the commutator between both operators $\hat{H}$ and $\hat{\boldsymbol{L}}^2$ is

$$\left[\hat{H},\hat{\boldsymbol{L}}^2\right]=0 \tag{A.0.9}$$

and, according to the compatibility theorem[1], if two operators commute, then they they have a common basis of eigenfunctions. From the eigenvalue equation

$$\hat{\boldsymbol{L}}^2Y^{\ell,m}(\theta,\phi)=\lambda Y^{\ell,m}(\theta,\phi) \tag{A.0.10}$$

the eigenvalues are

$$\lambda=-\ell(\ell+1) \tag{A.0.11}$$

where $\ell=0,1,2\ldots$ is the quantum number of angular number and $m=-\ell,\ldots,\ell$ is the azimuthal angular momentum number.

Now if our differential equation was

$$f\left[\frac{1}{r^2}\frac{\partial}{\partial r}\left(r^2 f\frac{\partial\psi}{\partial r}\right)+\frac{\hat{\boldsymbol{L}}^2}{r^2}\psi-\mu^2\psi\right]=-\omega^2\psi$$

that means that ψ is too a eigenfunction of $\hat{\boldsymbol{L}}^2$ meaning that $\hat{\boldsymbol{L}}^2\psi=-\ell(\ell+1)\psi$. Now separating variables once again[2], $\psi\left(r,\theta,\phi\right)=\rho(r)Y^{\ell,m}(\theta,\phi)$

$$f\left[\frac{1}{r^2}f\frac{\mathrm{d}}{\mathrm{d}r}\left(r^2 f\frac{\mathrm{d}\rho}{\mathrm{d}r}\right)-\frac{\ell(\ell+1)}{r^2}\rho(r)-\mu^2\rho\right]=-\omega^2\rho. \tag{A.0.12}$$

All we need to do is to solve equation (A.0.12). We will introduce now the Regge-Wheeler coordinate r^* which is defined as

$$\mathrm{d}r^*=\frac{\mathrm{d}r}{1-2M/r} \tag{A.0.13}$$

[1] See proof in Dirac (1981) for example.

[2] The function can be expanded in spherical harmonics. We will just work out with a specific wave mode for simplicity.

Let's define another function $R(r) = \rho(r)/r$. Now we can express equation (A.0.12) as

$$\frac{1}{r^2}\frac{\mathrm{d}}{\mathrm{d}r}\left[r^2 f \frac{\mathrm{d}}{\mathrm{d}r}\right] R(r)/r - \frac{\ell(\ell+1)}{r^2} - \mu^2 R(r)/r = -\omega^2 R(r)/r. \tag{A.0.14}$$

Let's focus only in this term

$$\frac{\mathrm{d}}{\mathrm{d}r}\left[r^2 f \frac{\mathrm{d}R(r)/r}{\mathrm{d}r}\right].$$

By the chain rule we can set everything in terms of $\mathrm{d}/\mathrm{d}r^*$ derivatives

$$r\frac{\mathrm{d}^2 R(r)}{\mathrm{d}r^{*2}}\frac{1}{f} - \frac{2M}{r^2}R(r)$$

and replacing this in equation (A.0.12)

$$f\left[\frac{1}{r^2}\left(-\ell(\ell+1)R/r + r\frac{\mathrm{d}^2 R}{\mathrm{d}r^{*2}}\frac{1}{f} - \frac{2M}{r^2}R\right) - \mu^2 R/r\right] = \omega^2 R/r \tag{A.0.15}$$

$$-\frac{\ell(\ell+1)f}{r^3}R + \frac{1}{r}\frac{\mathrm{d}^2 R}{\mathrm{d}r^{*2}} - \frac{2M}{r^4}Rf - f\mu^2 R/r = \omega^2 R/r \tag{A.0.16}$$

multiplying by r

$$-\frac{\ell(\ell+1)f}{r^2}R + \frac{\mathrm{d}^2 R}{\mathrm{d}r^{*2}} - \frac{2M}{r^3}Rf - f\mu^2 R = \omega^2 R \tag{A.0.17}$$

and we get

$$-\frac{\mathrm{d}^2 R(r)}{\mathrm{d}r^{*2}} + \left(1 - \frac{2M}{r}\right)\left(\frac{\ell\,(\ell+1)}{r^2} + \frac{2M}{r^3} + \mu^2\right) R(r) = \omega^2 R(r) \tag{A.0.18}$$

$$-\frac{\mathrm{d}^2 R(r)}{\mathrm{d}r^{*2}} + V_{\mathrm{eff}}^2(r)R(r) = \omega^2 R(r) \tag{A.0.19}$$

where

$$V_{\mathrm{eff}}^2(r) = \left(1 - \frac{2M}{r}\right)\left(\frac{\ell(\ell+1)}{r^2} + \frac{2M}{r^3} + \mu^2\right). \tag{A.0.20}$$

B Computation of the Recursion Coefficients

B.1 Quasi-bound states in Schwarzschild spacetime

An ansatz to solve equation (2.3.2) can be given by

$$R(r) = (r-2M)^{-2M\omega \mathrm{i}}\, r^{2M\omega \mathrm{i}+\chi} \mathrm{e}^{-r\sqrt{\mu^2-\omega^2}} \sum_{n=0}^{\infty} a_n \left(\frac{r-2M}{r}\right)^n .$$

We can make the following change of variable $x = 1-2M/r$ and rewrite equation (2.3.2) as

$$\frac{x^2\,(1-x)^4}{4M^2}R''(x) + \frac{x\,(1-x)^3\,(1-3x)}{4M^2}R'(x) - \left[\frac{(1-x)^3}{4M^2} + \frac{\ell(\ell+1)\,(1-x)^2}{4M^2} + \mu^2\right] R(x) = \omega^2 R(x) \quad \text{(B.1.1)}$$

where $R(x)$ is given by

$$R(x) = \left(\frac{2M}{1-x}\right)^{2M\omega \mathrm{i}+\chi} \left(\frac{2M}{1-x} - 2M\right)^{-2iM\omega} \exp\left(-\frac{2M\sqrt{\mu^2-\omega^2}}{1-x}\right) \sum_{n=0}^{\infty} a(n) x^n \quad \text{(B.1.2)}$$

and $'$ denotes the derivative of the function with respect to x.

Inserting equation (B.1.2) in equation (B.1.1) we have

$$\begin{aligned}\sum_{n=0}^{\infty} a_n x^n A + \sum_{n=0}^{\infty} a_n x^{n+1} B + \sum_{n=1}^{\infty} n a_n x^{n-1} C + \sum_{n=1}^{\infty} n a_n x^n D + \sum_{n=1}^{\infty} n a_n x^{n+1} E + \\ + \left(\mu^2-\omega^2\right)^{3/2} \sum_{n=2}^{\infty} n(n-1) a_n x^{n-1} - 2\left(\mu^2-\omega^2\right)^{3/2} \sum_{n=2}^{\infty} n(n-1) a_n x^n + \\ + \left(\mu^2-\omega^2\right)^{3/2} \sum_{n=2}^{\infty} n(n-1) a_n x^{n+1} = 0 \quad \text{(B.1.3)}\end{aligned}$$

where

$$
\begin{aligned}
A =& -\left(\ell^2+\ell+1\right)\left(\mu^2-\omega^2\right)^{3/2}+\sqrt{\mu^2-\omega^2}\left(\omega^2\mu^2 20M^2-\mu^4 4M^2\right)-\omega^3\mu^2 28\mathrm{i}M^2+\\
&\omega\mu^4 12\mathrm{i}M^2-16M^2\omega^4\left(\sqrt{\mu^2-\omega^2}-i\omega\right)+\left(\omega^2-\mu^2\right)\mu^2 3M+\\
&4M\omega\left(\mu^2-\omega^2\right)\left(\omega+\mathrm{i}\sqrt{(\mu^2-\omega^2)}\right)\\
B =& \left(\mu^2-\omega^2\right)^{3/2}+M^2\left[\mu^4\sqrt{\mu^2-\omega^2}+8\omega^4\left(\sqrt{\mu^2-\omega^2}-\mathrm{i}\omega\right)\right]-\sqrt{\mu^2-\omega^2}\omega^2\mu^2 8M^2\\
&+\omega^3\mu^2 12\mathrm{i}M^2-\omega\mu^4 4\mathrm{i}M^2+\left(\mu^2-\omega^2\right)\mu^2 2M+4M\omega\left(\omega^2-\mu^2\right)\left(\omega+\mathrm{i}\sqrt{\mu^2-\omega^2}\right)\\
C =& \left(\mu^2-\omega^2\right)^{3/2}(1-4\mathrm{i}M\omega)\\
D =& -4\left(\mu^2-\omega^2\right)^{3/2}-\left(\mu^2-\omega^2\right)\mu^2 6M+\left(\omega+\mathrm{i}\sqrt{\mu^2-\omega^2}\right)\left(\mu^2-\omega^2\right)8M\omega\\
E =& 3\left(\mu^2-\omega^2\right)^{3/2}+\left(-2\mathrm{i}\omega\sqrt{\mu^2-\omega^2}+\mu^2-2\omega^2\right)2M\left(\mu^2-\omega^2\right).
\end{aligned}
$$

Shifting the series we get

$$
\begin{aligned}
&\sum_{n=0}^{\infty}a_n x^n A+\sum_{n=1}^{\infty}a_{n-1}x^n B+\sum_{n=0}^{\infty}(n+1)a_{n+1}x^n C+\sum_{n=1}^{\infty}na_n x^n D+\\
&\quad+\sum_{n=2}^{\infty}(n-1)a_{n-1}x^n E+\left(\mu^2-\omega^2\right)^{3/2}\sum_{n=1}^{\infty}(n+1)na_{n+1}x^n-2\left(\mu^2-\omega^2\right)^{3/2}\times\\
&\qquad\times\sum_{n=2}^{\infty}n(n-1)a_n x^n+\sum_{n=3}^{\infty}(n-1)(n-2)a_{n-1}\left(\mu^2-\omega^2\right)^{3/2}x^n=0. \qquad \text{(B.1.4)}
\end{aligned}
$$

Now the series can be made to start at $n=1$, since when the new extra terms of the sums are zero, we can include them in the sum without changing the value of it. We must also strip out terms of the sums that are non-zero terms when $n<1$. So

$$
\begin{aligned}
&A\left(\sum_{n=1}^{\infty}a_n x^n+a_0\right)+B\sum_{n=1}^{\infty}a_{n-1}x^n+C\left(\sum_{n=1}^{\infty}(n+1)a_{n+1}x^n+a_1\right)+D\sum_{n=1}^{\infty}na_n x^n+\\
&\quad+E\sum_{n=1}^{\infty}(n-1)a_{n-1}x^n+\left(\mu^2-\omega^2\right)^{3/2}\sum_{n=1}^{\infty}(n+1)na_{n+1}x^n-2\left(\mu^2-\omega^2\right)^{3/2}\times\\
&\qquad\times\sum_{n=1}^{\infty}n(n-1)a_n x^n+\sum_{n=1}^{\infty}(n-1)(n-2)a_{n-1}\left(\mu^2-\omega^2\right)^{3/2}x^n=0. \qquad \text{(B.1.5)}
\end{aligned}
$$

It can be seen that everything can be factored in terms of x^n. Since the previous equation is a power series, then its coefficients for each x^n must be zero. For the coefficients of x^0 we have

$$
a_1\alpha_0+a_0\beta_0=0 \qquad \text{(B.1.6)}
$$

where

$$\begin{cases} \alpha_0 = \left(\mu^2-\omega^2\right)^{3/2}\left(1-4\mathrm{i}M\omega\right) \\ \beta_0 = -\left(\ell^2+\ell+1\right)\left(\mu^2-\omega^2\right)^{3/2} + 4M^2\left(\mu^2-\omega^2\right)\left[4\omega^2\left(\sqrt{\mu^2-\omega^2}-\mathrm{i}\omega\right)+\right. \\ \qquad \left. -\mu^2\left(\sqrt{\mu^2-\omega^2}-3\mathrm{i}\omega\right)\right] + 4M^2(\mu-\omega)(\mu+\omega)\times \\ \qquad \times\left(4\omega^2\left(\sqrt{\mu^2-\omega^2}-i\omega\right)-\mu^2\left(\sqrt{\mu^2-\omega^2}-3i\omega\right)\right). \end{cases} \tag{B.1.7}$$

The coefficients for $n>0$ are

$$a_{n+1}\alpha_n + a_n\beta_n + a_{n-1}\gamma_n = 0 \tag{B.1.8}$$

where

$$\begin{cases} \alpha_n = (n+1)\left(\mu^2-\omega^2\right)^{3/2}\left(n-4\mathrm{i}M\omega+1\right) \\ \beta_n = -\left(\ell^2+\ell+2n(n+1)+1\right)\left(\mu^2-\omega^2\right)^{3/2} + 4M^2\left(\mu^2-\omega^2\right)\left[4\omega^2\left(\sqrt{\mu^2-\omega^2}-\mathrm{i}\omega\right)+\right. \\ \qquad \left. -\mu^2\left(\sqrt{\mu^2-\omega^2}-3\mathrm{i}\omega\right)\right] - M(2n+1)\left(\mu^2-\omega^2\right)\left(-4\mathrm{i}\omega\sqrt{\mu^2-\omega^2}+3\mu^2-4\omega^2\right) \\ \gamma_n = M^2\left[\mu^4\left(\sqrt{\mu^2-\omega^2}-4\mathrm{i}\omega\right)+4\mu^2\omega^2\left(-2\sqrt{\mu^2-\omega^2}+3\mathrm{i}\omega\right)+8\omega^4\left(\sqrt{\mu^2-\omega^2}-\mathrm{i}\omega\right)\right] \\ \qquad +2Mn\left(\mu^2-\omega^2\right)\left(-2\mathrm{i}\omega\sqrt{\mu^2-\omega^2}+\mu^2-2\omega^2\right)+n^2\left(\mu^2-\omega^2\right)^{3/2}. \end{cases} \tag{B.1.9}$$

In order to get everything in units of M, we can multiply equations (B.1.6) and (B.1.8) by M^3, redefining our coefficients. Then we can effectively put everything in units of M in our coefficients by making the change of variables $M\omega=\omega^*$ and $M\mu=\mu^*$

$$\begin{cases} \alpha_n = (n+1)\left(\mu^{*2}-\omega^{*2}\right)^{3/2}\left(n-4\mathrm{i}\omega^*+1\right) \\ \beta_n = -\left(\ell^2+\ell+2n(n+1)+1\right)\left(\mu^{*2}-\omega^{*2}\right)^{3/2} + 4\left(\mu^{*2}-\omega^{*2}\right)\times \\ \qquad \left[4\omega^{*2}\left(\sqrt{\mu^{*2}-\omega^{*2}}-\mathrm{i}\omega^*\right)+-\mu^{*2}\left(\sqrt{\mu^{*2}-\omega^{*2}}-3\mathrm{i}\omega^*\right)\right]+ \\ \qquad -(2n+1)\left(\mu^{*2}-\omega^{*2}\right)\left(-4\mathrm{i}\omega^*\sqrt{\mu^{*2}-\omega^{*2}}+3\mu^{*2}-4\omega^{*2}\right) \\ \gamma_n = \left[\mu^{*4}\left(\sqrt{\mu^{*2}-\omega^{*2}}-4\mathrm{i}\omega^*\right)+4\mu^{*2}\omega^{*2}\left(-2\sqrt{\mu^{*2}-\omega^{*2}}+3\mathrm{i}\omega^*\right)+\right. \\ \qquad \left. 8\omega^{*4}\left(\sqrt{\mu^{*2}-\omega^{*2}}-\mathrm{i}\omega^*\right)\right]+2n\left(\mu^{*2}-\omega^{*2}\right)\left(-2\mathrm{i}\omega^*\sqrt{\mu^{*2}-\omega^{*2}}+\mu^{*2}-2\omega^{*2}\right) \\ \qquad +n^2\left(\mu^{*2}-\omega^{*2}\right)^{3/2} \end{cases} \tag{B.1.10}$$

which coincide with the coefficients calculated in Konoplya and Zhidenko (2005).

B.2 Quasi-normal modes in Schwarzschild spacetime

For scalar, vectorial and tensorial perturbations in Schwarzschild spacetime, their respective master equations can always be separated in all variables. In order to obtain the frequency eigenvalues to these

perturbations one must find an ansatz for the radial equation

$$-\frac{\mathrm{d}^2}{\mathrm{d}r^{*2}}R(r^*)+\left(1-\frac{2M}{r}\right)\left[\frac{\ell(\ell+1)}{r^2}-\frac{\epsilon}{r^3}\right]R(r^*)=\omega^2R(r^*),$$

where $\epsilon=1-s^2$, $-2M$ for scalar fields, 0 for vector fields like the electromagnetic one and $6M$ for tensor fields like a gravitational perturbation. We use as an ansatz

$$R(r)=(r-2M)^{-2M\omega\mathrm{i}}\,r^{4M\omega\mathrm{i}}\mathrm{e}^{\mathrm{i}\omega(r-2M)}\sum_{n=0}^{\infty}a_n\left(1-\frac{2M}{r}\right)^n$$

given in Leaver (1985). Making the replacement $x=1-2M/r$ we have

$$R(x)=\mathrm{e}^{-\frac{2\mathrm{i}Mx\omega}{x-1}}\left(\frac{M}{1-x}\right)^{4\mathrm{i}M\omega}\left(\frac{Mx}{2(1-x)}\right)^{-2\mathrm{i}M\omega}\sum_{n=0}^{\infty}a_nx^n \tag{B.2.1}$$

and

$$\frac{x^2\left(1-x\right)^4}{4M^2}R''(x)+\frac{x\left(1-x\right)^3\left(1-3x\right)}{4M^2}R'(x)-\left[\frac{\left(1-x\right)^3}{4M^2}+\frac{\ell(\ell+1)\left(1-x\right)^2}{4M^2}-\omega^2\right]R(x)=0.$$

Substituting the ansatz on the equation we get

$$\sum_{n=0}^{\infty}a_nx^n\left(-2\ell^2M-2\ell M+64M^3\omega^2+16\mathrm{i}M^2\omega+\epsilon\right)+\sum_{n=1}^{\infty}na_n\left(2M-8\mathrm{i}M^2\omega\right)x^{n-1}+$$
$$\sum_{n=0}^{\infty}a_nx^{n+1}\left(-32M^3\omega^2-16\mathrm{i}M^2\omega-\epsilon\right)+\sum_{n=1}^{\infty}2Mna_n(3-8\mathrm{i}M\omega)x^{n+1}+2M\sum_{n=2}^{\infty}n(n-1)a_nx^{n-1}+$$
$$2M\sum_{n=2}^{\infty}n(n-1)a_nx^{n+1}+\sum_{n=1}^{\infty}2Mna_n(-4+16\mathrm{i}M\omega)x^n-4M\sum_{n=2}^{\infty}n(n-1)a_nx^n=0.$$

Shifting the sums

$$\sum_{n=0}^{\infty}a_nx^n\left(-2\ell^2M-2\ell M+64M^3\omega^2+16\mathrm{i}M^2\omega+\epsilon\right)+\sum_{n=0}^{\infty}(n+1)a_{n+1}\left(2M-8\mathrm{i}M^2\omega\right)x^n+$$
$$\sum_{n=1}^{\infty}a_{n-1}x^n\left(-32M^3\omega^2-16\mathrm{i}M^2\omega-\epsilon\right)+\sum_{n=1}^{\infty}2Mna_n(-4+16\mathrm{i}M\omega)x^n+\sum_{n=2}^{\infty}2M(n-1)\times$$
$$(3-8\mathrm{i}M\omega)x^na_{n-1}+2M\sum_{n=3}^{\infty}(n-1)(n-2)a_{n-1}x^n+2M\sum_{n=1}^{\infty}(n+1)na_{n+1}x^n-4M\sum_{n=2}^{\infty}n(n-1)a_nx^n=0$$

and setting all the sums to start at $n = 1$ we end up with

$$\sum_{n=1}^{\infty} a_n x^n \left(-2\ell^2 M - 2\ell M + 64M^3\omega^2 + 16\mathrm{i}M^2\omega + \epsilon\right) + \sum_{n=1}^{\infty}(n+1)a_{n+1}\left(2M - 8\mathrm{i}M^2\omega\right)x^n +$$
$$\sum_{n=1}^{\infty} a_{n-1}x^n\left(-32M^3\omega^2 - 16\mathrm{i}M^2\omega - \epsilon\right) + \sum_{n=1}^{\infty} 2Mna_n(-4 + 16\mathrm{i}M\omega)x^n$$
$$+ \sum_{n=1}^{\infty} 2M(n-1)a_{n-1}(3 - 8\mathrm{i}M\omega)x^n + 2M\sum_{n=1}^{\infty}(n-1)(n-2)a_{n-1}x^n +$$
$$2M\sum_{n=1}^{\infty}(n+1)na_{n+1}x^n - 4M\sum_{n=1}^{\infty} n(n-1)a_n x^n +$$
$$a_0\left(-2\ell^2 M - 2\ell M + 64M^3\omega^2 + 16\mathrm{i}M^2\omega + \epsilon\right) + a_1\left(2M - 8\mathrm{i}M^2\omega\right) = 0.$$

It can be seen that everything can be factored in terms of x^n. Since the previous equation is a power series, then its coefficients for each x^n must be zero. For the coefficients of x^0 we have

$$\alpha_0 a_1 + \beta_0 a_0 = 0 \tag{B.2.2}$$

where

$$\begin{cases} \alpha_0 = 1 - 4\mathrm{i}M\omega \\ \beta_0 = -\ell^2 - \ell + 32M^2\omega^2 + 8\mathrm{i}M\omega + \dfrac{\epsilon}{2M} \end{cases} \tag{B.2.3}$$

The coefficients for $n > 0$ are

$$\alpha_n a_{n+1} + \beta_n a_n + \gamma_n a_{n-1} = 0 \tag{B.2.4}$$

where

$$\begin{cases} \alpha_n = (n+1)(n - 4\mathrm{i}M\omega + 1) \\ \beta_n = -\ell^2 - \ell + 32M^2\omega^2 + n(-2 + 16\mathrm{i}M\omega) + 8\mathrm{i}M\omega + \dfrac{\epsilon}{2M} - 2n^2 \\ \gamma_n = -16M^2\omega^2 - 8\mathrm{i}Mn\omega - \dfrac{\epsilon}{2M} + n^2 - 1. \end{cases} \tag{B.2.5}$$

B.3 Quasi-bound states in Kerr spacetime

B.3.1 Angular equation

The angular equation is given by

$$(1-u^2)\frac{\mathrm{d}^2 S(u)}{\mathrm{d}u^2} - 2u\frac{\mathrm{d}S(u)}{\mathrm{d}u} + \left[a^2u^2(\omega^2 - \mu^2) + \Lambda - \frac{m^2}{1-u^2}\right]S(u) = 0 \tag{B.3.1}$$

with $u = \cos\theta$. The ansatz proposed by Leaver (1985) is

$$S(u) = \mathrm{e}^{au\sqrt{\omega^2-\mu^2}}(1+u)^k(1-u)^k\sum_{n=0}^{\infty} b_n(1+u)^n \tag{B.3.2}$$

where $k = \frac{1}{2}|m|$. If we make the replacement $x = 1+u$, and inserting our ansatz in the angular equation we end up with

$$\left(a^2(x-1)^2(\omega^2-\mu^2) + \frac{4k^2}{(x-2)x} + \Lambda\right) S(x) - (x-2)x\frac{\mathrm{d}^2S(x)}{\mathrm{d}x^2} + (2-2x)\frac{\mathrm{d}S(x)}{\mathrm{d}x} = 0 \tag{B.3.3}$$

and

$$S(x) = (-((x-2)x))^k e^{a(x-1)\sqrt{\omega^2-\mu^2}}\sum_{n=0}^{\infty} b_n x^n. \tag{B.3.4}$$

Replacing the ansatz in the angular equation we have

$$\sum_{n=0}^{\infty} b_n x^n\left(a^2(\omega^2-\mu^2) + 2a(2k+1)\sqrt{\omega^2-\mu^2} - 4k^2 - 2k + \Lambda\right) +$$

$$\sum_{n=0}^{\infty} b_n x^{n+1}(-2a(2k+1)\sqrt{\omega^2-\mu^2}) + \sum_{n=1}^{\infty} n b_n x^n(4a\sqrt{\omega^2-\mu^2} - 4k - 2) + \sum_{n=1}^{\infty} n\left(-2a\sqrt{\omega^2-\mu^2}\right)\times$$

$$b_n x^{n+1} + \sum_{n=1}^{\infty}(4k+2)n b_n x^{n-1} + 2\sum_{n=2}^{\infty} n(n-1)b_n x^{n-1} - \sum_{n=2}^{\infty} n(n-1)b_n x^n = 0$$

and shifting the sum and making them start at $n = 1$ we have

$$\sum_{n=1}^{\infty} b_n x^n\left(a^2(\omega^2-\mu^2) + 2a(2k+1)\sqrt{\omega^2-\mu^2} - 4k^2 - 2k + \Lambda\right) +$$

$$\sum_{n=1}^{\infty} b_{n-1}x^n(-2a(2k+1)\sqrt{\omega^2-\mu^2}) + \sum_{n=1}^{\infty} n b_n x^n(4a\sqrt{\omega^2-\mu^2} - 4k - 2) +$$

$$\sum_{n=1}^{\infty}(n-1)(-2a\sqrt{\omega^2-\mu^2})b_{n-1}x^n + \sum_{n=1}^{\infty}(4k+2)(n+1)b_{n+1}x^n +$$

$$2\sum_{n=1}^{\infty} n(n+1)b_{n+1}x^n - \sum_{n=1}^{\infty} n(n-1)b_n x^n + b_0\left(a^2(\omega^2-\mu^2) + 2a(2k+1)\sqrt{\omega^2-\mu^2} - 4k^2 - 2k + \Lambda\right) +$$

$$b_1(4k+2) = 0.$$

It can be seen that everything can be factored in terms of x^n. Since the previous equation is a power series, then its coefficients for each x^n must be zero. For the coefficients of x^0 we have

$$\alpha_0 a_1 + \beta_0 a_0 = 0 \tag{B.3.5}$$

where

$$\begin{cases} \alpha_0 = (2k+1) \\ \beta_0 = k(4a\sqrt{\omega^2-\mu^2}-2) + a\sqrt{\omega^2-\mu^2}(a\sqrt{\omega^2-\mu^2}+2) - 4k^2 + \Lambda \end{cases} \tag{B.3.6}$$

The coefficients for $n > 0$ are

$$\alpha_n a_{n+1} + \beta_n a_n + \gamma_n a_{n-1} = 0 \tag{B.3.7}$$

where

$$\begin{cases} \alpha_n = 2(1+n)(1+2k+n) \\ \beta_n = k(4a\sqrt{\omega^2-\mu^2}-4n-2) + n(4a\sqrt{\omega^2-\mu^2}-1) + \\ \quad a\sqrt{\omega^2-\mu^2}(a\sqrt{\omega^2-\mu^2}+2) - 4k^2 + \Lambda - n^2 \\ \gamma_n = -2a\sqrt{\omega^2-\mu^2}(2k+n). \end{cases} \tag{B.3.8}$$

B.3.2 Radial equation

We set $2M = 1$ for the rest of the section. We need to solve the following radial equation

$$\frac{\mathrm{d}}{\mathrm{d}r}\left(\Delta\frac{\mathrm{d}R(r)}{\mathrm{d}r}\right) + \left[\frac{(\omega(r^2+a^2)-am)^2 + \Delta 2am\omega}{\Delta} - \omega^2a^2 - \mu^2r^2 - \Lambda\right]R(r) = 0$$

and we shall use the following ansatz as a solution

$$R(r) = (r-r_+)^{-\mathrm{i}\sigma}(r-r_-)^{-\mathrm{i}\sigma+\chi-1}\mathrm{e}^{-r\sqrt{\mu^2-\omega^2}}\sum_{n=0}^{\infty} d_n\left(\frac{r-r_+}{r-r_-}\right)^n.$$

Making the replacement $x = \frac{r-r_+}{r-r_-}$ we get

$$\left[\frac{(x-1)^2\left(a^2m^2+\omega^2\left(a^2+\frac{(r_+-r_-x)^2}{(x-1)^2}\right)^2+\frac{2am\omega(r_+-r_-x)}{x-1}\right)}{x(r_--r_+)^2} - a^2\omega^2 - \Lambda - \frac{\mu^2(r_+-r_-x)^2}{(x-1)^2}\right]R(x) +$$
$$\frac{(x-1)(-2r_-x+2r_++x-1)}{r_--r_+}R'(x) + (x-1)x\left((x-1)R''(x)+2R'(x)\right) = 0 \tag{B.3.9}$$

and the ansatz can be expressed as

$$R(x) = \left(\frac{x(r_--r_+)}{x-1}\right)^{-\mathrm{i}\sigma}\mathrm{e}^{\frac{\sqrt{\mu^2-\omega^2}(r_+-r_-x)}{x-1}}\left(\frac{r_--r_+}{x-1}\right)^{\mathrm{i}\sigma+\chi-1}\sum_{n=0}^{\infty} d_nx^n. \tag{B.3.10}$$

Then replacing it on the radial equation we get

$$\frac{A\sum_{n=0}^{\infty}x^{n+1}d_n}{\mu^2-\omega^2}+4\left(4a^2-1\right)\sum_{n=2}^{\infty}n(n-1)x^{n-1}d_n+B\sum_{n=1}^{\infty}nx^{n-1}d_n-\frac{C\sum_{n=0}^{\infty}x^nd_n}{\sqrt{\mu^2-\omega^2}}+$$
$$8\left(1-4a^2\right)\sum_{n=2}^{\infty}n(n-1)x^nd_n+\frac{D\sum_{n=1}^{\infty}nx^nd_n}{\sqrt{\mu^2-\omega^2}}+4\left(4a^2-1\right)\sum_{n=2}^{\infty}n(n-1)x^{n+1}d_n+E\sum_{n=1}^{\infty}nx^{n+1}d_n=0 \tag{B.3.11}$$

where

$$\begin{aligned}
A=&-b^2\mu^4+2\mu^2\left\{\left[8\left(\sqrt{\mu^2-\omega^2}+1\right)-4\mathrm{i}\omega\left(-2\mathrm{i}\omega+\sqrt{\mu^2-\omega^2}+2\right)\right]a^2-2\left(\sqrt{\mu^2-\omega^2}+1\right)\right.\\
&\left.-2\mathrm{i}abm\left(-2\mathrm{i}\omega+\sqrt{\mu^2-\omega^2}+2\right)+(b+1)\,\omega\left(2\omega+\mathrm{i}\left(\sqrt{\mu^2-\omega^2}+2\right)\right)\right\}\\
&-4\omega^2\left\{\left[8\sqrt{\mu^2-\omega^2}-4\omega\left(\omega+\mathrm{i}\left(\sqrt{\mu^2-\omega^2}+1\right)\right)+4\right]a^2-2\sqrt{\mu^2-\omega^2}\right.\\
&\left.-2\mathrm{i}abm\left(-\mathrm{i}\omega+\sqrt{\mu^2-\omega^2}+1\right)+(b+1)\,\omega\left(\omega+\mathrm{i}\left(\sqrt{\mu^2-\omega^2}+1\right)\right)-1\right\}\\
B=&\,4\mathrm{i}b\left(-2am+\omega+\mathrm{i}b+\omega b\right)\\
C=&\,2\left\{\left[16\mathrm{i}a^3m-2\mathrm{i}a\,(b+2)\,m+3\mathrm{i}\omega-2b-8a^4\sqrt{\mu^2-\omega^2}-\sqrt{\mu^2-\omega^2}-b\left(\sqrt{\mu^2-\omega^2}-3\mathrm{i}\omega\right)\right.\right.\\
&\left.+2a^2\left(4b-2\mathrm{i}\,(2b+3)\,\omega+2b\sqrt{\mu^2-\omega^2}+3\sqrt{\mu^2-\omega^2}+2\right)-1\right]\mu^2+\\
&2\left[2\mathrm{i}\left(-b+2a^2\,(b+2)-1\right)\omega^3+\left(\left(4b+4b\sqrt{\mu^2-\omega^2}+9\sqrt{\mu^2-\omega^2}+4\right)(-a^2)-8\mathrm{i}a^3m\right.\right.\\
&\left.+m2\mathrm{i}a\,(b+1)+4a^4\sqrt{\mu^2-\omega^2}+(b+1)\left(2\sqrt{\mu^2-\omega^2}+1\right)\right)\omega^2\\
&\left.\left.+\left(-2\mathrm{i}abm-\Lambda+4a^2(\Lambda+1)-1\right)\sqrt{\mu^2-\omega^2}+\left[\left(-4\mathrm{i}a^2-2abm+\mathrm{i}\,(b+1)\right)\omega\right]\sqrt{\mu^2-\omega^2}\right]\right\}\\
D=&\,4b\left\{\left(-8a^2+b+2\right)\mu^2-2\left(-4a^2+b+1\right)\omega^2+4\left(\mathrm{i}am+b\right)\sqrt{\mu^2-\omega^2}-2\mathrm{i}\,(b+1)\,\omega\sqrt{\mu^2-\omega^2}\right\}\\
E=&\,4\left\{12a^2-2\mathrm{i}abm+\mathrm{i}\omega\left(b^2+b\right)+\frac{-b^2\mu^2}{\sqrt{\mu^2-\omega^2}}+\frac{-2b^2\omega^2}{\sqrt{\mu^2-\omega^2}}-3\right\},
\end{aligned}$$

where $b=\sqrt{1-4a^2}$. Shifting the sums and making them start at $n=1$ we have

$$-\frac{Cd_0}{\sqrt{\mu^2-\omega^2}}+Bd_1+\frac{A\sum_{n=1}^{\infty}x^nd_{n-1}}{\mu^2-\omega^2}+E\sum_{n=1}^{\infty}(n-1)x^nd_{n-1}+$$
$$4\left(4a^2-1\right)\sum_{n=1}^{\infty}(n-1)(n-2)x^nd_{n-1}+B\sum_{n=1}^{\infty}(n+1)x^nd_{n+1}+$$

$$4\left(4a^2-1\right)\sum_{n=1}^{\infty}(n+1)nx^n d_{n+1}-\frac{C\sum_{n=1}^{\infty}x^n d_n}{\sqrt{\mu^2-\omega^2}}+8\left(1-4a^2\right)\sum_{n=1}^{\infty}n(n-1)x^n d_n+\frac{D\sum_{n=1}^{\infty}nx^n d_n}{\sqrt{\mu^2-\omega^2}}=0,$$

which results in

$$\alpha_0 a_1+\beta_0 a_0=0 \tag{B.3.12}$$

with

$$\begin{cases}\alpha_0=\dfrac{2\mathrm{i}am-\mathrm{i}(b+1)\omega+b}{b}\\ \beta_0=\dfrac{1}{4b\sqrt{\mu^2-\omega^2}}\Big\{-b\Big[-\omega^2\left(8\mathrm{i}am+7\sqrt{\mu^2-\omega^2}+4\right)+\mu^2\left(8\mathrm{i}am+\sqrt{\mu^2-\omega^2}-6\mathrm{i}\omega+2\right)\\ \quad+4\sqrt{\mu^2-\omega^2}(\Lambda+1)-4\mathrm{i}\omega\sqrt{\mu^2-\omega^2}+8\mathrm{i}\omega^3\Big]+\\ \quad 2\mathrm{i}(2am-\omega)\left(-\mu^2+2\omega\left(\omega+\mathrm{i}\sqrt{\mu^2-\omega^2}\right)-2\sqrt{\mu^2-\omega^2}\right)\\ \quad -b^3(\mu^2-\omega^2)^{3/2}+2b^2\left(2\omega^2\left(\sqrt{\mu^2-\omega^2}-\mathrm{i}\omega+1\right)-\mu^2\left(\sqrt{\mu^2-\omega^2}-2\mathrm{i}\omega+2\right)\right)\Big\}.\end{cases} \tag{B.3.13}$$

The coefficients for $n>0$ are

$$a_{n+1}\alpha_n+a_n\beta_n+a_{n-1}\gamma_n=0 \tag{B.3.14}$$

where

$$\begin{cases}\alpha_n=\dfrac{(n+1)(2\mathrm{i}am+bn-\mathrm{i}(b+1)\omega+b)}{b}\\ \beta_n=\dfrac{1}{4b\sqrt{\mu^2-\omega^2}}\Big\{-b\Big(-\omega^2\left(8\mathrm{i}am+7\sqrt{\mu^2-\omega^2}+8n+4\right)\\ \quad+\mu^2\left(8\mathrm{i}am+\sqrt{\mu^2-\omega^2}+4n-6\mathrm{i}\omega+2\right)+\\ \quad 4\sqrt{\mu^2-\omega^2}(\Lambda+2n(n+1)+1)-4\mathrm{i}(2n+1)\omega\sqrt{\mu^2-\omega^2}+8\mathrm{i}\omega^3\Big)+\\ \quad 2\mathrm{i}(2am-\omega)\left(-\mu^2+2\omega\left(\omega+\mathrm{i}\sqrt{\mu^2-\omega^2}\right)-2(2n+1)\sqrt{\mu^2-\omega^2}\right)\\ \quad -b^3(\mu^2-\omega^2)^{3/2}+2b^2\left(2\omega^2\left(\sqrt{\mu^2-\omega^2}+2n-\mathrm{i}\omega+1\right)-\mu^2\left(\sqrt{\mu^2-\omega^2}+4n-2\mathrm{i}\omega+2\right)\right)\Big\}\\ \gamma_n=\dfrac{1}{4b(\mu^2-\omega^2)^{3/2}}\Big\{4am(\mu^2-\omega^2)\left(2\omega\left(\sqrt{\mu^2-\omega^2}-\mathrm{i}\omega\right)+\mathrm{i}\mu^2+2\mathrm{i}n\sqrt{\mu^2-\omega^2}\right)+b\\ \quad\Big(\left(\mu^2-2\omega^2\right)\left(\mu^2\left(\sqrt{\mu^2-\omega^2}-2\mathrm{i}\omega\right)-2\omega^2\left(\sqrt{\mu^2-\omega^2}-\mathrm{i}\omega\right)\right)+\\ \quad 4n^2(\mu^2-\omega^2)^{3/2}+4n(\mu^2-\omega^2)\left(\mu^2+\omega\left(-2\omega-\mathrm{i}\sqrt{\mu^2-\omega^2}\right)\right)\Big)\\ \quad -2\mathrm{i}\omega(\mu^2-\omega^2)\left(-2\mathrm{i}\omega\sqrt{\mu^2-\omega^2}+\mu^2+2n\sqrt{\mu^2-\omega^2}-2\omega^2\right)\Big\}.\end{cases} \tag{B.3.15}$$

B.4 Quasi-normal modes in Kerr

B.4.1 Angular equation

B.4.2 Radial equation

Let us begin with equation (5.1.3). An ansatz for the solution of this equation is given by Leaver (1985) as

$$R(r) = \mathrm{e}^{\mathrm{i}\omega r}(r-r_-)^{-1-s+\mathrm{i}\omega+\mathrm{i}\sigma}(r-r_+)^{-s-\mathrm{i}\sigma}\sum_{n=0}^{\infty} d_n \left(\frac{r-r_+}{r-r_-}\right)^n .$$

Making the substitution $x = \frac{r-r_+}{r-r_-}$, the radial equation and the ansatz become

$$\left\{ \frac{(x-1)^2\left[a^2m^2 + \mathrm{i}s\left(a^2\omega + \frac{am(2r_-x-2r_+-x+1)}{x-1} - \frac{\omega(r_+-r_-x)^2}{(x-1)^2}\right) + \frac{2am\omega(r_+-r_-x)}{x-1}\right]}{x(r_- - r_+)^2} \right.$$
$$\left. + \frac{\omega^2\left(a^2 + \frac{(r_+-r_-x)^2}{(x-1)^2}\right)^2}{x(r_- - r_+)^2} - a^2\omega^2 - \Lambda + \frac{2\mathrm{i}s\omega(r_-x - r_+)}{x-1} \right\} R(x) +$$
$$\frac{(s+1)(x-1)(-2r_-x+2r_++x-1)}{r_- - r_+}R'(x) + (x-1)x\left((x-1)R''(x) + 2R'(x)\right) = 0 \tag{B.4.1}$$

$$R(x) = -\frac{\left((x-1)\mathrm{e}^{\frac{\mathrm{i}\omega(r_-x-r_+)}{x-1}}\left(\frac{x(r_--r_+)}{x-1}\right)^{-s-\mathrm{i}\sigma}\left(\frac{r_--r_+}{x-1}\right)^{-s+\mathrm{i}(\sigma+\omega)}\right)}{r_+ - r_-}\sum_{n=0}^{\infty} d_n x^n \tag{B.4.2}$$

which results in

$$\left(2\mathrm{i}\sqrt{1-4a^2}am + 4a^2(s+\mathrm{i}\omega-1) - \mathrm{i}\left(\sqrt{1-4a^2}+1\right)\omega - s + 1\right)\sum_{n=0}^{\infty} n d_n x^{n-1} +$$
$$x\left[-(2\omega+\mathrm{i})\left(-2\sqrt{1-4a^2}am - 4\mathrm{i}a^2(s-\mathrm{i}\omega+1) + \sqrt{1-4a^2}\omega + \mathrm{i}(s+1) + \omega\right)\sum_{n=0}^{\infty} d_n x^n \right.$$
$$+\left(-4\mathrm{i}\sqrt{1-4a^2}am + 8a^2\left(2 - \mathrm{i}\left(\sqrt{1-4a^2}+2\right)\omega\right) + 4\mathrm{i}\left(\sqrt{1-4a^2}\omega + \omega + \mathrm{i}\right)\right)\sum_{n=0}^{\infty} n d_n x^{n-1}$$
$$\left. + \left(1-4a^2\right)\sum_{n=0}^{\infty} n d_n\left(n x^{n-2} - x^{n-2}\right)\right] +$$

$$\left(1-4a^2\right)x^3\left(\sum_{n=0}^{\infty}nd_n\left(nx^{n-2}-x^{n-2}\right)\right)+x^2\left[2\left(4a^2-1\right)\sum_{n=0}^{\infty}nd_n\left(nx^{n-2}-x^{n-2}\right)\right.$$
$$\left.+\left(\mathrm{i}\sqrt{1-4a^2}(2am-\omega)-4a^2s+3\mathrm{i}\left(4a^2-1\right)(\omega+\mathrm{i})+s\right)\sum_{n=0}^{\infty}nd_nx^{n-1}\right]+$$
$$-\left[-4a^4\omega^2-8a^3m\omega+2am\left(2\sqrt{1-4a^2}\omega+\mathrm{i}\sqrt{1-4a^2}+\omega\right)+\right.$$
$$a^2\left[\omega\left(\left(8\sqrt{1-4a^2}+17\right)\omega+4\mathrm{i}\left(\sqrt{1-4a^2}+2\right)\right)-4\Lambda-4s-4\right]+$$
$$\left.-2\left(\sqrt{1-4a^2}+1\right)\omega(2\omega+\mathrm{i})+\Lambda+s+1\right]\sum_{n=0}^{\infty}d_nx^n.$$

Shifting the sums and making them start at $n=1$ we have

$$-(2\omega+\mathrm{i})\left(-2\sqrt{1-4a^2}am-4\mathrm{i}a^2(s-\mathrm{i}\omega+1)+\sqrt{1-4a^2}\omega+\mathrm{i}(s+1)+\omega\right)\sum_{n=1}^{\infty}d_{n-1}x^n+$$
$$\left(\mathrm{i}\sqrt{1-4a^2}(2am-\omega)-4a^2s+3\mathrm{i}\left(4a^2-1\right)(\omega+\mathrm{i})+s\right)\sum_{n=1}^{\infty}(n-1)d_{n-1}x^n+$$
$$\left(2\mathrm{i}\sqrt{1-4a^2}am+4a^2(s+\mathrm{i}\omega-1)-\mathrm{i}\left(\sqrt{1-4a^2}+1\right)\omega-s+1\right)\sum_{n=1}^{\infty}(n+1)d_{n+1}x^n+$$
$$\left(-4\mathrm{i}\sqrt{1-4a^2}am+8a^2\left(2-\mathrm{i}\left(\sqrt{1-4a^2}+2\right)\omega\right)+4\mathrm{i}\left(\sqrt{1-4a^2}\omega+\omega+\mathrm{i}\right)\right)\sum_{n=1}^{\infty}nd_nx^n+$$
$$\left(1-4a^2\right)\sum_{n=2}^{\infty}(n-1)(n-2)d_{n-1}x^n+\left(1-4a^2\right)\sum_{n=1}^{\infty}(n+1)nd_{n+1}x^n+2\left(4a^2-1\right)\sum_{n=1}^{\infty}n(n-1)d_nx^n$$
$$-\left[-4a^4\omega^2-8a^3m\omega+2am\left(2\sqrt{1-4a^2}\omega+\mathrm{i}\sqrt{1-4a^2}+\omega\right)+a^2\right.$$
$$\left(\omega\left(\left(8\sqrt{1-4a^2}+17\right)\omega+4\mathrm{i}\left(\sqrt{1-4a^2}+2\right)\right)-4\Lambda-4s-4\right)$$
$$\left.-2\left(\sqrt{1-4a^2}+1\right)\omega(2\omega+\mathrm{i})+\Lambda+s+1\right]\sum_{n=1}^{\infty}d_nx^n+$$
$$d_1\left(2\mathrm{i}\sqrt{1-4a^2}am+4a^2(s+\mathrm{i}\omega-1)-\mathrm{i}\left(\sqrt{1-4a^2}+1\right)\omega-s+1\right)-$$
$$d_0\left[-4a^4\omega^2-8a^3m\omega+2am\left(2\sqrt{1-4a^2}\omega+\mathrm{i}\sqrt{1-4a^2}+\omega\right)+a^2\right.$$
$$\left(\omega\left(\left(8\sqrt{1-4a^2}+17\right)\omega+4\mathrm{i}\left(\sqrt{1-4a^2}+2\right)\right)-4\Lambda-4s-4\right)+$$
$$\left.-2\left(\sqrt{1-4a^2}+1\right)\omega(2\omega+\mathrm{i})+\Lambda+s+1\right].$$

It can be seen that everything can be factored in terms of x^n. Since the previous equation is a power series, then its coefficients for each x^n must be zero. This results in two conditions

$$\alpha_0 d_1 + \beta_0 d_0 = 0$$

and

$$\alpha_n d_{n+1} + \beta_n d_n + \gamma_n d_{n-1} = 0 \; n > 1.$$

In order to get the same coefficients as Leaver (1985) we must divide our equations by b^2 resulting in

$$\begin{cases} \alpha_n = n(c_0 + 1) + c_0 + n^2 \\ \beta_n = n(c_1 + 2) + c_3 - 2n^2 \\ \gamma_n = n(c_2 - 3) - c_2 + c_4 + n^2 + 2 \end{cases}$$

where

$$\begin{aligned}
c_0 &= -\frac{2\mathrm{i}}{b}\left(\frac{\omega}{2} - am\right) - s - \mathrm{i}\omega + 1 \\
c_1 &= \frac{4\mathrm{i}}{b}\left(\frac{\omega}{2} - am\right) + 2\mathrm{i}(b+2)\omega - 4 \\
c_2 &= -\frac{2\mathrm{i}}{b}\left(\frac{\omega}{2} - am\right) + s - 3\mathrm{i}\omega + 3 \\
c_3 &= \omega^2\left(-a^2 + 2b + 4\right) + \frac{(4\omega + 2\mathrm{i})}{b}\left(\frac{\omega}{2} - am\right) - 2am\omega + \mathrm{i}(b+2)\omega - A_{\ell,m} - s - 1 \\
c_4 &= -\frac{(4\omega + 2\mathrm{i})}{b}\left(\frac{\omega}{2} - am\right) - \mathrm{i}(2s+3)\omega + s - 2\omega^2 + 1.
\end{aligned}$$

C

Fit data for event GW190521

C.1 Fundamental mode only $\ell = m = 2$ fit

Function parameters	Estimates	Standard Error
$A_{0,2,2}$	$-3.839334 \cdot 10^{127}$	$2.188576 \cdot 10^{-18}$
$\varrho_{0,2,2}$	0.532423	0.009856

Fit properties	
Adjusted R^2	0.734566
AIC	-12167.769000
BIC	-12148.764866
R^2	0.734694

C.2 Fit with $\ell = 2, 3$ and $m = -\ell, \ldots, \ell$

Function parameters	Estimates	Standard Error
$A_{0,2,2}$	$-3.962932 \cdot 10^{128}$	$2.019387 \cdot 10^{-16}$
$\varrho_{0,2,2}$	1.445611	0.008713
$A_{0,2,1}$	$-1.031247 \cdot 10^{130}$	$4.755333 \cdot 10^{-16}$
$\varrho_{0,2,1}$	-0.496468	0.011703
$A_{0,2,0}$	$-7.141702 \cdot 10^{132}$	$1.442403 \cdot 10^{-16}$
$\varrho_{0,2,0}$	-13922.393170	0.010448
$A_{0,2,-1}$	$5.088388 \cdot 10^{135}$	$7.505078 \cdot 10^{-17}$
$\varrho_{0,2,-1}$	$3.261298 \cdot 10^{6}$	0.011732
$A_{0,2,-2}$	$-5.031085 \cdot 10^{137}$	$3.678726 \cdot 10^{-17}$
$\varrho_{0,2,-2}$	$7.083380 \cdot 10^{8}$	0.014539
$A_{0,3,3}$	$-2.013120 \cdot 10^{130}$	$1.226625 \cdot 10^{-17}$
$\varrho_{0,3,3}$	33.139969	0.068196
$A_{0,3,2}$	$4.860586 \cdot 10^{132}$	$2.989783 \cdot 10^{-134}$
$\varrho_{0,3,2}$	-8476.624257	0.036770
$A_{0,3,1}$	$-3.553071 \cdot 10^{135}$	$1.017704 \cdot 10^{-136}$
$\varrho_{0,3,1}$	$3.416991 \cdot 10^{6}$	0.025212
$A_{0,3,0}$	$2.577785 \cdot 10^{138}$	$4.013109 \cdot 10^{-139}$
$\varrho_{0,3,0}$	$3.480170 \cdot 10^{9}$	0.017576
$A_{0,3,-1}$	$5.208828 \cdot 10^{140}$	$1.742343 \cdot 10^{-141}$
$\varrho_{0,3,-1}$	$-7.094043 \cdot 10^{11}$	0.011955
$A_{0,3,-2}$	$1.928109 \cdot 10^{142}$	$1.927743 \cdot 10^{-143}$
$\varrho_{0,3,-2}$	$-2.265400 \cdot 10^{13}$	0.009604
$A_{0,3,-3}$	$1.768381 \cdot 10^{142}$	$1.753499 \cdot 10^{-144}$
$\varrho_{0,3,-3}$	$1.411769 \cdot 10^{14}$	0.079959

Fit properties	
Adjusted R^2	0.994619
AIC	-28386.758562
BIC	-28228.390771
R^2	0.994650

D More numerical results for quasi-normal modes

We list here the quasi-normal modes for both Schwarzschild and Kerr. For the Kerr black hole we list only modes for $\ell = 0, \ldots, 50$, $m = -3, \ldots, 3$.

Table D.1: Scalar quasi-normal modes on Schwarzschild black holes

ℓ	$k=1$		$k=2$		$k=3$	
	$M\omega_R$	$-M\omega_I$	$M\omega_R$	$-M\omega_I$	$M\omega_R$	$-M\omega_I$
0	0.110455	0.104896	0.086089	0.348057	0.075515	0.600756
1	0.292936	0.097660	0.264449	0.306257	0.229539	0.540133
2	0.483644	0.096759	0.463851	0.295604	0.430544	0.508558
3	0.675366	0.096500	0.660671	0.292285	0.633626	0.496008
4	0.867416	0.096392	0.855808	0.290876	0.833692	0.490325
5	1.059612	0.096337	1.050041	0.290154	1.031498	0.487345
6	1.251887	0.096305	1.243752	0.289736	1.227845	0.485602
7	1.444208	0.096285	1.437139	0.289473	1.423235	0.484498
8	1.636560	0.096272	1.630311	0.289297	1.617974	0.483757
9	1.828933	0.096263	1.823334	0.289173	1.812253	0.483235
10	2.021320	0.096256	2.016250	0.289083	2.006196	0.482854
11	2.213719	0.096251	2.209086	0.289015	2.199886	0.482567
12	2.406125	0.096247	2.401861	0.288963	2.393384	0.482347
13	2.598538	0.096244	2.594589	0.288922	2.586729	0.482173

ℓ	$k=1$		$k=2$		$k=3$	
	$M\omega_R$	$-M\omega_I$	$M\omega_R$	$-M\omega_I$	$M\omega_R$	$-M\omega_I$
14	2.790957	0.096241	2.787278	0.288889	2.779953	0.482034
15	2.983379	0.096239	2.979937	0.288863	2.973078	0.481920
16	3.175805	0.096237	3.172570	0.288841	3.166123	0.481827
17	3.368233	0.096236	3.365183	0.288822	3.359101	0.481749
18	3.560664	0.096235	3.557778	0.288807	3.552022	0.481684
19	3.753097	0.096234	3.750359	0.288794	3.744895	0.481628
20	3.945531	0.096233	3.942926	0.288782	3.937728	0.481580
21	4.137967	0.096232	4.135483	0.288773	4.130525	0.481539
22	4.330404	0.096232	4.328030	0.288764	4.323292	0.481503
23	4.522843	0.096231	4.520570	0.288757	4.516031	0.481472
24	4.715282	0.096231	4.713101	0.288750	4.708748	0.481444
25	4.907722	0.096230	4.905627	0.288744	4.901443	0.481419
26	5.100163	0.096230	5.098147	0.288739	5.094120	0.481398
27	5.292604	0.096230	5.290662	0.288735	5.286781	0.481378
28	5.485046	0.096229	5.483172	0.288731	5.479427	0.481361
29	5.677489	0.096229	5.675678	0.288727	5.672059	0.481345
30	5.869932	0.096229	5.868180	0.288724	5.864680	0.481331
31	6.062376	0.096228	6.060680	0.288721	6.057290	0.481318
32	6.254820	0.096228	6.253176	0.288718	6.249890	0.481306
33	6.447264	0.096228	6.445669	0.288715	6.442481	0.481296
34	6.639709	0.096228	6.638160	0.288713	6.635065	0.481286
35	6.832154	0.096228	6.830649	0.288711	6.827640	0.481277
36	7.024599	0.096228	7.023135	0.288709	7.020209	0.481269
37	7.217045	0.096227	7.215620	0.288707	7.212771	0.481261
38	7.409490	0.096227	7.408102	0.288706	7.405328	0.481254
39	7.601936	0.096227	7.600583	0.288704	7.597879	0.481248

ℓ	$k=1$		$k=2$		$k=3$	
	$M\omega_R$	$-M\omega_I$	$M\omega_R$	$-M\omega_I$	$M\omega_R$	$-M\omega_I$
40	7.794383	0.096227	7.793063	0.288703	7.790425	0.481242
41	7.986829	0.096227	7.985541	0.288701	7.982967	0.481236
42	8.179276	0.096227	8.178018	0.288700	8.175504	0.481231
43	8.371722	0.096227	8.370494	0.288699	8.368038	0.481226
44	8.564169	0.096227	8.562968	0.288698	8.560567	0.481222
45	8.756616	0.096227	8.755442	0.288697	8.753093	0.481218
46	8.949063	0.096227	8.947914	0.288696	8.945616	0.481214
47	9.141511	0.096227	9.140385	0.288695	9.138136	0.481210
48	9.333958	0.096226	9.332856	0.288694	9.330653	0.481207
49	9.526405	0.096226	9.525326	0.288694	9.523167	0.481203
50	9.718853	0.096226	9.717795	0.288693	9.715679	0.481200

Table D.2: Gravitational quasi-normal modes on Schwarzschild black holes

ℓ	$k=1$		$k=2$		$k=3$	
	$M\omega_R$	$-M\omega_I$	$M\omega_R$	$-M\omega_I$	$M\omega_R$	$-M\omega_I$
2	0.373672	0.088962	0.346711	0.273915	0.301053	0.478277
3	0.599443	0.092703	0.582644	0.281298	0.551685	0.479093
4	0.809178	0.094164	0.796632	0.284334	0.772710	0.479908
5	1.012295	0.094871	1.002221	0.285817	0.982696	0.480328
6	1.212010	0.095266	1.203574	0.286650	1.187074	0.480564
7	1.409735	0.095510	1.402471	0.287164	1.388182	0.480709
8	1.606194	0.095671	1.599811	0.287504	1.587210	0.480804
9	1.801795	0.095783	1.796101	0.287741	1.784830	0.480870
10	1.996788	0.095864	1.991647	0.287912	1.981453	0.480917
11	2.191334	0.095925	2.186648	0.288040	2.177342	0.480952
12	2.385541	0.095971	2.381236	0.288138	2.372675	0.480979

ℓ	$k=1$		$k=2$		$k=3$	
	$M\omega_R$	$-M\omega_I$	$M\omega_R$	$-M\omega_I$	$M\omega_R$	$-M\omega_I$
13	2.579487	0.096008	2.575504	0.288215	2.567578	0.481001
14	2.773224	0.096037	2.769519	0.288277	2.762141	0.481017
15	2.966795	0.096060	2.963331	0.288327	2.956429	0.481031
16	3.160229	0.096080	3.156976	0.288368	3.150493	0.481042
17	3.353550	0.096096	3.350485	0.288402	3.344372	0.481051
18	3.546776	0.096110	3.543878	0.288431	3.538096	0.481059
19	3.739923	0.096121	3.737174	0.288456	3.731689	0.481066
20	3.933001	0.096131	3.930387	0.288477	3.925170	0.481072
21	4.126021	0.096140	4.123529	0.288495	4.118555	0.481076
22	4.318990	0.096147	4.316609	0.288510	4.311856	0.481081
23	4.511915	0.096154	4.509636	0.288524	4.505085	0.481084
24	4.704801	0.096159	4.702615	0.288536	4.698250	0.481088
25	4.897653	0.096164	4.895553	0.288547	4.891359	0.481091
26	5.090474	0.096169	5.088454	0.288556	5.084418	0.481093
27	5.283268	0.096173	5.281321	0.288565	5.277433	0.481096
28	5.476038	0.096176	5.474160	0.288573	5.470408	0.481098
29	5.668787	0.096180	5.666972	0.288579	5.663347	0.481099
30	5.861515	0.096183	5.859761	0.288586	5.856255	0.481101
31	6.054226	0.096185	6.052527	0.288591	6.049133	0.481103
32	6.246921	0.096188	6.245275	0.288596	6.241985	0.481104
33	6.439602	0.096190	6.438004	0.288601	6.434812	0.481105
34	6.632269	0.096192	6.630718	0.288605	6.627618	0.481106
35	6.824923	0.096194	6.823416	0.288609	6.820404	0.481107
36	7.017567	0.096195	7.016101	0.288613	7.013171	0.481108
37	7.210200	0.096197	7.208773	0.288616	7.205922	0.481109
38	7.402824	0.096198	7.401434	0.288619	7.398657	0.481110

ℓ	$k=1$		$k=2$		$k=3$	
	$M\omega_R$	$-M\omega_I$	$M\omega_R$	$-M\omega_I$	$M\omega_R$	$-M\omega_I$
39	7.595438	0.096200	7.594084	0.288622	7.591377	0.481111
40	7.788045	0.096201	7.786724	0.288624	7.784084	0.481112
41	7.980644	0.096202	7.979355	0.288627	7.976779	0.481112
42	8.173236	0.096203	8.171978	0.288629	8.169462	0.481113
43	8.365822	0.096204	8.364592	0.288631	8.362134	0.481113
44	8.558402	0.096205	8.557200	0.288633	8.554797	0.481114
45	8.750975	0.096206	8.749800	0.288635	8.747450	0.481114
46	8.943544	0.096207	8.942394	0.288637	8.940094	0.481115
47	9.136107	0.096208	9.134981	0.288638	9.132730	0.481115
48	9.328666	0.096208	9.327564	0.288640	9.325359	0.481116
49	9.521221	0.096209	9.520140	0.288641	9.517980	0.481116
50	9.713771	0.096210	9.712712	0.288642	9.710595	0.481116

Table D.3: Scalar quasi-normal modes on Kerr black holes for $a = 0.4M$

ℓ	$m=-3$		$m=-2$		$m=-1$		$m=0$	
	$M\omega_R$	$-M\omega_I$	$M\omega_R$	$-M\omega_I$	$M\omega_R$	$-M\omega_I$	$M\omega_R$	$-M\omega_I$
0	———	———	———	———	———	———	0.11170	0.10325
1	———	———	———	———	0.26690	0.09690	0.29608	0.09626
2	———	———	0.43306	0.09598	0.45932	0.09598	0.48886	0.09547
3	0.60029	0.09571	0.62547	0.09561	0.65285	0.09544	0.68265	0.09523
4	0.79245	0.09554	0.81872	0.09543	0.84678	0.09530	0.87676	0.09513
5	0.98539	0.09543	1.01240	0.09533	1.04091	0.09522	1.07103	0.09508
6	1.17877	0.09536	1.20631	0.09527	1.23516	0.09517	1.26537	0.09505
7	1.37243	0.09530	1.40038	0.09522	1.42947	0.09513	1.45976	0.09504
8	1.56628	0.09526	1.59455	0.09519	1.62383	0.09511	1.65418	0.09502
9	1.76026	0.09523	1.78879	0.09517	1.81823	0.09509	1.84863	0.09502

ℓ	$m=-3$		$m=-2$		$m=-1$		$m=0$	
	$M\omega_R$	$-M\omega_I$	$M\omega_R$	$-M\omega_I$	$M\omega_R$	$-M\omega_I$	$M\omega_R$	$-M\omega_I$
10	1.95435	0.09521	1.98308	0.09515	2.01265	0.09508	2.04308	0.09501
11	2.14850	0.09519	2.17741	0.09513	2.20708	0.09507	2.23755	0.09500
12	2.34271	0.09517	2.37177	0.09512	2.40153	0.09506	2.43203	0.09500
13	2.53697	0.09516	2.56615	0.09511	2.59599	0.09505	2.62651	0.09500
14	2.73126	0.09514	2.76055	0.09510	2.79046	0.09505	2.82100	0.09500
15	2.92558	0.09513	2.95497	0.09509	2.98493	0.09504	3.01550	0.09499
16	3.11992	0.09512	3.14940	0.09508	3.17941	0.09504	3.20999	0.09499
17	3.31428	0.09511	3.34383	0.09508	3.37390	0.09503	3.40449	0.09499
18	3.50866	0.09511	3.53828	0.09507	3.56839	0.09503	3.59900	0.09499
19	3.70306	0.09510	3.73274	0.09506	3.76288	0.09503	3.79350	0.09499
20	3.89746	0.09509	3.92720	0.09506	3.95738	0.09503	3.98801	0.09499
21	4.09188	0.09509	4.12167	0.09506	4.15187	0.09502	4.18251	0.09499
22	4.28631	0.09508	4.31614	0.09505	4.34637	0.09502	4.37702	0.09499
23	4.48074	0.09508	4.51061	0.09505	4.54087	0.09502	4.57153	0.09499
24	4.67518	0.09508	4.70509	0.09505	4.73538	0.09502	4.76604	0.09499
25	4.86963	0.09507	4.89958	0.09504	4.92988	0.09502	4.96055	0.09499
26	5.06408	0.09507	5.09406	0.09504	5.12439	0.09501	5.15505	0.09499
27	5.25854	0.09507	5.28855	0.09504	5.31889	0.09501	5.34960	0.09499
28	5.45300	0.09506	5.48304	0.09504	5.51340	0.09501	5.54410	0.09499
29	5.64746	0.09506	5.67753	0.09504	5.70791	0.09501	5.73860	0.09499
30	5.84193	0.09506	5.87203	0.09503	5.90242	0.09501	5.93310	0.09498
31	6.03641	0.09505	6.06652	0.09503	6.09693	0.09501	6.12765	0.09498
32	6.23088	0.09505	6.26102	0.09503	6.29144	0.09501	6.32215	0.09498
33	6.42536	0.09505	6.45552	0.09503	6.48595	0.09501	6.51665	0.09498
34	6.61984	0.09505	6.65002	0.09503	6.68047	0.09501	6.71120	0.09498
35	6.81432	0.09505	6.84452	0.09503	6.87498	0.09500	6.90570	0.09498

ℓ	$m=-3$		$m=-2$		$m=-1$		$m=0$	
	$M\omega_R$	$-M\omega_I$	$M\omega_R$	$-M\omega_I$	$M\omega_R$	$-M\omega_I$	$M\omega_R$	$-M\omega_I$
36	7.00881	0.09504	7.03902	0.09502	7.06949	0.09500	7.10020	0.09498
37	7.20330	0.09504	7.23353	0.09502	7.26401	0.09500	7.29475	0.09498
38	7.39779	0.09504	7.42803	0.09502	7.45852	0.09500	7.48925	0.09498
39	7.59228	0.09504	7.62254	0.09502	7.65303	0.09500	7.68375	0.09498
40	7.78677	0.09504	7.81705	0.09502	7.84755	0.09500	7.87830	0.09498
41	7.98126	0.09504	8.01155	0.09502	8.04206	0.09500	8.07280	0.09498
42	8.17576	0.09504	8.20606	0.09502	8.23658	0.09500	8.26730	0.09498
43	8.37025	0.09503	8.40057	0.09502	8.43110	0.09500	8.46185	0.09498
44	8.56475	0.09503	8.59508	0.09502	8.62561	0.09500	8.65635	0.09498
45	8.75925	0.09503	8.78959	0.09502	8.82013	0.09500	8.85085	0.09498
46	8.95375	0.09503	8.98410	0.09501	9.01464	0.09500	9.04540	0.09498
47	9.14825	0.09503	9.17861	0.09501	9.20916	0.09500	9.23990	0.09498
48	9.34275	0.09503	9.37312	0.09501	9.40368	0.09500	9.43445	0.09498
49	9.53725	0.09503	9.56763	0.09501	9.59820	0.09500	9.62895	0.09498
50	9.73175	0.09503	9.76214	0.09501	9.79271	0.09500	9.82345	0.09498

Table D.4: Scalar quasi-normal modes on Kerr black holes for $a = 0.4M$

ℓ	$m=1$		$m=2$		$m=3$	
	$M\omega_R$	$-M\omega_I$	$M\omega_R$	$-M\omega_I$	$M\omega_R$	$-M\omega_I$
0	———	———	———	———	———	———
1	0.33157	0.09579	———	———	———	———
2	0.52214	0.09515	0.55965	0.09493	———	———
3	0.71512	0.09501	0.75052	0.09481	0.78909	0.09468
4	0.90883	0.09496	0.94313	0.09479	0.97981	0.09466
5	1.10284	0.09494	1.13647	0.09480	1.17200	0.09468
6	1.29702	0.09494	1.33019	0.09482	1.36495	0.09471

ℓ	$m=1$		$m=2$		$m=3$	
	$M\omega_R$	$-M\omega_I$	$M\omega_R$	$-M\omega_I$	$M\omega_R$	$-M\omega_I$
7	1.49129	0.09493	1.52414	0.09483	1.55834	0.09473
8	1.68563	0.09493	1.71822	0.09484	1.75201	0.09475
9	1.88000	0.09494	1.91241	0.09485	1.94587	0.09477
10	2.07441	0.09494	2.10666	0.09486	2.13986	0.09479
11	2.26883	0.09494	2.30095	0.09487	2.33394	0.09481
12	2.46327	0.09494	2.49529	0.09488	2.52810	0.09482
13	2.65773	0.09494	2.68965	0.09489	2.72231	0.09483
14	2.85219	0.09494	2.88404	0.09489	2.91657	0.09484
15	3.04666	0.09495	3.07844	0.09490	3.11086	0.09485
16	3.24114	0.09495	3.27286	0.09490	3.30518	0.09485
17	3.43562	0.09495	3.46729	0.09490	3.49952	0.09486
18	3.63010	0.09495	3.66173	0.09491	3.69389	0.09487
19	3.82459	0.09495	3.85618	0.09491	3.88827	0.09487
20	4.01909	0.09495	4.05064	0.09491	4.08266	0.09488
21	4.21358	0.09495	4.24510	0.09492	4.27707	0.09488
22	4.40808	0.09495	4.43957	0.09492	4.47148	0.09489
23	4.60258	0.09496	4.63404	0.09492	4.66591	0.09489
24	4.79708	0.09496	4.82852	0.09492	4.86034	0.09489
25	4.99159	0.09496	5.02300	0.09493	5.05480	0.09490
26	5.18609	0.09496	5.21748	0.09493	5.24925	0.09490
27	5.38060	0.09496	5.41197	0.09493	5.44370	0.09490
28	5.57511	0.09496	5.60645	0.09493	5.63815	0.09491
29	5.76961	0.09496	5.80095	0.09493	5.83260	0.09491
30	5.96412	0.09496	5.99544	0.09494	6.02705	0.09491
31	6.15863	0.09496	6.18993	0.09494	6.22155	0.09491
32	6.35314	0.09496	6.38443	0.09494	6.41600	0.09491

ℓ	$m=1$		$m=2$		$m=3$	
	$M\omega_R$	$-M\omega_I$	$M\omega_R$	$-M\omega_I$	$M\omega_R$	$-M\omega_I$
33	6.54765	0.09496	6.57893	0.09494	6.61050	0.09492
34	6.74217	0.09496	6.77343	0.09494	6.80495	0.09492
35	6.93668	0.09496	6.96793	0.09494	6.99945	0.09492
36	7.13119	0.09496	7.16243	0.09494	7.19395	0.09492
37	7.32571	0.09496	7.35693	0.09494	7.38840	0.09492
38	7.52022	0.09496	7.55144	0.09494	7.58290	0.09492
39	7.71473	0.09496	7.74594	0.09495	7.77740	0.09493
40	7.90925	0.09496	7.94045	0.09495	7.97190	0.09493
41	8.10376	0.09497	8.13495	0.09495	8.16635	0.09493
42	8.29828	0.09497	8.32946	0.09495	8.36085	0.09493
43	8.49279	0.09497	8.52397	0.09495	8.55535	0.09493
44	8.68731	0.09497	8.71848	0.09495	8.74985	0.09493
45	8.88183	0.09497	8.91299	0.09495	8.94435	0.09493
46	9.07634	0.09497	9.10749	0.09495	9.13885	0.09493
47	9.27086	0.09497	9.30201	0.09495	9.33335	0.09494
48	9.46538	0.09497	9.49652	0.09495	9.52785	0.09494
49	9.65989	0.09497	9.69103	0.09495	9.72235	0.09494
50	9.85441	0.09497	9.88554	0.09495	9.91685	0.09494

Table D.5: Gravitational quasi-normal modes on Kerr black holes for $a = 0.4M$

ℓ	$m=-3$		$m=-2$		$m=-1$		$m=0$	
	$M\omega_R$	$-M\omega_I$	$M\omega_R$	$-M\omega_I$	$M\omega_R$	$-M\omega_I$	$M\omega_R$	$-M\omega_I$
2	———	———	0.33246	0.08913	0.35463	0.08848	0.37968	0.08783
3	0.53233	0.09265	0.55529	0.09235	0.58024	0.09197	0.60737	0.09154
4	0.73946	0.09370	0.76429	0.09350	0.79078	0.09326	0.81907	0.09298
5	0.94179	0.09420	0.96779	0.09405	0.99522	0.09387	1.02418	0.09367

ℓ	$m=-3$		$m=-2$		$m=-1$		$m=0$	
	$M\omega_R$	$-M\omega_I$	$M\omega_R$	$-M\omega_I$	$M\omega_R$	$-M\omega_I$	$M\omega_R$	$-M\omega_I$
6	1.14168	0.09447	1.16848	0.09435	1.19653	0.09421	1.22590	0.09405
7	1.34013	0.09463	1.36751	0.09453	1.39600	0.09441	1.42565	0.09429
8	1.53767	0.09474	1.56548	0.09465	1.59429	0.09455	1.62414	0.09445
9	1.73457	0.09481	1.76273	0.09473	1.79179	0.09465	1.82178	0.09455
10	1.93103	0.09486	1.95946	0.09479	1.98871	0.09471	2.01881	0.09463
11	2.12716	0.09490	2.15581	0.09483	2.18522	0.09476	2.21541	0.09469
12	2.32303	0.09492	2.35187	0.09486	2.38141	0.09480	2.41167	0.09474
13	2.51871	0.09494	2.54770	0.09489	2.57735	0.09483	2.60767	0.09477
14	2.71423	0.09496	2.74336	0.09491	2.77310	0.09485	2.80346	0.09480
15	2.90962	0.09497	2.93887	0.09492	2.96869	0.09487	2.99909	0.09482
16	3.10491	0.09498	3.13426	0.09493	3.16415	0.09489	3.19459	0.09484
17	3.30012	0.09499	3.32955	0.09494	3.35950	0.09490	3.38997	0.09486
18	3.49525	0.09499	3.52476	0.09495	3.55476	0.09491	3.58526	0.09487
19	3.69032	0.09500	3.71990	0.09496	3.74995	0.09492	3.78047	0.09488
20	3.88533	0.09500	3.91498	0.09497	3.94507	0.09493	3.97561	0.09489
21	4.08030	0.09500	4.11001	0.09497	4.14014	0.09493	4.17070	0.09490
22	4.27524	0.09501	4.30500	0.09497	4.33516	0.09494	4.36573	0.09491
23	4.47013	0.09501	4.49994	0.09498	4.53014	0.09495	4.56072	0.09491
24	4.66500	0.09501	4.69485	0.09498	4.72508	0.09495	4.75568	0.09492
25	4.85984	0.09501	4.88973	0.09498	4.91998	0.09495	4.95059	0.09492
26	5.05465	0.09501	5.08460	0.09498	5.11485	0.09496	5.14550	0.09493
27	5.24945	0.09501	5.27940	0.09499	5.30970	0.09496	5.34035	0.09493
28	5.44425	0.09501	5.47420	0.09499	5.50455	0.09496	5.53520	0.09493
29	5.63900	0.09501	5.66900	0.09499	5.69935	0.09496	5.73000	0.09494
30	5.83375	0.09501	5.86380	0.09499	5.89415	0.09497	5.92480	0.09494
31	6.02845	0.09501	6.05855	0.09499	6.08890	0.09497	6.11955	0.09494

ℓ	$m=-3$		$m=-2$		$m=-1$		$m=0$	
	$M\omega_R$	$-M\omega_I$	$M\omega_R$	$-M\omega_I$	$M\omega_R$	$-M\omega_I$	$M\omega_R$	$-M\omega_I$
32	6.22320	0.09501	6.25330	0.09499	6.28365	0.09497	6.31435	0.09495
33	6.41790	0.09501	6.44800	0.09499	6.47840	0.09497	6.50910	0.09495
34	6.61260	0.09501	6.64270	0.09499	6.67315	0.09497	6.70380	0.09495
35	6.80725	0.09501	6.83745	0.09499	6.86785	0.09497	6.89855	0.09495
36	7.00195	0.09501	7.03215	0.09499	7.06255	0.09497	7.09325	0.09495
37	7.19660	0.09501	7.22680	0.09499	7.25725	0.09497	7.28795	0.09495
38	7.39125	0.09501	7.42150	0.09499	7.45195	0.09498	7.48265	0.09496
39	7.58590	0.09501	7.61615	0.09499	7.64665	0.09498	7.67735	0.09496
40	7.78055	0.09501	7.81080	0.09500	7.84130	0.09498	7.87200	0.09496
41	7.97520	0.09501	8.00550	0.09500	8.03595	0.09498	8.06670	0.09496
42	8.16985	0.09501	8.20015	0.09500	8.23065	0.09498	8.26135	0.09496
43	8.36450	0.09501	8.39475	0.09500	8.42530	0.09498	8.45600	0.09496
44	8.55910	0.09501	8.58940	0.09500	8.61995	0.09498	8.65065	0.09496
45	8.75370	0.09501	8.78405	0.09500	8.81455	0.09498	8.84530	0.09496
46	8.94835	0.09501	8.97865	0.09500	9.00920	0.09498	9.03995	0.09496
47	9.14295	0.09501	9.17330	0.09500	9.20385	0.09498	9.23455	0.09496
48	9.33755	0.09501	9.36790	0.09500	9.39845	0.09498	9.42920	0.09497
49	9.53215	0.09501	9.56255	0.09500	9.59310	0.09498	9.62380	0.09497
50	9.72675	0.09501	9.75715	0.09500	9.78770	0.09498	9.81845	0.09497

Table D.6: Gravitational quasi-normal modes on Kerr black holes for $a = 0.4M$

ℓ	$m=1$		$m=2$		$m=3$	
	$M\omega_R$	$-M\omega_I$	$M\omega_R$	$-M\omega_I$	$M\omega_R$	$-M\omega_I$
2	0.40798	0.08726	0.43984	0.08688	———	———
3	0.63687	0.09107	0.66892	0.09062	0.70365	0.09022
4	0.84928	0.09268	0.88152	0.09237	0.91590	0.09208

ℓ	$m=1$		$m=2$		$m=3$	
	$M\omega_R$	$-M\omega_I$	$M\omega_R$	$-M\omega_I$	$M\omega_R$	$-M\omega_I$
5	1.05474	0.09346	1.08699	0.09324	1.12102	0.09303
6	1.25665	0.09389	1.28885	0.09373	1.32255	0.09356
7	1.45650	0.09416	1.48862	0.09403	1.52205	0.09389
8	1.65506	0.09434	1.68709	0.09422	1.72028	0.09411
9	1.85273	0.09446	1.88469	0.09436	1.91768	0.09427
10	2.04979	0.09455	2.08168	0.09447	2.11450	0.09438
11	2.24640	0.09462	2.27822	0.09454	2.31089	0.09447
12	2.44267	0.09467	2.47443	0.09460	2.50697	0.09453
13	2.63867	0.09471	2.67038	0.09465	2.70281	0.09459
14	2.83447	0.09474	2.86613	0.09469	2.89846	0.09463
15	3.03010	0.09477	3.06172	0.09472	3.09396	0.09466
16	3.22559	0.09479	3.25717	0.09474	3.28934	0.09469
17	3.42097	0.09481	3.45252	0.09477	3.48462	0.09472
18	3.61626	0.09483	3.64777	0.09478	3.67981	0.09474
19	3.81147	0.09484	3.84295	0.09480	3.87493	0.09476
20	4.00661	0.09485	4.03806	0.09481	4.06999	0.09478
21	4.20169	0.09486	4.23312	0.09483	4.26500	0.09479
22	4.39672	0.09487	4.42813	0.09484	4.45997	0.09480
23	4.59171	0.09488	4.62310	0.09485	4.65489	0.09481
24	4.78666	0.09489	4.81803	0.09485	4.84979	0.09482
25	4.98157	0.09489	5.01290	0.09486	5.04465	0.09483
26	5.17645	0.09490	5.20780	0.09487	5.23950	0.09484
27	5.37130	0.09490	5.40265	0.09487	5.43430	0.09485
28	5.56615	0.09491	5.59745	0.09488	5.62910	0.09485
29	5.76095	0.09491	5.79225	0.09489	5.82385	0.09486
30	5.95575	0.09492	5.98705	0.09489	6.01860	0.09486

ℓ	$m=1$		$m=2$		$m=3$	
	$M\omega_R$	$-M\omega_I$	$M\omega_R$	$-M\omega_I$	$M\omega_R$	$-M\omega_I$
31	6.15055	0.09492	6.18180	0.09489	6.21335	0.09487
32	6.34530	0.09492	6.37655	0.09490	6.40810	0.09487
33	6.54005	0.09492	6.57130	0.09490	6.60280	0.09488
34	6.73480	0.09493	6.76600	0.09491	6.79750	0.09488
35	6.92950	0.09493	6.96070	0.09491	6.99220	0.09489
36	7.12420	0.09493	7.15540	0.09491	7.18690	0.09489
37	7.31890	0.09493	7.35010	0.09491	7.38155	0.09489
38	7.51360	0.09494	7.54480	0.09492	7.57625	0.09490
39	7.70830	0.09494	7.73945	0.09492	7.77090	0.09490
40	7.90295	0.09494	7.93415	0.09492	7.96555	0.09490
41	8.09760	0.09494	8.12880	0.09492	8.16020	0.09490
42	8.29230	0.09494	8.32345	0.09492	8.35485	0.09491
43	8.48695	0.09494	8.51810	0.09493	8.54945	0.09491
44	8.68160	0.09495	8.71275	0.09493	8.74410	0.09491
45	8.87625	0.09495	8.90735	0.09493	8.93870	0.09491
46	9.07085	0.09495	9.10200	0.09493	9.13335	0.09491
47	9.26550	0.09495	9.29665	0.09493	9.32795	0.09492
48	9.46015	0.09495	9.49125	0.09493	9.52255	0.09492
49	9.65475	0.09495	9.68585	0.09494	9.71720	0.09492
50	9.84935	0.09495	9.88050	0.09494	9.91180	0.09492

E Scripts for numerical computations

All of our previous numerical results were obtained using the following scripts in Mathematica 12.3. In order to find all the roots in a certain range at once we used the function `FindRoots2D` found in Wagon (2010). In order to obtain the gravitational quasi-normal modes for the Kerr black hole we used a Mathematica package `SpinWeightedSpheroidalHarmonics` from the *Black Hole Perturbation Kit*. Sometimes further refinement with the `FindRoot` function is needed to obtain missing frequency values. Some of these calculations might take more than 6 hours even on a modern desktop computer.

E.1 Numerical results up to $\ell = 50$ for quasi-normal modes for scalar fields on Schwarzschild black holes

```
FindRoots2D::usage = "FindRoots2D[funcs,{x,a,b},{y,c,d}] finds all \
nontangential solutions to\n   {f=0, g=0} in the given rectangle.";
Options[FindRoots2D] = {PlotPoints -> Automatic,
   MaxRecursion -> Automatic};
FindRoots2D[funcs_, {x_, a_, b_}, {y_, c_, d_}, opts___] :=
   Module[{fZero, seeds, signs, fy},
     fy = Compile[{x, y}, Evaluate[funcs[[2]]]];
      fZero =
   Cases[Normal[ContourPlot[funcs[[1]] == 0, {x, a - (b - a)/97,
               b + (b - a)/103}, {y, c - (d - c)/98,
       d + (d - c)/102},
              Evaluate[FilterRules[{opts}, Options[ContourPlot]]]]],
          Line[z_] :> z, Infinity];
      seeds = Flatten[((signs = Sign[Apply[fy, #1, {1}]];
                 #1[[1 +
           Flatten[Position[Rest[signs*RotateRight[signs]],
```

```
                          -1]]]]) & ) /@ fZero, 1];
  If[seeds == {}, {},
        Select[Union[({x, y} /. FindRoot[{funcs[[1]], funcs[[2]]},
                     {x, #1[[1]]}, {y, #1[[2]]},
          Evaluate[FilterRules[{opts},
                        Options[FindRoot]]]] & ) /@ seeds,
            SameTest -> (Norm[#1 - #2] < 10^(-6) & )],
          a <= #1[[1]] <= b && c <= #1[[2]] <= d & ]]]

α[n_, ω_, l_] := (1 + n)*(1 + n - 4*I*ω);
β[n_, ω_, l_] := -1 - l - l^2 - 2*n^2 + 8*I*ω +
   32*ω^2 +
       n*(-2 + 16*I*ω);
γ[n_, ω_, l_] := (n - 4*I*ω)^2;
b0[ω_, l_] := -1 - l - l^2 + 8*I*ω + 32*ω^2;
a0[ω_, l_] := 1 - 4*I*ω;
F[ω_, l_] :=
  b0[ω, l]/a0[ω, l] - ContinuedFractionK[
         (-α[i - 1, ω, l])^(1 -
        KroneckerDelta[1, i])*γ[i, ω, l],
          β[i, ω, l], {i, 1, 200}];
R[ω_, l_] := Re[F[ω, l]];
Imag[ω_, l_] := Im[F[ω, l]];

ClearSystemCache[]
f[l_, a_] := FindRoots2D[{R[x + I*y, l], Imag[x + I*y, l]},
       {x, 0 + a*0.5, 1 + a}, {y, -0.6, -0.05}, MaxRecursion -> 5];
mytable = Table[{j, f[j, 0.25*(j - 1)]}, {j, 0, 50, 1}];
TableForm[mytable]
Export["out.csv", mytable]
```

E.2 Numerical results up to $\ell = 50$ for gravitational quasi-normal modes on Schwarzschild black holes

```
FindRoots2D::usage = "FindRoots2D[funcs,{x,a,b},{y,c,d}] finds all
 ↪  nontangential solutions to\n   {f=0, g=0} in the given
 ↪  rectangle.";
Options[FindRoots2D] = {PlotPoints -> Automatic, MaxRecursion ->
 ↪  Automatic};
```

```
FindRoots2D[funcs_, {x_, a_, b_}, {y_, c_, d_}, opts___] :=
 ↪  Module[{fZero, seeds, signs, fy}, fy = Compile[{x, y},
 ↪  Evaluate[funcs[[2]]]];
    fZero = Cases[Normal[ContourPlot[funcs[[1]] == 0, {x, a - (b -
 ↪  a)/97, b + (b - a)/103}, {y, c - (d - c)/98, d + (d - c)/102},
        Evaluate[FilterRules[{opts}, Options[ContourPlot]]]]],
 ↪  Line[z_] :> z, Infinity];
    seeds = Flatten[((signs = Sign[Apply[fy, #1, {1}]]; #1[[1 +
 ↪  Flatten[Position[Rest[signs*RotateRight[signs]], -1]]]) & ) /@
 ↪  fZero, 1];
    If[seeds == {}, {}, Select[Union[({x, y} /. FindRoot[{funcs[[1]],
 ↪  funcs[[2]]}, {x, #1[[1]]}, {y, #1[[2]]},
           Evaluate[FilterRules[{opts}, Options[FindRoot]]]] & ) /@
 ↪  seeds, SameTest -> (Norm[#1 - #2] < 10^(-6) & )], a <= #1[[1]] <=
 ↪  b && c <= #1[[2]] <= d & ]]]
α[n_, ω_, l_] := (1 + n)*(1 + n - 4*I*ω);
β[n_, ω_, l_] := -l - l^2 + 3 + 8*I*ω + 32*ω^2 - 2*n^2 + n*(-2 +
 ↪  16*I*ω);
γ[n_, ω_, l_] := -1 + n^2 - 3 - 8*I*n*ω - 16*ω^2;
b0[ω_, l_] := -l - l^2 + 3 + 8*I*ω + 32*ω^2;
a0[ω_, l_] := 1 - 4*I*ω;
F[ω_, l_] := b0[ω, l]/a0[ω, l] - ContinuedFractionK[(-α[i - 1, ω,
 ↪  l])^(1 - KroneckerDelta[1, i])*γ[i, ω, l], β[i, ω, l], {i, 1,
 ↪  200}];
R[ω_, l_] := Re[F[ω, l]];
Imag[ω_, l_] := Im[F[ω, l]];
ClearSystemCache[]
f[l_, a_] := FindRoots2D[{R[x + I*y, l], Imag[x + I*y, l]}, {x, 0 +
 ↪  a*0.5, 1 + a}, {y, -0.6, -0.05}];
mytable = Table[{j, f[j, 0.25*(j - 1)]}, {j, 2, 50, 1}];
TableForm[mytable]
Export["out.csv", mytable]
```

E.3 Numerical results for scalar quasi-bound modes on Kerr

```
FindRoots2D::usage =
  "FindRoots2D[funcs,{x,a,b},{y,c,d}] finds all nontangential \
solutions to
   {f=0, g=0} in the given rectangle.";
```

```
Options[FindRoots2D] = {PlotPoints -> Automatic,
   MaxRecursion -> Automatic};

FindRoots2D[funcs_, {x_, a_, b_}, {y_, c_, d_}, opts___] :=
 Module[{fZero, seeds, signs, fy},
  fy = Compile[{x, y}, Evaluate[funcs[[2]]]];
  fZero =
   Cases[Normal[
     ContourPlot[
      funcs[[1]] == 0, {x, a - (b - a)/97, b + (b - a)/103}, {y,
       c - (d - c)/98, d + (d - c)/102},
      Evaluate[FilterRules[{opts}, Options[ContourPlot]]]]],
    Line[z_] :> z, Infinity];
  seeds = Flatten[((signs = Sign[Apply[fy, #1, {1}]];
        #1[[
         1 + Flatten[
           Position[Rest[signs*RotateRight[signs]], -1]]]]) &) /@
     fZero, 1];
  If[seeds == {}, {}, Select[Union[({x, y} /.
         FindRoot[{funcs[[1]],
           funcs[[2]]}, {x, #1[[1]]}, {y, #1[[2]]},
          Evaluate[FilterRules[{opts}, Options[FindRoot]]]] &) /@
      seeds, SameTest -> (Norm[#1 - #2] < 10^(-6) &)],
    a <= #1[[1]] <= b && c <= #1[[2]] <= d &]]]

b = Sqrt[1 - a^2];
\[Alpha]r[n_, \[Omega]_, l_, m_, \[Mu]_] :=
  1 + (I a m)/b + 2 n + (I a m n)/b + n^2 - 2 I \[Omega] - (
   2 I \[Omega])/b - 2 I n \[Omega] - (2 I n \[Omega])/b;

\[Beta]r[n_, \[Omega]_, l_, m_, \[Mu]_] := -1 - (I a m)/b - 2 n - (
   2 I a m n)/b -
   2 n^2 - (SpheroidalEigenvalue[l,
      m, \[Sqrt](a^2 (\[Mu]^2 - \[Omega]^2))] +
     a^2 (\[Mu]^2 - \[Omega]^2)) - \[Mu]^2 - 2 b \[Mu]^2 -
   b^2 \[Mu]^2 + 2 I \[Omega] + (2 I \[Omega])/b - (2 a m \[Omega])/
   b + 4 I n \[Omega] + (4 I n \[Omega])/b + 7 \[Omega]^2 + (
   4 \[Omega]^2)/b + 4 b \[Omega]^2 + b^2 \[Omega]^2 - \[Mu]^2/
   Sqrt[\[Mu]^2 - \[Omega]^2] - (I a m \[Mu]^2)/(
   b Sqrt[\[Mu]^2 - \[Omega]^2]) + (2 n \[Mu]^2)/
```

```
   Sqrt[\[Mu]^2 - \[Omega]^2] + (6 I \[Mu]^2 \[Omega])/
   Sqrt[\[Mu]^2 - \[Omega]^2] + (2 I \[Mu]^2 \[Omega])/(
   b Sqrt[\[Mu]^2 - \[Omega]^2]) + (2 \[Omega]^2)/
   Sqrt[\[Mu]^2 - \[Omega]^2] + (2 I a m \[Omega]^2)/(
   b Sqrt[\[Mu]^2 - \[Omega]^2]) - (8 I \[Omega]^3)/
   Sqrt[\[Mu]^2 - \[Omega]^2] - (4 I \[Omega]^3)/(
   b Sqrt[\[Mu]^2 - \[Omega]^2]) - 2 b Sqrt[\[Mu]^2 - \[Omega]^2] -
   2 I a m Sqrt[\[Mu]^2 - \[Omega]^2] -
   4 n Sqrt[\[Mu]^2 - \[Omega]^2] -
   4 b n Sqrt[\[Mu]^2 - \[Omega]^2] +
   4 I b \[Omega] Sqrt[\[Mu]^2 - \[Omega]^2];

\[Gamma]r[n_, \[Omega]_, l_, m_, \[Mu]_] :=
  1/(b Sqrt[\[Mu]^2 - \[Omega]^2] (-\[Mu]^2 + \[Omega]^2)) (-I a m \
\[Mu]^4 - 2 b n \[Mu]^4 + 2 I \[Mu]^4 \[Omega] +
     2 I b \[Mu]^4 \[Omega] + 3 I a m \[Mu]^2 \[Omega]^2 +
     6 b n \[Mu]^2 \[Omega]^2 - 6 I \[Mu]^2 \[Omega]^3 -
     6 I b \[Mu]^2 \[Omega]^3 - 2 I a m \[Omega]^4 -
     4 b n \[Omega]^4 + 4 I \[Omega]^5 + 4 I b \[Omega]^5 -
     I a m n \[Mu]^2 Sqrt[\[Mu]^2 - \[Omega]^2] -
     b n^2 \[Mu]^2 Sqrt[\[Mu]^2 - \[Omega]^2] -
     b \[Mu]^4 Sqrt[\[Mu]^2 - \[Omega]^2] -
     2 a m \[Mu]^2 \[Omega] Sqrt[\[Mu]^2 - \[Omega]^2] +
     2 I n \[Mu]^2 \[Omega] Sqrt[\[Mu]^2 - \[Omega]^2] +
     2 I b n \[Mu]^2 \[Omega] Sqrt[\[Mu]^2 - \[Omega]^2] +
     I a m n \[Omega]^2 Sqrt[\[Mu]^2 - \[Omega]^2] +
     b n^2 \[Omega]^2 Sqrt[\[Mu]^2 - \[Omega]^2] +
     4 \[Mu]^2 \[Omega]^2 Sqrt[\[Mu]^2 - \[Omega]^2] +
     4 b \[Mu]^2 \[Omega]^2 Sqrt[\[Mu]^2 - \[Omega]^2] +
     2 a m \[Omega]^3 Sqrt[\[Mu]^2 - \[Omega]^2] -
     2 I n \[Omega]^3 Sqrt[\[Mu]^2 - \[Omega]^2] -
     2 I b n \[Omega]^3 Sqrt[\[Mu]^2 - \[Omega]^2] -
     4 \[Omega]^4 Sqrt[\[Mu]^2 - \[Omega]^2] -
     4 b \[Omega]^4 Sqrt[\[Mu]^2 - \[Omega]^2]);


Fr[\[Omega]_, l_,
   m_, \[Mu]_] := \[Beta]r[0, \[Omega], l, m, \[Mu]]/\[Alpha]r[
     0, \[Omega], l, m, \[Mu]] -
   ContinuedFractionK[(-\[Alpha]r[i - 1, \[Omega], l, m, \[Mu]])^(
```

```
     1 - KroneckerDelta[1, i])*\[Gamma]r[i, \[Omega], l,
      m, \[Mu]], \[Beta]r[i, \[Omega], l, m, \[Mu]], {i, 1, 200}];
Rr[\[Omega]_, l_, m_, \[Mu]_] := Re[Fr[\[Omega], l, m, \[Mu]]];
Imagr[\[Omega]_, l_, m_, \[Mu]_] := Im[Fr[\[Omega], l, m, \[Mu]]];

(*User must give a value to a (dimensionalized spin parameter)*)
TableForm[
 ParallelTable[
  FindRoots2D[{Rr[x + I y, l, 0, \[Mu]],
    Imagr[x + I y, l, 0, \[Mu]]}, {x, \[Mu] - 0.1, \[Mu] +
     0.01}, {y, -0.1, 0.1}, MaxRecursion -> 5], {\[Mu], 0.1, 0.8,
   0.1}, {l, 0, 3}]]

(*user must specify l,m*)
TableForm[
 ParallelTable[
  FindRoots2D[{Rr[x + I y, 2, 2, \[Mu]],
    Imagr[x + I y, 2, 2, \[Mu]]}, {x, \[Mu] - 0.1, \[Mu] +
     0.01}, {y, -0.1, 0.1},
   MaxRecursion -> 5], {a, {0.2, 0.4, 0.6, 0.8, 0.9, 0.99}}, {\[Mu],
   0.1, 0.8, 0.1}]]
```

E.4 Numerical results for scalar quasi-normal modes on Kerr

The following code is in Leaver units, where $2M = 1$. All frequencies must be divided by two to obtain results in geometric units.

```
FindRoots2D::usage =
  "FindRoots2D[funcs,{x,a,b},{y,c,d}] finds all nontangential \
solutions to
   {f=0, g=0} in the given rectangle.";

Options[FindRoots2D] = {PlotPoints -> Automatic,
   MaxRecursion -> Automatic};

FindRoots2D[funcs_, {x_, a_, b_}, {y_, c_, d_}, opts___] :=
 Module[{fZero, seeds, signs, fy},
  fy = Compile[{x, y}, Evaluate[funcs[[2]]]];
  fZero =
   Cases[Normal[
```

```
    ContourPlot[
     funcs[[1]] == 0, {x, a - (b - a)/97, b + (b - a)/103}, {y,
      c - (d - c)/98, d + (d - c)/102},
     Evaluate[FilterRules[{opts}, Options[ContourPlot]]]]],
   Line[z_] :> z, Infinity];
 seeds = Flatten[((signs = Sign[Apply[fy, #1, {1}]];
      #1[[
       1 + Flatten[
         Position[Rest[signs*RotateRight[signs]], -1]]]]) &) /@
    fZero, 1];
 If[seeds == {}, {}, Select[Union[({x, y} /.
       FindRoot[{funcs[[1]],
         funcs[[2]]}, {x, #1[[1]]}, {y, #1[[2]]},
        Evaluate[FilterRules[{opts}, Options[FindRoot]]]] &) /@
     seeds, SameTest -> (Norm[#1 - #2] < 10^(-6) &)],
   a <= #1[[1]] <= b && c <= #1[[2]] <= d &]]]

\[Alpha]r[n_, \[Omega]_, l_,
  m_] := ((1 + n) (Sqrt[1 - 4 a^2] + 2 I a m +
    Sqrt[1 - 4 a^2] (n - I \[Omega]) - I \[Omega]))/Sqrt[1 - 4 a^2];

\[Beta]r[n_, \[Omega]_, l_, m_] := -1 -
  2 n - (SpheroidalEigenvalue[l, m, Sqrt[-a^2 \[Omega]^2]] -
    a^2 \[Omega]^2) + 2 I \[Omega] +
  1/Sqrt[1 -
    4 a^2] (-2 Sqrt[1 - 4 a^2] n^2 +
     4 I (1 + Sqrt[1 - 4 a^2]) n \[Omega] +
     2 \[Omega] (I + 2 (1 + Sqrt[1 - 4 a^2]) \[Omega]) +
     2 a m (-I - 2 I n - (2 + Sqrt[1 - 4 a^2]) \[Omega]) -
     a^2 \[Omega] (4 I + 8 I n + (8 + Sqrt[1 - 4 a^2]) \[Omega]));

\[Gamma]r[n_, \[Omega]_, l_,
 m_] := ((2 I a m + Sqrt[1 - 4 a^2] (n - I \[Omega]) -
   I \[Omega]) (n - 2 I \[Omega]))/Sqrt[1 - 4 a^2]


Fr[\[Omega]_, l_,
  m_] := \[Beta]r[0, \[Omega], l, m]/\[Alpha]r[0, \[Omega], l, m] -
  ContinuedFractionK[(-\[Alpha]r[i - 1, \[Omega], l, m])^(
    1 - KroneckerDelta[1, i])*\[Gamma]r[i, \[Omega], l, m],
↪  \[Beta]r[
```

```
     i, \[Omega], l, m], {i, 1, 200}];
Rr[\[Omega]_, l_, m_] := Re[Fr[\[Omega], l, m]];
Imagr[\[Omega]_, l_, m_] := Im[Fr[\[Omega], l, m]];

(*To look for overtones*)

(*User must give a value to a in Leaver's units*)
TableForm[
 ParallelTable[
  FindRoots2D[{Rr[x + I y, i, m], Imagr[x + I y, i, m]}, {x, 0,
    3}, {y, -2, -0.05}, MaxRecursion -> 3 ], {i, 0, 6}, {m, -i, i}]]

(*Fundamental frequencies only*)

(*Replace m with the azimuthal ang. mom. number. Change domain if \
necessary*)
ParallelTable[
 FindRoots2D[{Rr[x + I y, l, m], Imagr[x + I y, l, m]}, {x, 0,
   25}, {y, -0.23, -0.15}, MaxRecursion -> 3], {l, 2, 50}]

(*Choose a value for l and m*)
ParallelTable[
 FindRoots2D[{Rr[x + I y, l, m], Imagr[x + I y, l, m]}, {x, 0,
   10}, {y, -0.21, 0}], {a, {0, 0.1, 0.2, 0.3, 0.4, 0.45, 0.495}}]
```

E.5 Numerical results for gravitational quasi-normal modes on Kerr

The following code is in Leaver units, where $2M = 1$. All frequencies must be divided by two to obtain results in geometric units. Some of these calculations might take a very long time.

```
FindRoots2D::usage =
  "FindRoots2D[funcs,{x,a,b},{y,c,d}] finds all nontangential \
solutions to
   {f=0, g=0} in the given rectangle.";

Options[FindRoots2D] = {PlotPoints -> Automatic,
   MaxRecursion -> Automatic};

FindRoots2D[funcs_, {x_, a_, b_}, {y_, c_, d_}, opts___] :=
```

```
 Module[{fZero, seeds, signs, fy},
  fy = Compile[{x, y}, Evaluate[funcs[[2]]]];
  fZero =
   Cases[Normal[
     ContourPlot[
      funcs[[1]] == 0, {x, a - (b - a)/97, b + (b - a)/103}, {y,
       c - (d - c)/98, d + (d - c)/102},
      Evaluate[FilterRules[{opts}, Options[ContourPlot]]]]],
    Line[z_] :> z, Infinity];
  seeds = Flatten[((signs = Sign[Apply[fy, #1, {1}]];
        #1[[
         1 + Flatten[
           Position[Rest[signs*RotateRight[signs]], -1]]]]) &) /@
     fZero, 1];
  If[seeds == {}, {}, Select[Union[({x, y} /.
         FindRoot[{funcs[[1]],
           funcs[[2]]}, {x, #1[[1]]}, {y, #1[[2]]},
          Evaluate[FilterRules[{opts}, Options[FindRoot]]]] &) /@
      seeds, SameTest -> (Norm[#1 - #2] < 10^(-6) &)],
    a <= #1[[1]] <= b && c <= #1[[2]] <= d &]]]

b = Sqrt[1 - 4 a^2];
s = -2;
\[CapitalLambda][\[Omega]_, l_, m_] :=
  SpinWeightedSpheroidalEigenvalue[s, l, m, a \[Omega]] +
   2 a \[Omega]  m - a^2 \[Omega]^2;

c0[\[Omega]_, m_] := 1 - s - I \[Omega] - (2 I)/b (\[Omega]/2 - a m);
c1[\[Omega]_, m_] := -4 +
   2 (2 + b) I \[Omega] + (4 I)/b (\[Omega]/2 - a m);
c2[\[Omega]_, m_] := s + 3 - 3 I \[Omega] - (2 I)/b (\[Omega]/2 - a
 ↪  m);
c3[\[Omega]_, l_, m_] := \[Omega]^2 (4 + 2 b - a^2) - 2 a m \[Omega]
 ↪  -
    s - 1 - \[CapitalLambda][\[Omega], l, m] + (2 + b) I \[Omega] + (
    4 \[Omega] + 2 I)/b (\[Omega]/2 - a m);
c4[\[Omega]_, m_] :=
  s + 1 - 2 \[Omega]^2 - (2 s + 3) I \[Omega] - (4 \[Omega] + 2 I)/
    b (\[Omega]/2 - a m);
```

```
\[Alpha]r[n_, \[Omega]_, l_, m_] :=
  n^2 + (c0 [\[Omega], m] + 1) n + c0[\[Omega], m];

\[Beta]r[n_, \[Omega]_, l_, m_] := -2 n^2 + (c1[\[Omega], m] + 2) n +
   c3[\[Omega], l, m];

\[Gamma]r[n_, \[Omega]_, l_, m_] :=
  n^2 + (c2[\[Omega], m] - 3) n + c4[\[Omega], m] - c2[\[Omega], m] +
   2;


Fr[\[Omega]_, l_,
   m_] := \[Beta]r[0, \[Omega], l, m]/\[Alpha]r[0, \[Omega], l, m] -
   ContinuedFractionK[(-\[Alpha]r[i - 1, \[Omega], l, m])^(
     1 - KroneckerDelta[1, i])*\[Gamma]r[i, \[Omega], l, m],
 ↪  \[Beta]r[
     i, \[Omega], l, m], {i, 1, 200}];
Rr[\[Omega]_, l_, m_] := Re[Fr[\[Omega], l, m]];
Imagr[\[Omega]_, l_, m_] := Im[Fr[\[Omega], l, m]];

DistributeDefinitions[SpinWeightedSpheroidalEigenvalue]

(*User must give a value to "a" in Leaver's units*)
ParallelTable[
 FindRoots2D[{Rr[x + I  y, l, m], Imagr[x + I  y, l, m]}, {x, 0.5,
   3}, {y, -2, -0.15}], {l, 2, 6}, {m, -l, l}]

(*Change y domain to obtain more overtones*)
TableForm[
 ParallelTable[
  FindRoots2D[{Rr[x + I  y, l, l], Imagr[x + I  y, l, l]}, {x, 0.5,
    3}, {y, -0.21, -0.14},
   MaxRecursion -> 3], {a, {0.1, 0.2, 0.3, 0.4, 0.45, 0.495}}, {l, 2,
   6}]]
```

References

"Black Hole Perturbation Toolkit," (bhptoolkit.org).

Abbott, B. P., R. Abbott, T. D. Abbott, M. R. Abernathy, F. Acernese, *et al.* (LIGO Scientific Collaboration and Virgo Collaboration) (2016), Physical Review Letters **116** (6), 061102, arXiv: 1602.03837.

Abbott, R., T. D. Abbott, S. Abraham, F. Acernese, Ackley, *et al.* (LIGO Scientific Collaboration and Virgo Collaboration) (2020), Phys. Rev. Lett. **125**, 101102.

Alcubierre, M. (2012), *Introduction to 3+1 Numerical Relativity* (Oxford University Press).

Arvanitaki, A., S. Dimopoulos, S. Dubovsky, N. Kaloper, and J. March-Russell (2010), Physical Review D **81** (12), 123530, arXiv: 0905.4720.

Bambi, C. (2020), *Proceedings of Multifrequency Behaviour of High Energy Cosmic Sources - XIII — PoS(MULTIF2019)*, PoS **MULTIF2019**, 028.

Barranco, J., A. Bernal, J. C. Degollado, A. Diez-Tejedor, M. Megevand, M. Alcubierre, D. Núñez, and O. Sarbach (2011), Physical Review D **84** (8), 083008, arXiv: 1108.0931.

Baumann, D., H. S. Chia, J. Stout, and L. ter Haar (2019), Journal of Cosmology and Astroparticle Physics **2019** (12), 006, arXiv:1908.10370 [gr-qc].

Birkhoff, G. D. (1923), *Relativity and Modern Physics* (Cambridge, Mass.).

Chandrasekhar, S. (1983), *The Mathematical Theory of Black Holes* (Oxford University Press).

Detweiler, S. (1980), Physical Review D **22** (10), 2323.

d'Inverno, R. (1992), *Introducing Einstein's Relativity* (Clarendon Press).

Dirac, P. A. M. (1981), *The Principles of Quantum Mechanics* (Oxford University Press).

Dolan, S. R. (2007), Physical Review D **76** (8), 084001.

Ferrari, V., and B. Mashhoon (1984), Physical Review D **30** (2), 295.

Goebel, C. J. (1972), The Astrophysical Journal Letters **172**, L95.

Herdeiro, C. A. R., and E. Radu (2014), Physical Review Letters **112** (22), 221101, arXiv: 1403.2757.

Isi, M., M. Giesler, W. M. Farr, M. A. Scheel, and S. A. Teukolsky (2019), Physical Review Letters **123** (11), 111102, arXiv: 1905.00869.

Kerr, R. P. (1963), Physical Review Letters **11** (5), 237.

Kokkotas, K. D., and B. G. Schmidt (1999), Living Reviews in Relativity **2** (1), 2.

Konoplya, R. A., and A. V. Zhidenko (2005), Physics Letters B **609** (3-4), 377, arXiv:gr-qc/0411059 [gr-qc].

Leaver, E. W. (1985), Proceedings of the Royal Society of London. Series A, Mathematical and Physical Sciences **402** (1823), 285.

Li, P.-C., T.-C. Lee, M. Guo, and B. Chen (2021), arXiv:2105.14268 [gr-qc].

Martel, K., and E. Poisson (2005), Physical Review D **71** (10), 104003.

Misner, C. W., K. S. Thorne, and J. A. Wheeler (2017), *Gravitation* (Princeton University Press).

Nollert, H.-P. (1993), Physical Review D **47** (12), 5253.

Penrose, R. (1969), Rivista del Nuovo Cimento **1** (7), 252.

Regge, T., and J. A. Wheeler (1957), Physical Review **108** (4), 1063.

Richartz, M. (2016), Physical Review D **93** (6), 064062, arXiv: 1509.04260.

Schutz, B. (2009), *A First Course in General Relativity*, 2nd ed. (Cambridge University Press, Cambridge).

Schwarzschild, K. (1916), Abh. Konigl. Preuss. Akad. Wissenschaften Jahre 1906,92, Berlin,1907 **1916**, 189.

Teukolsky, S. A. (1973), The Astrophysical Journal **185**, 635.

Townsend, P. K. (1997), Black Holes: Lecture notes, arXiv:gr-qc/9707012.

Wagon, S. (2010), *Mathematica® in Action* (Springer-Verlag GmbH).

Yang, H., D. A. Nichols, F. Zhang, A. Zimmerman, Z. Zhang, and Y. Chen (2012), Physical Review D **86** (10), 104006, arXiv:1207.4253 [gr-qc].

Zouros, T. J., and D. M. Eardley (1979), Annals Phys. **118** (1), 139.

Zyla, P., *et al.* (Particle Data Group) (2020), PTEP **2020** (8), 083C01.